Aus der
Franz-Volhard-Klinik
Kardiologie, Charité Campus Buch
Direktor: Univ.-Prof. Dr. med. Rainer Dietz

Habilitationsschrift

Die Kardiale Magnetresonanztomographie in der Diagnostik myokardialer Erkrankungen

Zur Erlangung der Lehrbefähigung für das Fach Innere Medizin

vorgelegt dem Fakultätsrat der

Medizinischen Fakultät Charité

der Universitätsmedizin Berlin

von

Dr. med. Jeanette Esther Schulz-Menger

Dekan: Prof. Dr. Martin Paul

Gutachter:
1. Prof. Stefan Neubauer, Oxford
2. Prof. Ruth Strasser, Dresden

eingereicht Mai 2006
Vortrag vor dem Fakultätsrat 6. Februar 2007

Für meinen Sohn Alex

Inhaltsverzeichnis

Abstrakt

In der Kardiologie stellt die nichtinvasive Differenzierung von Myokardschäden noch immer eine diagnostische Herausforderung dar. In dieser Arbeit wurde die kardiale Magnetresonanztomographie genutzt, um Myokardschäden zu differenzieren und Zusammenhänge zu funktionellen Veränderungen, insbesondere bei primären und sekundären Kardiomyopathien zu untersuchen. Es ist gelungen, Einsatzmöglichkeiten der Methode aufzuzeigen, die bereits auch Verbreitung in der klinischen Routine gefunden haben.

Bei der Hypertrophischen Kardiomyopathie führten wir die Planimetrie der Fläche des linksventrikulären Ausflusstraktes zur Quantifizierung der Obstruktion ein und konnten nicht nur Patienten nach Septumablation kontrollieren, sondern erstellten auch Normwerte zur Differenzierung der Obstruktion. Nach der Intervention wurden im zeitlichen Verlauf die Evolution des peri-infarziellen Ödemes und der Infarktnarbe, einschließlich des Zusammenhanges zur funktionellen und klinischen Verbesserung untersucht. Durch die Anwendung einer Kombination von T2-gewichteten und kontrastverstärkten T1-gewichteten Sequenzen im zeitlichen Verlauf konnten sowohl die sehr frühen als auch die späten Myokardveränderungen dargestellt werden. Da die therapeutisch indizierte Intervention ohne Induktion einer alkoholbedingten Kolliquationsnekrose mit Schaumstoffpartikeln durchführt wurde, ist das Ergebnis mit einer nicht iatrogenen akuten Koronararterienokklusion vergleichbar. Dies erlaubt Rückschlüsse auf die Darstellung eines akuten Infarkt mittels Magnetresonanztomographie.

Der echokardiographische Nachweis von Wandbewegungsstörungen ist eine grundlegende diagnostische Information, allerdings ist die Unterscheidung zwischen einer entzündlichen oder ischämischen Genese nicht möglich. Diese Lücke kann nunmehr durch die kardiale Magnetresonanztomographie geschlossen werden. Das von uns eingeführte multisequentielle Protokoll führte zum Beispiel bei der Myokarditis zu einer Verbesserung der diagnostischen Genauigkeit der magnetresonanztomographischen Untersuchungen. Ebenso konnte eine myokardiale Mitbeteiligung bei Sarkoidose bereits bei normaler linksventrikulärer Funktion gezeigt werden.

Für die Darstellung der Koronararterien wurde eine 3D-Steady-State-Free-Precession-Sequenz bei gesunden Probanden und in klinischer Umgebung geprüft, sie erwies sich als verlässlich, muss aber noch weiter evaluiert werden.

Die kardiale MRT hat in einigen kardiologischen Bereichen bereits Eingang in die Routine gefunden. Die Methode hat das Potenzial, prospektiv reversible und irreversible myokardiale Veränderungen zu unterscheiden und sie darüber hinaus im Verlauf zu untersuchen. Es ist zu erwarten, dass auf dem Gebiet der myokardialen Erkrankungen nichtinvasive bildgebende Differenzierungen zur Charakterisierung des klinischen Status und Therapieerfolges beitragen werden. Weitere Studien werden gestatten, die prognostische Relevanz frühzeitig erfasster Veränderungen zur bewerten.

Schlagworte: Hypertrophische Kardiomyopathie, Kardiomyopathie, Magnetresonanztomographie, Myokarditis, Systemerkrankungen,

Abstract

Non-invasive differentiation of myocardial injury is an ongoing diagnostic challenge in cardiology. We used cardiac magnetic resonance to characterize myocardial injuries and to investigate their relations to functional changes, especially in primary and secondary cardiomyopathies. We were able to describe novel applications of CMR, which are currently used in routine settings.

The planimetry of the left ventricular outflow tract area to quantify obstruction was developed to characterize hypertrophic cardiomyopathies (HCM). We applied the method in patients after septal artery embolization to monitor the success of the intervention. We then extended our observations to establish cut-off values to differentiate between the obstructive and non-obstructive forms of HCM and to provide the first reference standard for planimetric values in healthy volunteers. After intervention infarct related edema and fibrosis was detected during follow-up and correlated to functional and clinical improvement of the patients. Combining of T2-weighted and contrast-enhanced T1-weighted images allowed the detection of very early and late myocardial changes during follow-up. As the intervention was performed using foam gel instead of alcohol, the therapeutically induced infarction was similar to an abrupt coronary occlusion in the clinical setting in contrast to the non-physiological alcohol-like colliquation-necrosis. As such, we were able not only to monitor the intervention-related tissue injuries but also to gain novel insights into the very early myocardial tissue injuries in acute myocardial infarction

Assessment of wall motion abnormalities applying echocardiography is a basic diagnostic information, but it is not possible to differentiate between e.g.

inflammatory or ischemic aetiologies. Applying cardiac magnetic resonance (CMR), this information can be provided. Exploiting the unique tissue characterization capabilities of CMR, we introduced a multi-sequential approach, which was shown to increase the diagnostic accuracy of magnetic resonance imaging to detect myocarditis. Applying a similar approach we were able to detect myocardial involvement in sarcoidosis even when left ventricular function was still preserved.

A 3D-steady-state-free-precession pulse sequence was applied in volunteers and patients and could be shown to be applicable, but has to be improved.

Cardiac magnetic resonance is routinely applied in many areas of cardiology. The method has the potential to differentiate prospectively between reversible and irreversible myocardial injuries. The changes can be detected during follow-up.

One could expect, that in the field of myocardial diseases the differentiation by non-invasive imaging modalities will improve clinical characterization and monitor the success of therapy or (therapeutic success). Further studies will allow identifying the prognostic values of the early-detected injuries.

Key words: cardiomyopathy, hypertrophic cardiomyopathy, magnetic resonance tomography, myocarditis, systemic disorder

Abkürzungsverzeichnis

DCM	Dilatative Kardiomyopathie
DG	Druckgradient
FSE	Fast-Spinechosequenz
gRE	globales relatives Enhancement
GRE	Gradientenechosequenzen
HCM	Hypertrophische Kardiomyopathie
HOCM	Hypertrophische obstruktive Kardiomyopathie
IR	Inversion Recovery
KM	Kontrastmittel
KMP	Kardiomyopathie
MRT	Magnetresonanztomographie
LHE	Late Hyperenhancement
LVOT	Linksventrikulärer Ausflusstrakt
PTSMA	Perkutane transluminale septale Myokadablation
SSFP	Steady State Free Precession
TE	Echozeit
RCM	Restriktive Kardiomyopathie
TR	Repititionszeit

I Darstellung von Myokardschäden als diagnostische Herausforderung in der Kardiologie

Der Nachweis regionaler Wandbewegungsstörungen, morphologischer Veränderungen, als auch Funktionsmessungen geben Hinweise auf kardiale Erkrankungen und werden in der täglichen klinischen Routine eingesetzt. Es ist davon auszugehen, dass eine darüber hinaus gehende nichtinvasive Differenzierung der Krankheitsursache und eine prospektive Einschätzung der Reversibilität die Diagnostik bereichert und die Festlegung therapeutischer Strategien erleichtert.

Dies erscheint insbesondere deshalb relevant, da bei myokardialen Erkrankungen der weitere Krankheitsverlauf oftmals von einer frühen Diagnose abhängig ist.

1. Nicht-ischämische Herzkrankheiten

Im Folgenden wird nur auf die Erkrankungen nicht koronarer Ursache eingegangen, für die im Rahmen dieser Arbeit neue diagnostische Konzepte entwickelt wurden.

1.1. Kardiomyopathien

Kardiomyopathien sind chronische, vorwiegend genetisch bedingte Erkrankungen, die meist progredient verlaufen. Sie werden in 4 Hauptformen unterteilt: Dilatative Kardiomyopathie (DCM), Hypertrophische Kardiomyopathie (HCM), Restriktive Kardiomyopathie (RCM), und arrhythmogene rechtsventrikuläre Kardiomyopathie (ARVC).[1]

Ein Schwerpunkt unserer Arbeit ist die kardiale Magnetresonanztomographie (MRT) bei der HCM. Die HCM wird durch unterschiedliche Mutationen verursacht, die für das Sarkomer kodieren. Phänotypisch imponiert eine nicht allein durch die Hämodynamik oder andere Erkrankungen erklärbare Hypertrophie unterschiedlichen Ausmaßes. Allerdings liegt bei einigen, durchaus malignen Formen keine ausgeprägte Hypertrophie vor oder prägt sich erst im späteren Lebensalter aus (z.B. Troponin T- und Protein C-Mutationen).[2-4] Umso entscheidender ist es, alternative Wege der Phänotypisierung zu beschreiten.

Die heute übliche Einteilung unterscheidet nach nichtobstruktiven, latent obstruktiven und obstruktiven Formen, die Letzteren werden nach der Lokalisation der Obstruktion in subaortal (linksventrikulärer Ausflusstrakt, LVOT) respektive mitventrikulär gelegene unterteilt.[5] Der Nachweis der Obstruktion wird durch den invasiv gemessenen und/oder den echokardiographisch berechneten Druckgradienten (DG) erbracht. Allerdings weist der DG eine große spontane Variabilität auf, die zusätzlich durch hämodynamische Veränderungen beeinflusst wird. [6, 7] Es gibt Hinweise darauf, dass einer LVOT-Obstruktion eine prognostische Bedeutung zukommt. [8]

Sowohl bei den obstruktiven, als auch bei den nicht obstruktiven Erkrankungen ist das histologische Bild geprägt durch ein irreguläres Anordnungsmuster der Myozyten, sogenanntes myocardial disarray, darüber hinaus sind in einigen Fällen auch diffuse, intramyokardial gelegene Fibrosen nachweisbar. Die Progredienz der fibrotischen Umwandlung scheint mit einer Verschlechterung des klinischen Befundes einherzugehen.[9]

1.2. Sekundäre Myokarderkrankungen

Sekundäre oder auch spezifische Kardiomyopathien werden definiert als myokardiale Erkrankungen mit bekannter Ursache (z.B. ischämisch, hypertensiv oder entzündlich). Eine häufige Ursache der DCM ist eine Myokarditis, die in unseren Breiten vorwiegend durch virale Infektionen (z.B Coxsackievirus, Parvovirus B 19, Herpesviren), aber auch durch bakterielle, allergische oder toxische Reaktionen induziert werden kann.[10] Die histologischen Veränderungen variieren in Abhängigkeit von dem auslösenden Agens, dem Stadium der Myokarditis und umfassen sowohl fokale als auch diffuse Läsionen.[11] Histologisch können entzündliche zelluläre Infiltrationen mit und ohne myozytäre Nekrosen vorliegen.[12] Die Ausprägung der myokardialen Schäden und deren rasche Diagnose prägen den Verlauf der Erkrankung, der von einer restititio ad integrum bis zum Tod reichen kann.[10]

Bei Systemerkrankungen bestimmt insbesondere die myokardiale Mitbeteiligung die Prognose. Obwohl bei einigen Systemerkrankungen spezifische Veränderungen (z.B. Granulome bei der Sarkoidose) auftreten, wird Autopsiestudien zufolge, die klinische Diagnose viel zu selten gestellt. Als Beispiel sei wiederum die Sarkoidose genannt, bei der gemessen an autoptischen Befunden nur 50% der post mortem nachgewiesenen Myokardbeteiligungen bereits klinisch erfasst wurden.[13] Neben den Granulomen konnten histologisch im Myokard in einigen Fällen auch ausgedehnte Fibrosen nachgewiesen werden.[14] Auch bei Vaskulitiden, wie dem Churg-Strauss-Syndrom imponieren myokardiale Nekrosen. Perimyokarditiden stellen in 48% der Fälle die Todesursache dar.[15] Bei der sich vorwiegend als RCM ausprägenden kardialen Amyloidose liegen

extrazelluläre Amyloideinlagerungen vor.[16] Nach der Diagnosestellung der myokardialen Beteiligung beträgt die mittlere Überlebensdauer nur noch 13 Monate.[17] Ebenso sind beim Lupus erythematodes vielfältige Formen der kardialen Beteiligung beschrieben[18], aber insbesondere bei der inflammatorischen myokardialen Beteiligung bestehen große Unterschiede zwischen der autoptisch nachgewiesenen Häufigkeit (bis zu 40%) und dem klinischen Nachweis (8 - 14%).[19, 20]

2. Koronare Herzkrankheit

Bevor es zu einer hämodynamisch relevanten Einengung der subepikardialen Koronargefäße kommt, liegen bereits eine endotheliale Dysfunktion und Lipideinlagerungen in der Gefäßwand vor.[21] Bei einem fortgeschrittenen Stadium wird die Myokardperfusion in den abhängigen Gebieten durch die progrediente Einengung der Koronargefäße vermindert. Durch Plaquerupturen können Koronarobliterationen induziert werden, die zu einer akuten Myokardischämie und dann Nekrose führen.[22] Die in solchen Situationen meist entstehenden Myokardinfarkte sind durch Nekrosen charakterisiert, die sich im Verlauf von subendokardial nach subepikardial ausdehnen können.[23] Während innerhalb der ersten halben Stunde nach Beginn einer Ischämie die Schäden reversibel sind, erwiesen sich die danach entstehenden Nekrosen und Einblutungen als irreversibel. Elektronenmikroskopisch wurden mittels Triphenytetrazolium Chlorid (TTC)-Färbung bereits nach 3,5 Stunden Nekrosen, fokale Einblutungen und Ödeme nachgewiesen. Man geht bei einem nicht reperfundierten Myokardinfarkt

davon aus, dass sich nach ungefähr sechs Wochen die Fibrose vollständig ausgebildet hat.[24]

3. Differenzierung von Krankheitsstadien und - ursachen

Im Verlauf myokardialer Erkrankungen kann sich die Lokalisation der Schädigung ändern, z.B. können sich primär fokale Veränderungen wie bei der Myokarditis diffus ausbreiten und das histologische Substrat kann eine Wandlung erfahren. [12] Während anfänglich häufig, wie auch beim Myokardinfarkt beobachtet, reversible Schäden erfassbar sind, bestehen zu bestimmten Zeitpunkten reversible und irreversible Veränderungen nebeneinander. Übergänge zur Irreversibilität sind möglich, deren Ausdehnung potenzielle Funktionseinbußen bestimmen und die Prognose mit beeinflussen können. Während die klinische Manifestation und die klassischen paraklinischen Parameter bei kardialen Erkrankungen sehr ähnlich sein können, unterscheidet sich die therapeutische Konsequenz erheblich. Sowohl eine Myokarditis als auch ein Myokardinfarkt können klinisch als ein akutes Koronarsyndrom imponieren. Obwohl in den meisten Fällen die Differenzierung gelingt, würde eine direkte Visualisierung der Pathologie einen Zugewinn an Sicherheit erbringen.

Ein wesentlicher Aspekt unserer Arbeit ist es, funktionelle und myokardiale Veränderungen nachzuweisen, Krankheitsverläufe darzustellen und Myokardschäden zu differenzieren.

II Die MRT in der Kardiologie

1. Integrative Bildgebung in der Diagnostik kardialer Erkrankungen- Rolle der MRT

Eine ideale Bildgebung in der Kardiologie ist dadurch gekennzeichnet, dass sie ohne jede Belastung für den Patienten rasch funktionelle und morphologische Veränderungen detektiert, die ursächlichen Gewebeveränderungen differenziert, schnell anwendbar und weit verbreitet ist. Die meist in der Routine eingesetzte Echokardiographie erfüllt eine Reihe dieser Anforderungen, kann aber Myokardschäden (z.B. entzündlicher vs. ischämischer Schaden) nicht unterscheiden und ist darüber hinaus in ca. 20% limitiert durch eingeschränkte Schallbedingungen.[25] Szintigraphische Methoden, z.B. die Single-Photon-Emmission-Computertomographie gestatten durch die Beurteilung von Nuklidanreicherungen den Nachweis von Durchblutungsstörungen und der linksventrikulären Funktion. Allerdings liegt die räumliche Auflösung bei etwa 7-10mm Bildelementkantenlänge und damit deutlich über der MRT, wodurch Detektion kleinerer mit MRT darstellbarer Defekte (wie z.B. subendokardialer Infarkte) unmöglich wird.[26] Die Positronen-Emmissions-Tomographie (PET) gilt gegenwärtig noch als der Goldstandard bei Vitatilitäts- und Ischämieuntersuchungen, allerdings ist die sehr teure Methode schlecht verfügbar und spielt in der Routinediagnostik kaum eine Rolle. Die kardiale MRT weist eine exzellente Korrelation zur PET sowohl bei der Vitalitäts-, als auch bei der Perfusionsdiagnostik auf.[27, 28 29, 30] Während die Echokardiographie sicherlich in den nächsten Jahren die Methode der ersten Wahl zur Erfassung von Wandbewegungsstörungen und morphologischen Veränderungen sein wird, hat

die MRT die Möglichkeit, zusätzlich Ödeme[31, 32], Infarktnarben[33] oder Fibrosen anderer Genese[34] darzustellen. Da die nicht invasive, strahlenfreie MRT-Technik mit hoher räumlicher Auflösung entstandene morphologische und funktionelle Veränderungen aufzeigen kann, hat man eine Methode zur Verfügung, die ein neues Verständnis von Erkrankungen erlaubt. Gegenwärtig ist, in Abhängigkeit von der Indikation, die Untersuchungsdauer noch relativ lang (zwischen 10-60 min, durchschnittlich 30 min). Es ist zu erwarten, dass es mit einer weiteren Entwicklung der Technik zur Verkürzung kommt. Allerdings ist die kardiale MRT bisher nur eingeschränkt verfügbar, da es erst wenige hochqualifizierte Zentren gibt, deren Zahl sich aber ständig vermehrt.

2. Gerätetechnische Voraussetzungen [35]

Die von uns durchgeführten MRT-Untersuchungen wurden anfangs an einem 1.0T System (Expert, Siemens-Medical Solution, Erlangen, Deutschland), später an 1.5T Scannern (CVi GE, Waukesha, Wisconsin, USA respektive Sonata Siemens-Medical Solution, Erlangen, Deutschland) durchgeführt. Gegenwärtig sind die 1.5T Magneten am weitesten verbreitet in der kardiologischen Anwendung und gestatten eine zuverlässige Durchführung von Untersuchungen mit hoher Qualität.

Eine wesentliche Rolle für die MRT-Bildgebung spielen die Hochfrequenzspulen, die das Signal-Rausch-Verhältnis verbessern können, ohne dass es zu einer Verschlechterung der räumlichen Auflösung oder zu einer Messzeitverlängerung kommt. In unseren Arbeiten kamen Volumen-Hochfrequenz-Spulen (als Körperspule „body-coil“) und Matrixanordnungen von Oberflächen-Hochfrequenz-Empfangsspulen, so genannte „Phased-Array-Spulen“ zum Einsatz.

Die Körperspule zeichnet sich durch ihre große Signalhomogenität aus und wurde insbesondere bei geplanter Quantifizierung des Signals eingesetzt, z.B. in der Texturanalyse bei Myokarditis. Ansonsten wurden Phased-Array-Spulen verwendet, die aus mehreren parallel geschalteten Spulenelementen bestehen. Diese Spulen gestatten auf Grund ihres Signal-Rausch-Vorteiles eine höhere räumliche und zeitliche Auflösung. Außerdem unterstützen sie neue Entwicklungen der schnellen Bildgebung, wie zum Beispiel die parallele Bildgebung. In Abhängigkeit vom Durchmesser der Spulenelemente und der Superposition des Signals der einzelnen Elemente weisen Phased-Array Spulen stark ausgeprägte Gradienten in der Signalintensität auf.

Mit zunehmendem Abstand von den Spulenelementen wird die Signalintensität geringer, so dass eine zuverlässige Quantifizierung der absoluten Signalintensität zusätzliche aufwendige Korrekturen erfordert.

3. **Überblick über verwendete Bildgebungstechniken** [35]

3.1. Kardiale Funktion und Morphologie

Durch die Anwendung von Gradientenecho-Sequenzen (GRE) können Bilder über den gesamten Herzzyklus im cine-Mode aufgenommen und dargestellt werden. Dies gestattet durch die Quantifizierung von Volumen und Masse die Berechnung von Funktionsparametern, darüber hinaus die Detektion von Wandbewegungsstörungen. Da bei dieser Technik sehr kurze Repititionszeiten erreicht werden, ist im Vergleich zu Spinecho-Techniken (Kapitel II 3.2.; Seite 18) eine schnellere Bildaufnahme möglich. Die GRE sind damit weniger anfällig für Bewegungsartefakte; weisen auf Grund der kurzen Repititionszeit ein

vergleichsweise geringes Signal-Rausch-Verhältnis („signal-noise ratio“, SNR) auf. Um insbesondere Suszeptibilitätsartefakte zu vermeiden, wird die Echozeit (TE) so kurz wie möglich gehalten und beträgt in der Praxis zwischen 2-6 ms. Anfänglich standen vorwiegend so genannte „spoiled“ GRE-Techniken zur Verfügung, bei denen das von der vorherigen Anregung verbliebene Signal vor der nächsten Messung durch spezielle Hochfrequenzpulse zerstört wird. Seit Ende der 90iger Jahre stehen zunehmend „Steady State Free Precession“ (SSFP)-Techniken zur Verfügung. Hier wird das verbleibende Signal nicht zerstört sondern die transversale Magnetisierung trägt zu mehreren Echos bei. Die Bildgebung mit SSFP-Techniken offeriert einen SNR-Vorteil gegenüber GRE-Techniken, außerdem wird durch die Verwendung großer Anregungswinkel (alpha > 45°) ein im Vergleich zu Gradientenechotechniken größerer Blut-Myokard-Kontrast erreicht. Dieser wird durch das Verhältnis von T_2 zu T_1 geprägt und ist im Vergleich zu Gradientenechotechniken unabhängiger vom Einstrom ungesättigten Blutes in die Schicht. Somit kann das Myokard besser von Blut abgegrenzt werden, dies ermöglicht im Vergleich zu GRE-Techniken eine deutlich bessere Beurteilung der regionalen und globalen Ventrikelfunktion.

Die bessere Detailerkennbarkeit muss bei der Erstellung von Normwerten berücksichtigt werden, da im Vergleich zu spoiled GRE-Techniken Unterschiede bei der Bestimmung von Volumen und Masse Unterschiede auftreten können.[36] Insbesondere im Rahmen von Studien müssen die Parameter konstant gehalten werden, da bereits eine Änderung der zeitlichen Auflösung (z.B. durch eine Änderung der Phasenkodierschritte pro Herzphase (views per segment)) und die dadurch induzierten Änderungen der Bildqualität zu signifikant unterschiedlichen

Werten führen können.[37] Gegenwärtig werden in der kardiologischen Routineanwendung bei entsprechenden Fragestellungen in der Mehrheit SSFP-Techniken eingesetzt. Bei den hier vorgestellten Arbeiten wurden in Abhängigkeit von der vorhandenen Sequenztechnik anfangs vorrangig spoiled GRE verwendet, die bereits im frühen Stadium der Entwicklung der SSFP-Techniken durch diese ergänzt bzw. ersetzt wurden.

3.2. Myokarddifferenzierung

Es kommen Fast-Spinecho (FSE)- und Inversion-Recovery (IR)-Sequenzen mit und ohne Kontrastmittelverstärkung zum Einsatz.

FSE sind modifizierte Spinecho-Sequenzen, bei denen die Bildaufnahmezeit durch das sequentielle Auslesen multipler Echos pro Anregung reduziert wird. Dadurch werden im Vergleich zur konventionellen Spin-Echo Technik längere Wiederholzeiten (TR) benötigt, die insbesondere für T_2- und protonengewichtete Bilder geeignet sind. Der Vorteil von FSE-Techniken gegenüber GRE liegt in der Unempfindlichkeit gegenüber statischen Magnetfeldinhomogenitäten. Sie kommen im Kardio-MRT insbesondere bei der anatomischen Bildgebung zum Einsatz und sind geeignet für die Myokarddifferenzierung. Dabei kann bereits der native Gewebekontrast genutzt werden, da in Abhängigkeit von der eingesetzten Kontrastwichtung bzw. den benutzten Bildgebungsparametern Flüssigkeiten hell dargestellt werden (T2-Wichtung) können. Zusätzlich können Muskel- oder/und Fettsignalbeiträge durch den Einsatz von Sättigungsvorbereitungsmodulen unterdrückt werden. IR-Sequenzen werden vorwiegend zur Aufnahme von T1-gewichteten Bildern verwendet, wobei über eine Veränderung der Inversionszeit

die T1-Wichtung beeinflusst wird. Dies wird unter anderem genutzt, um Signalanteile ausgewählter Gewebe zu unterdrücken und die Darstellung von Gewebskomponenten mit einem hohen Kontrast-Rausch-Verhältnis zu erreichen. Bei Myokardinfarkten gelang mit dieser Technik eine Steigerung des Kontrast-Rausch-Verhältnis[38] im Vergleich zu den Erstbeschreibungen Anfang der 80iger Jahre.[39]

Bei unseren Untersuchungen kamen T_1- und T_2-gewichtete Sequenzen zum Einsatz. Durch die Einführung eines Turbofaktors bei der FSE konnte die Messzeit deutlich verkürzt werden. Für die Quantifizierung eines Ödems verwendeten wir eine T_2-gewichtete Triple Inversion Recovery Sequenz (STIR).

Die Sequenzparameter der in den Publikationen verwendeten Sequenz sind:

TR 2 x RR, TE 65 ms, TI 140 ms, Schichtdicke 15 mm, Schichtabstand 5 mm, Field of View 34 bis 38 cm, Matrix: 256 x 256, eine Mittelung. Das Signal wurde quantifiziert durch die Plazierung einer Region of Interest (ROI) im Myokard und zum internen Vergleich im Skelettmuskel.

Dies ist exemplarisch in Abbildung 1 auf der Seite 21 dargestellt.

Unter Anwendung von T_1-gewichteten Sequenzen erfolgte die Analyse der Kontrastmittelauswaschung zu unterschiedlichen Zeitpunkten. Für die Phase der frühen Auswaschung wurde das Signal über die ersten vier Minuten nach Kontrastmittelapplikation quantifiziert. Dafür kam eine nicht atemangehaltene Mehrschicht-T_1-gewichtete FSE-Technik zur Anwendung. Der Signalanstieg wurde im Verhältnis zu dem vor der KM-Applikation aufgenommenen Signal berechnet.

Die Sequenzparameter der publizierten Sequenz sind: TR 475 – 480 ms,

TE 30 ms, Matrix 256 x 256; Schichtdicke 6 mm, 4 - 6 Mittelungen.

Der Signalanstieg wurde im Verhältnis zum vor der KM-Applikation akquirierten Signal sowohl im Myokard als auch im Skelettmuskel berechnet. Das Verhältnis der beiden Werte wird durch das so genannte globale relative Enhancement (gRE) widerspiegelt. Zum besseren Verständnis ist dies in der Abbildung 2 auf der Seite 21 dargestellt.

Abbildung 1:

Darstellung der Signalquantifizierung in den T_2-gewichteten Sequenzen Region of Interest (ROI) exemplarisch für das Myokard (gelb) und den Skelettmuskel (weiss)

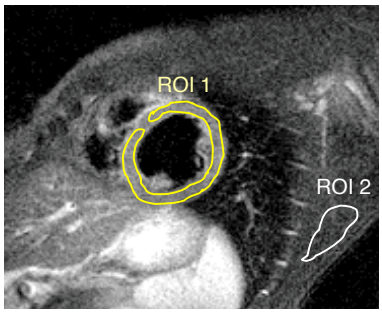

$$\text{T2 Ratio} = \frac{\text{Signalintensität}_{\text{Myokard (ROI 1)}}}{\text{Signalintensität}_{\text{Skelettmuskell (ROI 2)}}}$$

Abbildung 2:

Darstellung der Signalquantifizierung in den T_1-gewichteten Sequenzen Region of Interest (ROI) exemplarisch für das Myokard (gelb) und den Skelettmuskel (weiss)

Links axiale Schicht vor und rechts nach Kontrastmittelapplikation

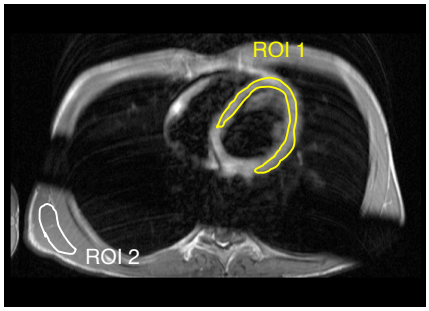

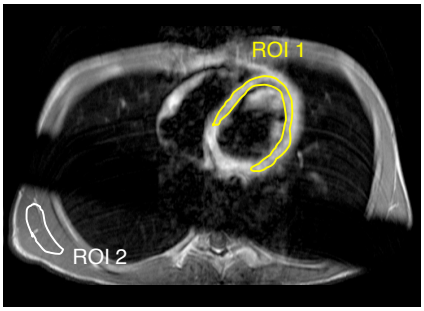

$$\text{Enhancement Ratio} = \frac{\text{Signal}_{\text{post Gd-DTPA}} - \text{Signal}_{\text{pre Gd-DTPA}}}{\text{Signal}_{\text{pre Gd-DTPA}}}$$

$$\text{gRE} = \frac{\text{Enhancement ratio}_{\text{Myokard ROI 1}}}{\text{Enhancement ratio}_{\text{Skelettmuskel ROI 2}}}$$

Die quantifizierten Werte wurden im Vergleich zu Normalpersonen beurteilt. Um spulenbedingte Signalinhomogenitäten auszuschließen, wurde eine Körperspule verwendet. Diese Technik wurde bereits 1998 von uns publiziert.[40] Nach der Implementierung eines zweiten Scanners einer anderen Herstellerfirma passten wir anhand eines Normalkollektives (n=47 gesunde Probanden) die verwendeten Techniken und Protokolle an und re-evaluierten die Normwerte.[41] Die späte Kontrastmittelauswaschung wurde mittels IR-GRE dargestellt. Die Auswertung erfolgte in Abhängigkeit von der Fragestellung qualitativ oder quantitativ. Die quantitative Analyse beruht auf einem von uns entwickelten Algorithmus, der eine gut reproduzierbare Auswertung gestattet.[42]

Da viele unserer Arbeiten auf der kombinierten Anwendung aller genannten Sequenzen beruhen, wird das Untersuchungsprotokoll in der folgenden Abbildung 3 zusammengefasst dargestellt.

Abbildung 3:

Darstellung des multi-sequentiellen MRT-Protokolles

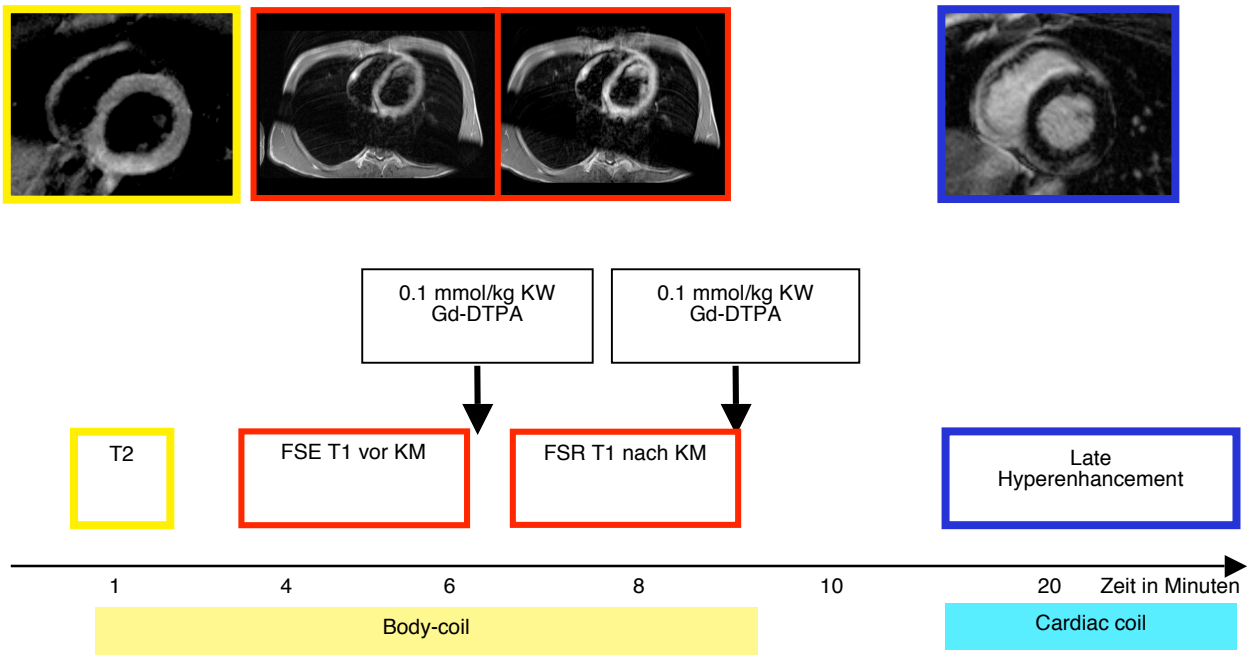

Ohne Zweifel wäre eine direkte Quantifizierung der T1-Zeiten anstrebenswert, um eine Myokarddifferenzierung vornehmen zu können.

Bei der Darstellung der Myokardperfusion wird die initiale Passage des KM genutzt. Hierbei kommen bisher T_1-gewichtete Techniken unter Anwendung verschiedener Kontrastmitteldosierungen zum Einsatz. Es besteht gegenwärtig keine Einigung über das optimale Vorgehen bei dieser Untersuchung. Direkte Vergleichstudien innerhalb und unterhalb der Hersteller sind nicht verfügbar. Um eine prospektive Studie mit geplanter quantitativer Auswertung effektiv durchführen zu können, prüften wir vorhandene Techniken und stellten insbesondere die Optimierung der Kontrastmitteldosis in den Vordergrund. Die in der Studie verwendete Techniken/Protokolle (Firma Siemens Medical Solution Erlangen/Germany) sind:

a) Fast Low-Angle Shot (FLASH), TR/TE = 172 ms/1.25 ms/, TI = 100 ms, Flipwinkel = 12°, Matrix 192 x 94, Schichtdicke 10 mm, parallele Bildgebung (generalized autocalibrating partially parallel acquisition, GRAPPA) Beschleunigungsfaktor 2, Bandweite 500 Hz/pixel;

b) Segmented Echo Planar Imaging (EPI), TR/TE = 5.6/1.17 ms, TI = 135 ms, Flipwinkel = 25°, Matrix 128 x 80, Schichtdicke 8 mm, EPI Faktor 4, Bandweite 1860 Hz/pixel.

3.3. Parallele Bildgebung

Die parallele Bildgebung bietet eine Möglichkeit zur supplementären Ortskodierung, die über die Ausnutzung der Signalintensitätsprofile von Matrixanordnungen von Oberflächenspulen realisiert wird. Jedes dieser

Spulenelemente besitzt ein charakteristisches Signalintensitätsprofil über einen räumlich begrenzten Abbildungsbereich, das zur Ortskodierung genutzt wird. Kernkomponente der spulenintensitätsprofilkodierten parallelen MRT ist die gleichzeitige Aufnahme von Teilortsfrequenzraumdaten für jedes Spulenelement und den dazugehörigen räumlich begrenzten Abbildungsbereich.

Im Unterschied zum konventionellen Ansatz wird zur Datenaufnahme eine verminderte Anzahl von gradientenbasierten Phasenkodierungsschritten zur Füllung des *k*-Raumes verwendet. Der entsprechende Beschleunigungsfaktor ist durch die Verringerung der Abtastdichte der Phasenkodierungsgradienten definiert. Jedes Teilbild zeichnet sich aufgrund der Datenreduktion durch einen entsprechend reduzierten Abbildungsbereich entlang der Phasenkodierungsrichtung aus, so dass für Objekte mit einer Ausdehnung größer als das reduzierte Field of View eingefaltete Bildkopien entstehen.

Parallele Rekonstruktionsmethoden erlauben unter Einbeziehung der Signalintensitätsprofile der einzelnen Spulenelemente die Erstellung eines korrekten und vollständigen Gesamtbildes.[43, 44] Der mit der parallelen Bildgebung verbundene Geschwindigkeitsvorteil gegenüber konventioneller sequentieller Ortsauflösung mittels Phasenkodierungsgradienten kann in einen Zugewinn der räumlichen und/oder zeitlichen Auflösung umgesetzt werden. Durch das Risiko einer potenziellen Neurostimulation oder Gewebeerwärmung sind in der konventionellen Bildgebung einem weiteren Geschwindigkeitszuwachs Grenzen gesetzt, die durch zu schnelles Schalten der Gradienten diktiert sind. Die parallele Bildgebung unterstützt durch die Reduktion der zur Phasenkodierung notwendigen Gradientenschaltpunkte die Herabsetzung physiologischer dB/dt-Einflüsse. Der

Geschwindigkeitsvorteil der parallelen Bildgebung wird in der kardiovaskulären MRT vielfältig genutzt.[45] Gegenwärtig werden meist 6-8 Elementspulen in der Routine eingesetzt. Erste 32-Kanal-Spulen sind im Einsatz.[46]

In dieser Arbeit wurde die parallele Bildgebung sowohl bei der Anwendung der SSFP-basierten Sequenzen, bei der Perfusionsbildgebung und bei den IR-GRE angewandt.

4. Kontrastmittel

Das in der kardialen MRT am häufigsten verwendete Kontrastmittel (KM) ist Gadolinium (Gd). Prinzipiell beruht die Wirksamkeit der paramagnetischen Substanz auf der Verkürzung der Relaxationszeiten T_1 und T_2, die durch die Kontrastmittelanreicherung und der damit verbundenen Veränderung des lokalen Magnetfeldes induziert werden. Um die Anreicherung von Gd in pathologisch verändertem Gewebe darzustellen, werden T_1-gewichtete Bilder aufgenommen.[47] Die KM-Anreicherung führt zu einer Signalverstärkung, die quantifiziert werden kann. Gadolinium selbst ist eine toxische Substanz und wird deshalb in gebundener Form angewendet. Wir verwendeten in diesen Arbeiten Gd-DTPA, das sich durch eine sehr gute Verträglichkeit auszeichnet. Die Nebenwirkungen übersteigen nicht die von Placebo, solange die zugelassene Höchstdosis nicht überschritten wird.[48]

Gd-DTPA ist ein extrazelluläres Kontrastmittel, das bei intravasaler Applikation eine Signalintensitätszunahme in Abhängigkeit von der Gewebeperfusion und Kapillarpermeabilität bewirkt. Insbesondere bei Fibrosen kommt es zu einer verzögerten Auswaschung aus dem extrazellulären Raum.[49] Die verwendete Dosis

hängt von der Indikation ab. Die unterschiedlichen Pathologien können insbesondere anhand der Ein- und Auswaschkinetik des KM differenziert werden.

III MRT in der Diagnostik kardialer Erkrankungen – eigene wissenschaftliche Arbeiten

Im Mittelpunkt der eigenen Arbeiten steht die weitere Phänotypisierung und Gewebedifferenzierung bei verschiedenen myokardialen Erkrankungen unter Anwendung der kardialen MRT. Dieser Schwerpunkt begründet sich auf der Möglichkeit der MRT, Pathologien dreidimensional zu erfassen, diese mit hoher Genauigkeit zu quantifizieren und über die Funktionsdarstellung hinaus Myokardschäden zu differenzieren und im Verlauf darzustellen.

Übersichten über die Rolle der MRT bei Kardiomyopathien konnten bereits im Jahre 2000 und 2005 publiziert werden.[50] Das Interesse an dieser Thematik fand Ausdruck in weiteren eingeladenen Übersichtsarbeiten.

Magnetic Resonance Imaging in Patients with Cardiomyopathies: When and Why

Jeanette Schulz-Menger, Matthias G. Friedrich[1]

Abstract

Cardiac magnetic resonance imaging (MRI) is a noninvasive tool which is able to diagnose and differentiate cardiomyopathies in a single study. The assessment of essential information such as alterations of myocardial and ventricular geometry and function is possible with a high degree of accuracy and reproducibility, based on a small inter- and intraobserver variability. Thus, very small morphological and functional changes in different types of cardiomyopathy are detectable, thereby enabling the cardiologist to increase the safety of therapeutic decisions. Furthermore, MRI bears the potential to characterize tissue transformation in the different types of myocardial affections including ischemic, toxic, infiltrative or inflammatory forms.

Key Words: Cardiomyopathy · Magnetic resonance imaging

Magnetresonanztomographie bei Kardiomyopathien: wann und warum

Zusammenfassung

Die kardiale Magnetresonanztomographie (MRT) bietet als nichtinvasives Verfahren die Möglichkeit, innerhalb einer Untersuchung die für die verschiedenen Formen der Kardiomyopathien charakteristischen funktionellen und morphologischen Veränderungen darzustellen. In dieser Übersicht werden die Einsatzmöglichkeiten der MRT bei den verschiedenen Formen dieser Erkrankung diskutiert.

Die geringe Variabilität der MRT-Messungen gestattet ge-naue Verlaufskontrollen im klinischen Alltag, eröffnet aber auch die Möglichkeit, Therapiestudien mit einer geringeren Anzahl von einzuschließenden Patienten zu sicheren Ergebnissen zu führen. Damit erweitert sich das Spektrum der Indikationen über die Präzisierung unklarer Befunde hinaus auf die Verlaufsbeobachtung während einer pharmakologischen Intervention und auf alle wissenschaftlichen Fragestellungen.

Der Vorzug der MRT, nichtinvasiv Gewebe charakterisieren zu können, verdeutlicht das Potential dieser Technik bei sekundären Kardiomyopathien sowie bei entzündlichen und infiltrativen Formen myokardialer Erkrankungen.

Schlüsselwörter: Kardiomyopathie · Magnetresonanztomographie

Cardiomyopathies are chronic, progressive myocardial diseases associated with altered cardiac function [42]. They are classified into 4 main forms: dilated cardiomyopathy (DCM), hypertrophic cardiomyopathy (HCM), restrictive cardiomyopathy (RCM), and arrhythmogenic right ventricular cardiomyopathy (ARVCM). Specific cardiomyopathies have been defined as myocardial diseases based on certain cardiac or systemic disorders, such as ischemic, hypertensive or inflammatory cardiomyopathy. The typical morphological feature of dilated cardiomyopathy is rather uniform and characterized by progressive left ventricular dilation and loss of contractile function. This phenotype can also be the result of extensive ischemic injury of the myocardium with subsequent remodeling (sometimes called ischemic cardiomyopathy) or long-term pressure overload in arterial hypertension (known as hypertensive cardiomyopathy).

For establishing the diagnosis of cardiomyopathy the exclusion of other cardiac diseases is necessary, mostly done by echocardiography, cardiac catheterization, radionuclide ventriculography, and recently magnetic resonance imaging (MRI).

Echocardiography as a bedside tool is the work horse of a routine clinical approach to cardiomyopathies. However, the quality of echocardiographic results

[1] Franz-Volhard-Klinik, Charite, Humboldt-University, Berlin, Germany.

depends on the ultrasound window of the patient and the experience of the investigator [5]. Thus, the standard transthoracic approach may suffer from a significant interstudy and intraobserver variability, which limits its usefulness to accurately visualize cardiomyopathic features and observe changes during follow-up [18, 35, 57]. In this review we will discuss the value of MRI as a diagnostic tool for cardiomyopathies.

In a diagnostic approach to cardiomyopathy MRI can be used to evaluate morphological, functional parameters and to measure flow velocities [3, 18, 36]. MRI visualizes left and right ventricular morphology and function with a high degree of accuracy and reproducibility [2, 37].

Published guidelines such as those of the Task Force of the European Society of Cardiology and the Association of European Pediatric Cardiologists, recommend the use of MRI as an alternative in hypertrophic and restrictive cardiomyopathy. Concerning dilated cardiomyopathy, other imaging techniques are accepted as usually adequate. The application of MRI in the diagnosis of arrhythmogenic right ventricular dysplasia is described as investigational [32].

Thus MRI is accepted to be applicable in all forms of cardiomyopathies, but not clearly advantageous when compared to other techniques. However, in the future the advantage of MRI over echocardiography to more precisely measure functional parameters may become very important as patients need precise measurements during pharmacological interventions [33], where subtle changes may have an important impact on therapeutical decision-making. Furthermore, MRI may detect or exclude early changes in members of families with inherited forms of cardiomyopathies, including frequent forms of hypertrophic cardiomyopathy [51], dilated cardiomyopathy [42] and arrhythmogenic right ventricular cardiomyopathy [11, 60]. Moreover, the statistically adequate sample size of clinical studies could be markedly reduced by the choice of methods with a small inter- and intraobserver variability [6, 12, 18, 50].

Metabolic alterations frequently occur in cardiomyopathy and can be assessed by the use of MR spectroscopy. Clinical results have been reported for ^{31}P-MR of dilated cardiomyopathy [31] and hypertrophic cardiomyopathy [20] This approach is not yet used in a routine clinical setting, because it is time-consuming and needs a lot of expertise. However, this may change in the future, when the clinical impact is further elucidated.

The ability of MRI to obtain information about myocardial tissue changes is currently being investigated. T1-weighted, black-blood spin echo sequences visualize the myocardium with a high contrast to adjacent structures such as epicardial fat and intracavital blood. The application of gadolinium may be helpful to identify inflammatory and infiltrative processes. T2-weighted spin-echo sequences are suitable to detect fluid accumulation such as myocardial edema or pericardial effusion. It is to be expected that this unique capability of MRI will further increase its importance for the understanding and clinical assessment of cardiomyopathies and underlying processes.

The main advantages of MRI are the lack of ionizing radiation and its non-invasiveness. The rapid development of cardiovascular MR techniques will further expand the spectrum of suitable applications and thus make frequent updates of indication lists necessary.

Hypertrophic Cardiomyopathy

Hypertrophic cardiomyopathy is characterized by an inappropriate myocardial hypertrophy with a diminished diastolic function. The obstructive forms feature an additional narrowing of the left ventricular outflow tract (LVOT). Echocardiography with the use of Doppler and two-dimensional (2-D) imaging is established as the method of choice for the clinical diagnosis of hypertrophic cardiomyopathy. Its characterization depends on an accurate display of the morphological and functional changes [17, 19, 44]. For MRI studies of left ventricular volume and mass gradient echo sequences are applied. Breathhold sequences in a short-axis orientation from the mitral valve to the apex are suitable for an accurate assessment of locally hypertrophied myocardium. The quantification of left ventricular mass is more reliable than 2-D-echo which uses geometric assumptions [3, 28].

Apical hypertrophic cardiomyopathy may be very difficult to assess by echocardiography [37, 44, 54]. In contrast, of MRI exactly depicts the morphological pattern in very early stages of apical [54] or other localized forms of hypertrophy [40, 41].

Using cine gradient-echo imaging and velocity mapping, functional measurements, including estimation of the outflow tract gradient, are possible. However, the reliability of MRI measurements is not superior to echocardiography [1, 19, 30, 59]. MRI planimetry of the transplanar flow in the outflow tract may serve as an alternative to assess the degree of obstruction, thereby overcoming the problem of a low reproducibility of an echocardiographic determination of pressure gradients [22, 45] (Figure 1).

Using tagging techniques it is possible to quantify small changes in regional wall motion [52], and also to reveale specific functional differences to patients with other causes of hypertrophy and healthy subjects [24, 53]. Metabolic changes of the myocardium in hypertrophic cardiomyopathy can already be detected by ^{31}P-NMR spectroscopy in asymptomatic patients [20].

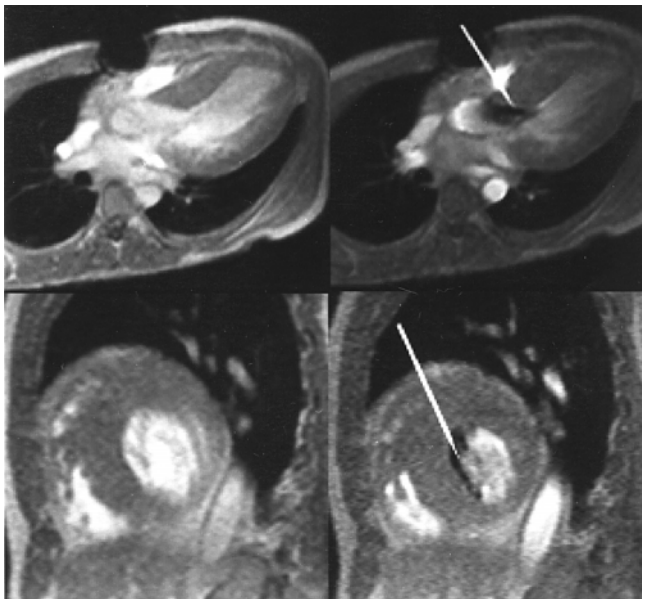

Figure 1
Hypertrophic obstructive cardiomyopathy with a history of myectomy 10 years ago. Diastolic (left) and systolic (right) gradient echo images in the 4-chamber view, long axis view (upper panel) and short axis (lower panel). The systolic signal void in the left ventricular outflow tract is due to turbulent flow within the obstructed outflow tract.

Abbildung 1
Hypertrophische obstruktive Kardiomyopathie, Zustand nach Myektomie vor zehn Jahren. Diastolische (links) und systolische (rechts) Gradienten-Echo-Sequenz). Vier-Kammer-Blick lange Achse (obere Abbildung) und kurze Achse (untere Abbildung). Die Signalauslöschung im systolischen Bild widerspiegelt den turbulenten Fluss im linksventrikulären Ausflusstrakt, der durch die Obstruktion induziert wird.

Studies on the prognostic relevance of these findings are not yet available.

MRI may reveal specific signal patterns in different forms of left ventricular hypertrophy [9, 55]. Myocardial ischemia and reduced coronary vasodilator reserve as estimated by invasive procedures or PET are frequent findings in hypertrophic cardiomyopathy and seem be of prognostic value for these patients. Assessment of myocardial blood flow is also possible using velocity-encoded cine MR without breathhold in healthy subjects was successfully applied [56], and this technique has recently been applied for evaluating coronary blood flow and coronary flow reserve in patients with hypertrophic cardiomyopathy [21]. Therefore, MR techniques open new roads in the evaluation of hypertrophied myocardium.

Dilated Cardiomyopathy

Functional and anatomical changes in patients with dilated cardiomyopathy are easily quantified using MRI. In general, echocardiography provides basic information of left ventricular changes. However, MRI may serve as a valuable alternative in the diagnostic work-up of patients with limited ultrasound conditions and when data on the right ventricular morphology and function are requested [8, 43]. Furthermore, MRI provides a more accurate detection of endocardial border resulting in a very low variability of functional measurements [48] (Figures 2a and 2b). Thus, MRI may be preferable in the follow-up during medical therapy [8, 12].

Pilot studies revealed that MRI may be able to differentiate between acute and chronic alterations of the myocardium, e. g. in acute myocarditis [14, 15] which may lead to the clinical pattern of dilated cardiomyopathy. Contrast-enhanced T1-weighted MRI may visualize reversible myocardial changes in acute myocarditis [15]. During follow-up there is a correlation between ongoing symptoms related to myocarditis and MRI findings [13]. Although contrast-enhanced MRI may be more sensitive for detecting subtle myocardial changes associated with acute myocarditis, edema associated with acute inflammation may also be detected using T2-weighted spin-echo sequences [14, 16] (Figures 3a and 3b)

Changes of high-energy phosphate metabolism as demonstrated by MRI were shown to have a prognostic impact in patients with dilated cardiomyopathy [31].

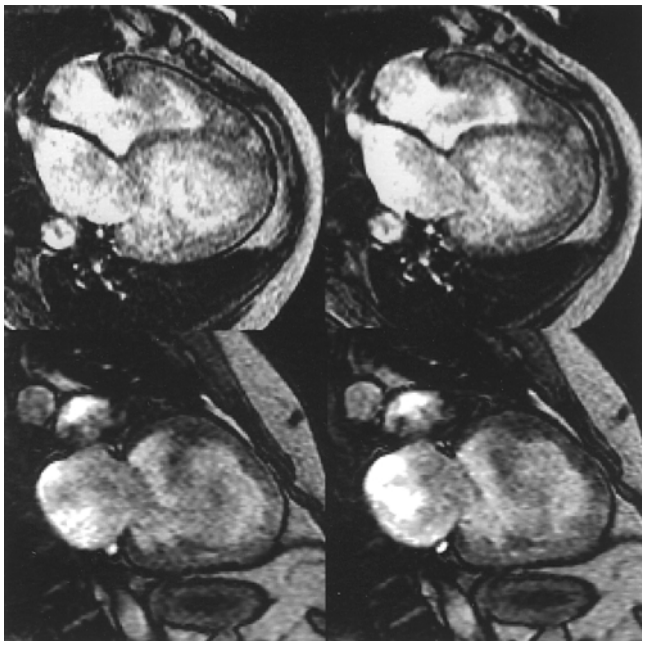

Figure 2a – Abbildung 2a

Figures 2a and 2b
a) Dilative cardiomyopathy. Diastolic (left) and systolic (right) gradient-echo images in the long axis orientation. Upper panel: 4-chamber- view. Lower panel: 2-chamber view. A biplanar volumetry resulted in a left ventricular ejection fraction as low as 20%. b) short axis view as contiguous slice set of a short axis view from base to apex used for the detection of small changes.

Abbildungen 2a und 2b
a) Dilatative Kardiomyopathie. Diastolische Bilder (links) und systolische Bilder (rechts) (Gradientenechosequenzen) in den langen Achsen. Obere Abbildung: Vier-Kammer-Blick. Untere Abbildung: Zwei-Kammer-Blick. Die biplane Volumetrie ergab eine links-ventrikuläre Ejektionsfraktion unter 20%. b) Kurzachsenschnitte durch den gesamten linken Ventrikel zur Erfassung geringer Veränderungen nachweisbar.

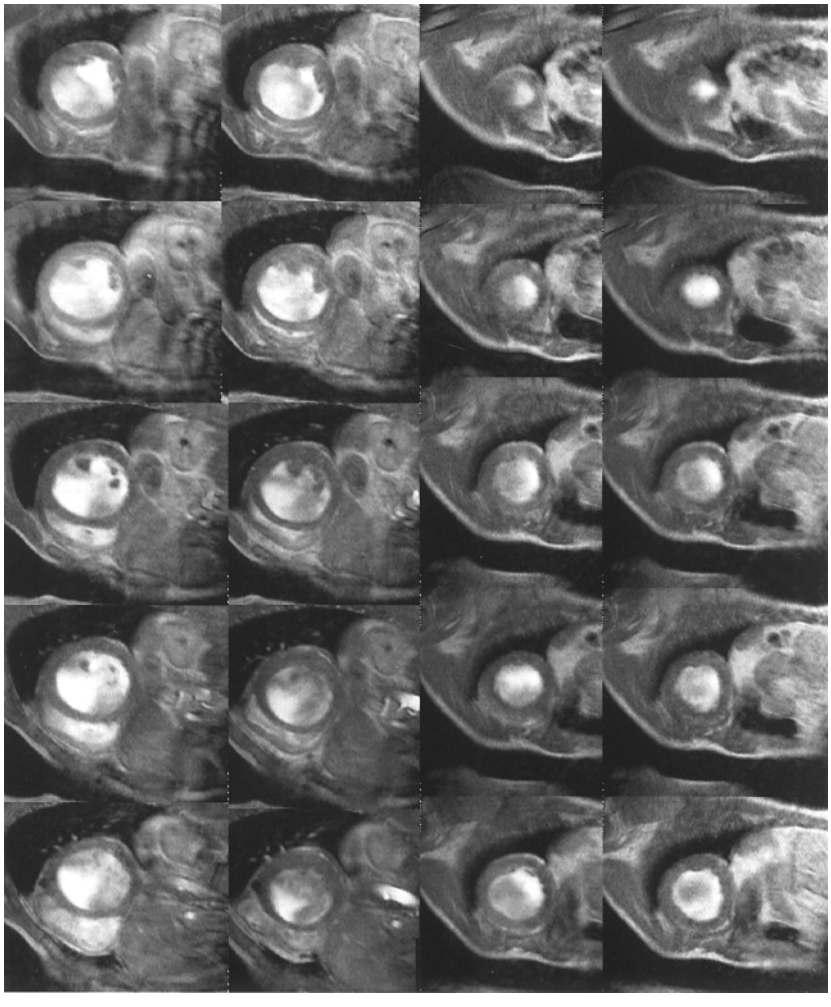

Figure 2b – Abbildung 2b

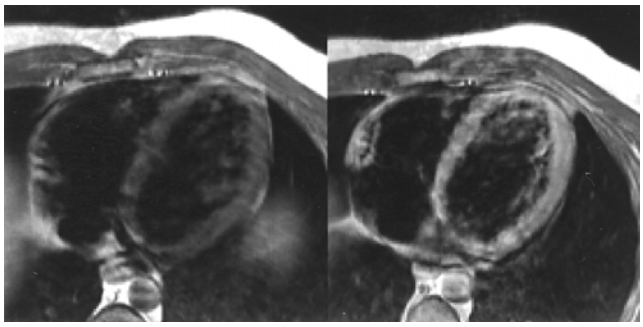

Figure 3a
Myocarditis:32-year-old patient with acute precordial discomfort, ECG-changes, positive creatine kinase, history of respiratory infection a week ago and invasive exclusion of coronary artery disease. Axial T1-weighted spin-echo images before (right) and after (left) application of contrast medium (Gd-DTPA). There is an increased myocardial contrast enhancement.

Abbildung 3a
Myokarditis: 32-jähriger Patient mit akuten thorakalen Beschwerden, EKG-Veränderungen, erhöhter CK, einem Atemwegsinfekt vor einer Woche und nachgewiesenen unauffälligen Koronararterien. Axiale T1-gewichtete Spin-Eecho-Sequenzen vor (rechts) und nach (links) Applikation von Kontrastmittel (Gd-DTPA). Erhöhte myokardiale Kontrastmittelanreicherung.

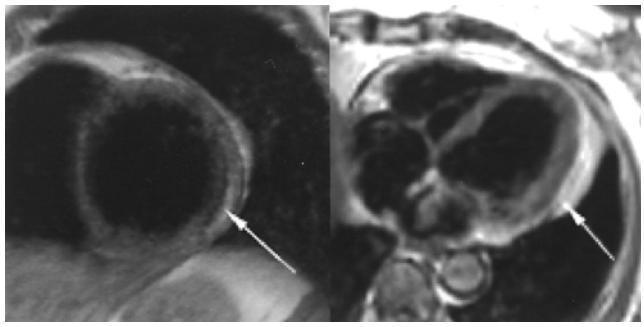

Figure 4
Pericarditis constrictiva: T1-weighted spin-echo sequences in a short axis view (left) and axial (right) showing thickenend pericardium (arrows).

Abbildung 4
Pericarditis constrictiva: T1-gewichtete Spin-Echo-Sequenzen in kurzer Achse (links) und axial (rechts) mit Darstellung des verdickten Perikards (Pfeile).

Figure 3b
Myocarditis in systemic lupus erythematodes (sLE): 25year-old patient with known sLE, precordial discomfort-short axis: T2- weighted (STIR) spin-echo images (left) visualising a little pericardial effusion (bright signal) and a myocardial edema was detectable. T1-weighted spin-echo images before (middle) and after (left) application of contrast medium (Gd-DTPA). There is an increased relative enhancement of the myocardium demonstrable.

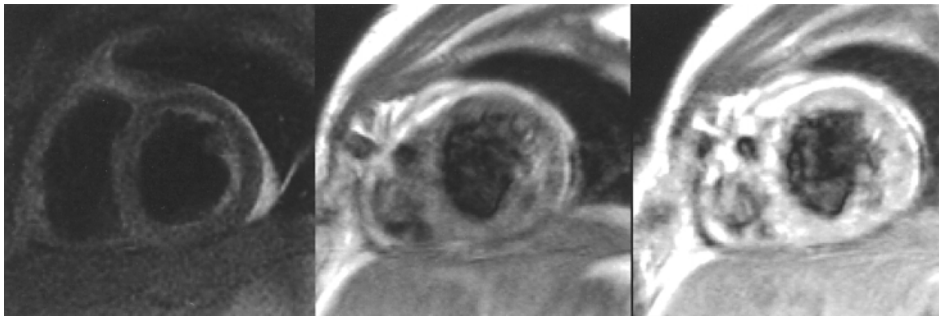

Abbildung 3b
Myokarditis bei systemischem Lupus erythematodes: 25-jähriger Patient mit gesichertem systemischem Lupus erythematodes (sLE). Kurze Achsen: Die T2-gewichteten Spinechosequenzen (links) zeigen einen kleinen Perikarderguss (helles Signal), und es war ein myokardiales Ödem nachweisbar. T1-gewichtete Spin-Echo-Bilder vor (mittleres Bild) und nach (rechts) Gabe von Kontrastmittel (Gd-DTPA). Ein erhöhtes relatives Enhancement war nachweisbar.

In conclusion, MRI may contribute significantly to the scientific assessment and the clinical care of patients with dilated cardiomyopathy.

Restrictive Cardiomyopathy

Restrictive cardiomyopathy is a rare condition. The main diagnostic challenge is to differentiate the disease from constrictive pericarditis. MRI is able to detect functional changes associated with constrictive pericarditis. Moreover, it can be especially useful to detect pericardial thickening (above 4 mm) as the typical feature of constrictive pericarditis [27, 29, 46] (Figure 4). The sensitivity and specificity of MRI using spin echo techniques were found to be as high as 88% and 100%, respectively, with a diagnostic accuracy of 93% [25].

Arrhythmogenic Right Ventricular Cardiomyopathy

One of the accepted major criteria of arrhythmogenic right ventricular cardiomyopathy is fibrofatty replacement of myocardium as found in biopsy specimens [26]. This phenomenon, as well as regional wall thinning can be visualized by T1-weighted spin-echo tech-

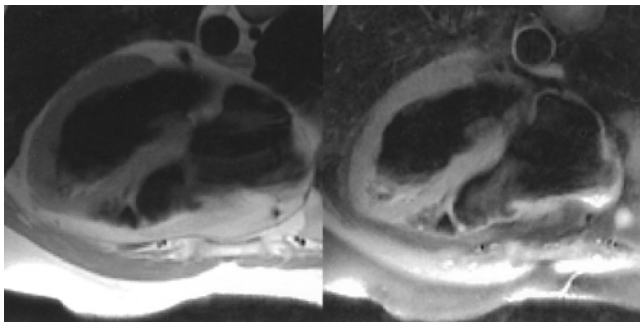

Figure 5
Arrhythmogenic right ventricular cardiomyopathy. Axial T1-weighted images without (right) and with (left) fat saturation in a 50-year-old patient with electrocardiographic features suggestive for ARVC and frequent ventricular extrasystoles and invasive exclusion of coronary artery disease. Fatty replacement of the myocardium leading to a bright signal (left), which is suppressed in a fat-saturated image (right). A regional dyskinesia was detected in gradient-echo images (not shown).

Abbildung 5
Arrhythmogene rechtsventrikuläre Dysplasie. Axiale T1-gewichtete Bilder mit (rechts) und ohne (links) Fettsättigung bei einem 50-jährigen Patienten mit elektrokardiographischen Hinweisen für eine ARVC, gehäuften ventrikulären Extrasystolen und invasiv ausgeschlossener koronarer Herzkrankheit. Fettige Degeneration des Myokards, erkennbar an einem hellen Signal, welches in den fettgesättigten Bildern (rechts) unterdrückt ist. In diesem Bereich war eine Dyskinesie nachweisbar (nicht abgebildet).

niques, although these MRI findings are not yet accepted formally as diagnostic criteria (Figure 5). Recent reviews indicate that MRI may become an importa nt tool to diagnose the disease [11, 60]. Typical functional disturbances, such as global and/or regional dysfunction, and morphological features such as global or segmental dilation, localized aneurysms (akinetic or dyskinetic areas with diastolic bulging) are accurately detected by MRI [59] and accepted additional features for the diagnosis of arrhythmogenic right ventricular cardiomyopathy (generally in combination with ECG abnormalities) [26].

Secondary Forms – Infiltrative and Inflammatory Disease

Systemic diseases may be complicated by myocardial involvement leading to impairment of ventricular function. Typical so-called "infiltrative cardiomyopathies" include sarcoidosis, amyloidosis, and hemochromatosis. The incidence of myocardial involvement in systemic sarcoidosis is about 20 to 30% [10] with a substantial risk of subsequent death [39]. The sarcoid lesions can be visualized using T2-weighted and/or contrast-enhanced

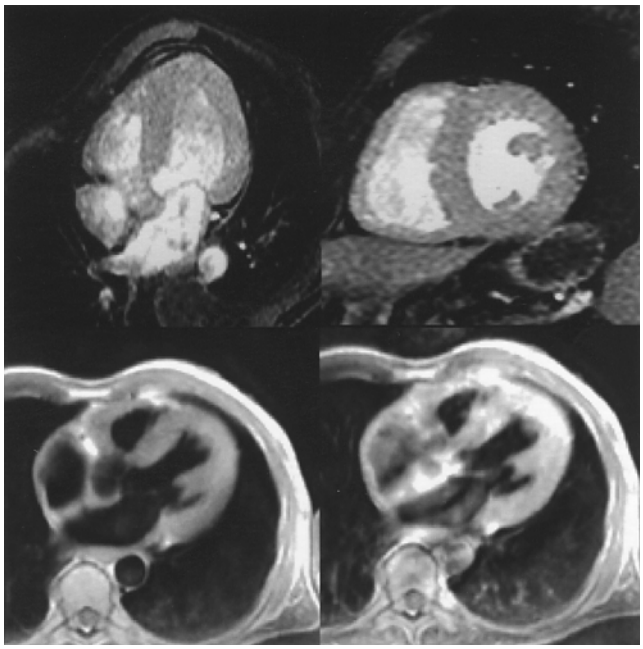

Figure 6
Infiltrative cardiomyopathy caused by amyloidosis. Upper panel: Thickened wall gradient-echo images in a 4-chamber view (left panel) and in a short axis view. Lower panel: Axial T1-weighted spin-echo images before (left) and after (right) application of Gd-DTPA with an increased contrast media accumulation in the myocardium.

Abbildung 6
Infiltrative Kardiomyopathie – Amyloidose. Oben: Darstellung der linksventrikulären Hypertrophie (rechts im Vier-Kammer-Blick, links in der kurzen Achse) – Gradientenechosequenzen. Unten: T1-gewichtete Spin-Echo-Sequenzen vor (links) und nach (rechts) Applikation von Gd-DTPA mit global vermehrter Kontrastmittelaufnahme.

T1 spin-echo sequences in muscular sarcoidosis [34] and in the brain [47]. There are some reports on patients with similar findings in the myocardium [4, 7]. This may be useful to guide biopsy and valuable for monitoring the patient during therapy.

Infiltration of the heart by amyloidosis may lead to a loss of atrial and/or left ventricular function and subsequent congestive left heart failure [23]. Changes of the signal intensity after application of Gd-DTPA may discriminate myocardial amyloidosis from simple hypertrophy [9] (Figure 6).

Cardiac hemochromatosis is not very common, but may lead to a significant loss of contractile function. The characteristic iron deposits lead to a signal drop in spin-echo studies due to the paramagnetic properties of iron, a well known phenomenon in body MRI

[49, 58]. However, these MRI signal intensity changes may – with the exception of hemosiderosis – be not very specific for the disease, and the diagnosis of cardiac hemochromatosis should currently not solely be based on MR findings.

When and Why – Making an Attempt to Summarize

The diagnosis of cardiomyopathy can comprehensively be established in virtually all the patients by a single MRI study. In follow-up investigations even small changes in myocardial function, mass and morphology are detectable, thereby reducing the sample size and duration of clinical trials and furthermore improving the safety of patients undergoing therapeutic interventions.

At time of writing this, the main clinical application of MRI is in patients who are suspected to having a cardiomyopathy but cannot be adequately evaluated by echocardiography due to impaired ultrasound windows. The higher accuracy of MRI is helpful during pharmaceutical interventions and in clinical trials on cardiomyopathy. Furthermore, MRI may be valuable for the detection of early changes in asymptomatic members of families with a patient suffering from cardiomyopathy.

Further scientific work will need to exploit the potential of MRI to investigate ischemic, toxic or inflammatory injuries of the myocardium as well as involvement in systemic diseases.

MRI will serve not only as in-vivo gold standard in diagnosis of cardiomyopathies but also as the tool of choice in their investigation leading to better understanding of myocardial disease.

References

1. Arrive L, Assayag P, Russ G, et al. MRI and cine MRI of asymmetric septal hypertrophic cardiomyopathy. J Comput Assist Tomogr 1994;18:376–82.
2. Benjelloun H, Cranney G, Kirk K, et al. Interstudy reproducibilty of biplane cine nuclear magnetic resonance measurements of left ventricular function. Am J Cardiol 1991;67:1413–20.
3. Bottini P, Carr A, Prisant L, et al. Magnetic resosance imaging compared to echocardiography to assess left ventricular mass in the hypertensive patient. Am J Hypertens 1995;8:221–8.
4. Chandra M, Silvermann M, Oshinski J, et al. Diagnosis of cardiac sarcoidosis aided by MRI. Chest 1996;110:562–5.
5. Cheitlin M. ACC/AHA guidelines for the clinical application of echocardiography. Circulation 1997;95:1686–744.
6. Devlin AM, Moore NR, Ostman-Smith I. A comparison of MRI and echocardiography in hypertrophic cardiomyopathy. Br J Radiol 1999;72:258–64.
7. Doherty M, Kumar S, Nicholson A, et al. Cardiac sarcoidosis: the value of magnetic resonance imaging in diagnosis and assessment of response to treatment. Respir Med 1998;92:697–9.
8. Doherty NE, Fujita N, Caputo GR, et al. Measurement of right ventricular mass in normal and dilated cardiomyopathic ventricles using cine magnetic resonance imaging. Am J Cardiol 1992;69: 1223–8.
9. Fattori R, Rocchi G, Celletti F, et al. Contribution of magnetic resonance imaging in the differential diagnosis of cardiac amyloidosis and symmetric hypertrophic cardiomyopathy. Am Heart J 1998; 136:824–30.
10. Flora G, Sharma O. Myocardial sarcoidosis: a review. Sarcoidosis 1989;6:97–106.
11. Fontaine G, Fontaliran F, Hebert JL, et al. Arrhythmogenic right ventricular dysplasia. Annu Rev Med 1999;50:17–35.
12. Friedrich M, Strohm O, Osterziel K, et al. Growth hormone therapy in dilated cardiomyopathy monitored with MRI. MAGMA 1998;6:152–4.
13. Friedrich M, Strohm O, Schulz-Menger J, Marciniak H, Luft F, Dietz R. Noninvasive diagnosis of acute myocarditis by contrast enhanced magnetic resonance imaging. Proc ISMRM 6th Annual Meeting, Sydney, 1998:912.
14. Friedrich M, Strohm O, Schulz-Menger J, et al. Response to the author. Circulation 1999;99:458–9.
15. Friedrich MG, Strohm O, Schulz Menger J, et al. Contrast media-enhanced magnetic resonance imaging visualizes myocardial changes in the course of viral myocarditis. Circulation 1998;97:1802–9.
16. Gagliardi M, Poletta B, Di Renzi P. MRI for the diagnosis and follow up of myocarditis (letter). Circulation 1999;99:458–9.
17. Gardin J, Dabestani A, Glasgow G, et al. Echocardiographic and Doppler flow observations in obstructed and non-obstructed hypertrophic cardiomyopathy. Am J Cardiol 1985;56:614–21.
18. Germain P, Roul G, Kastler B, et al. Inter-study variability in left ventricular mass measurement. Comparison between M-mode echocardiography and MRI. Eur Heart J 1992;13:1011–9.
19. Higgins C, Byrd B, Stark D. Magnetic resonance imaging of hypertrophic cardiomyopathy. Am J Cardiol 1985;1985:1121–6.
20. Jung W, Sieverding L, Breuer J, et al. 31P NMR spectroscopy detects metabolic abnormalities in asymptomatic patients with hypertrophic cardiomyopathy. Circulation 1998;97:2536–42.
21. Kawada N, Sakuma H, Yamakado T, et al. Hypertrophic cardiomyopathy: MR measurement of coronary blood flow and vasodilator flow reserve in patients and healthy subjects. Radiology 1999;211:129–35.
22. Kizilbash AM, Heinle SK, Grayburn PA. Spontaneous variability of left ventricular outflow tract gradient in hypertrophic obstructive cardiomyopathy. Circulation 1998;97:461–6.
23. Kyle R, Spittell P, Gertz M, et al. The premortem recognition of systemic senile amyloidosis with cardiac involvement. Am J Med 1996;101:395–400.
24. Maier S, Fischer S, McKinnon G, et al. Evaluation of left ventricular segmental wall motion in hypertrophic cardiomyopathy with myocardial tagging. Circulation 1992;86:1919–28.
25. Masui T, Finck S, Higgings C. Constrictive pericarditis and restrictive cardiomyopathy: evaluation with magnetic resonance imaging. Radiology 1992;182:369–72.
26. McKenna WJ, Thiene G, Nava A, et al. Diagnosis of arrhythmogenic right ventricular dysplasia/cardiomyopathy. Task Force of the Working Group Myocardial and Pericardial Disease of the European Society of Cardiology and of the Scientific Council on Cardiomyopathies of the International Society and Federation of Cardiology. Br Heart J 1994;71:215–8.
27. Mehta A, Mehta M, Jain A. Constrictive pericarditis. Clin Cardiol 1999;22:334–44.

28. Missouris CG, Forbat SM, Singer DR, et al. Echocardiography overestimates left ventricular mass: a comparative study with magnetic resonance imaging in patients with hypertension. J Hypertens 1996;14:1005–10.
29. Myers BH, Spodick DH. Constrictive pericarditis: Clinical and pathophysiologic characteristics. Am Heart J 1999;138:219–32.
30. Nakatani S, White RD, Powell KA, et al. Dynamic magnetic resonance imaging assessment of the effect of ventricular wall curvature on regional function in hypertrophic cardiomyopathy. Am J Cardiol 1996;77:618–22.
31. Neubauer S, Horn M, Cramer M, et al. Myocardial phosphocreatine-to-ATP ratio is a predictor of mortality in patients with dilated cardiomyopathy. Circulation 1997;96:2190–6.
32. Neubauer S, Revel D, de Roos A, et al. The clinical role of magnetic resonance in cardiovascular disease - Task force of the European Society of Cardiology, in Collaboration with the Association of European Paediatric Cardiologists. Eur Heart J 1198,19:19–39
33. Osterziel K, Strohm O, Schuler J, et al. Randomised, double-blind, placebo-controlled trial ofhuman recombinant growth hormone inpatients with chronic heart failure due to dilated cardiomyopathy. Lancet 1998;351:1233–7.
34. Otake S, Banno T, Ohba S, et al. Muscular sarcoidosis: findings at MR-imaging. Radiology 1990;176:1227–33.
35. Otterstad J, Froeland E, Jon Sutton M, et al. Accuracy and reproducibility of biplane two-dimensional echocardiographic measurements of left ventricular dimensions and function [see comments]. Eur Heart J 1997;18:507–13.
36. Park JH, Kim YM. MR imaging of cardiomyopathy. Magn Reson Imag Clin N Am 1996;4:269–86.
37. Park JH, Kim YM, Chung JW, Park YB, Han JK, Han MC. MR imaging of hypertrophic cardiomyopathy. Radiology 1992;185:441–6.
38. Pattynama P, Lamb H, van der Velde E, et al. Reproducibility of MRI-derived measurements of right ventricular volumes and myocardial mass. Magn Reson Imag 1995;13:53–63.
39. Perry A, Vuitch F. Causes of death in patients with sarcoidosis. A morphological study of 38 autopsies with clinicopathological correlations. Arch Pathol Lab Med 1996;119:167–72.
40. Pons Llado G, Carreras F, Borras X, et al. Comparison of morphologic assessment of hypertrophic cardiomyopathy by magnetic resonance versus echocardiographic imaging. Am J Cardiol 1997;79:1651–6.
41. Posma JL, Blanksma PK, van der Wall EE, et al. Assessment of quantitative hypertrophy scores in hypertrophic cardiomyopathy: magnetic resonance imaging versus echocardiography. Am Heart J 1996;132:1020–7.
42. Richardson P, McKenna W. Report of the 1995 World Health Organization/International Society and Federation of Cardiology Task Force on the Definition and Classification of Cardiomyopathies. Circulation 1996;93:841–2.
43. Rominger MB, Bachmann GF, Geuer M, et al. [Comparison of left and right ventricular ejection and filling parameters of the heart using cine-MRI with breath holding technique. Clinical study of 42 patients with cardiomyopathy and coronary heart disease]. Fortschr Geb Rontgenstr Neuen Bildgeb Verfahr 1999;170:534–41.
44. Sardanelli F, Molinari G, Petillo A, et al. MRI in hypertrophic cardiomyopathy: a morphofunctional study. J Comput Assist Tomogr 1993;17:862–72.
45. Schulz-Menger J, Strohm O, Waigand J, et al. Magnetic resonance imaging accurately detects delayed improvement in left ventricular outflow tract following septal artery embolisation in hypertrophic obtructive cardiomyopathy. Circulation 1997;96:1054.abstract.
46. Sechtem U, Tscholakoff D, Higgings C. MRI of the abnormal pericardium. Am J Roentgenol 1986;147:239–44.
47. Seltzer S, Mark A, Atlas S. CNS-sarcoidosis: evaluation with contrast-enhanced MR imaging. AJNR 1991;12:1227–33.
48. Semelka R, Tomei E, Wagner S. Interstudy reproducibility of dimensional and functional measurements between cine magnetic resonance studies in the morphological abnormal left ventricle. Am Heart J 1990;1990:1367–73.
49. Siegelmann E, Mitchell D, Semelka R. Abdominal iron deposition: metabolism, MR findings, and clinical importance. Radiology 1997;199:13–22.
50. Soler R, Rodriguez E, Marini M. Left ventricular mass in hypertrophic cardiomyopathy: assessment by three-dimensional and geometric MR methods. J Comput Assist Tomogr 1999;23:577–82.
51. Spirito P, Seidman CE, McKenna WJ, et al. The management of hypertrophic cardiomyopathy [see comments]. N Engl J Med 1997; 336:775–85.
52. Stuber M, Nagel E, Fischer SE, et al. Quantification of the local heartwall motion by magnetic resonance myocardial tagging. Comput Med Imag Graph 1998;22:217–28.
53. Stuber M, Scheidegger M, Fischer S, et al. Alteration in the local myocardial motion pattern in patients suffering from pressure overload due to aortic stenosis. Circulation 2000;101:1764–6.
54. Suzuki J, Shimamato R, Nishikawa J, et al. Morphological onset and early diagnosis in apical hypertrophic cardiomyopathy: a long term analysis with nuclear magnetic resonance imaging. J Am Coll Cardiol 1999;33:146–51.
55. Tsukihashi H, Ishibashi Y, Shimada T, et al. [Changes in gadolinium-DTPA enhanced magnetic resonance signal intensity ratio in hypertrophic cardiomyopathy]. J Cardiol 1994;24:185–91.
56. van Rossum A, Visser F, Hofman M, et al. Global left ventricular perfusion: noninvasive measurement with cine MR imaging and phase velocity mapping of coronary venous outflow. Radiology 1992;182:685–91.
57. van Royen N, Jaffe C, Krumholz H, et al. Comparison and reproducibility of visual echocardiographic and quantitative radionuclide imaging for measuring left ventricular ejection fraction . Am J Cardiol 1996;77:843–50.
58. Waxmann S, Eustace S, Haernell G. Myocardial involvment in primary hemochromatosis demonstrated by magnetic resonance imaging. Am Heart J 1994;128:1047–9.
59. White RD, Obuchowski NA, Gunawardena S, et al. Left ventricular outflow tract obstruction in hypertrophic cardiomyopathy: presurgical and postsurgical evaluation by computed tomography magnetic resonance imaging. Am J Card Imag 1996;10:1–13.
60. Wichter T, Borggrefe M, Breithardt G. [Arrhythmogenic right ventricular cardiomyopathy. Etiology, diagnosis and therapy]. Med Klin 1998;93:268–77.

Address for Correspondence:
Dr. Jeanette Schulz-Menger, Franz-Volhard-Klinik, Charité,
Humboldt-Universität, Wiltbergstraße 50,
D-13125 Berlin, Germany,
Phone (+49/30) 9417-2593, Fax -2560,
e-mail: schulzmenger@fvk-berlin.de

J. Schulz-Menger

Kardiomyopathien und Magnetresonanztomographie

Cardiomyopathies and magnetic resonance imaging

Die kardiale Magnetresonanztomographie (MRT) stößt durch ihre Möglichkeit, Gewebe und Funktion zu charakterisieren, zunehmend auf Interesse in der Kardiologie und somit auch bei der Diagnostik der unterschiedlichen Kardiomyopathieformen.

Untersuchungstechniken

Durch die Anwendung unterschiedlicher Techniken können in einem Untersuchungsgang morphologische und funktionelle Veränderungen erfasst, Flussgeschwindigkeiten gemessen und Gefäßdarstellungen durchgeführt werden.

Für eine kardiologische „State of the Art"-Diagnostik sind 1,5 Tesla MRT-Scanner, mit einer entsprechend Aufrüstung notwendig. Eine Untersuchung dauert in Abhängigkeit von der Fragestellung zwischen 30 – 60 Minuten. Neben speziellen Fragestellungen kommt die Methode auch bei eingeschränkten echokardiographischen Untersuchungsbedingungen zum Einsatz.

Zur Beurteilung der kardialen Funktion und Wandbewegungsanalyse werden Gradientenechosequenzen (heute meist als „steady state free precession") eingesetzt. Die freie Schichtwahl ermöglicht die Darstellung auch atypisch gelegener pathologischer Strukturen. Zur genauen Darstellung der Ejektionsfraktion, der Volumina und der Masse sollten dreidimensionale Datensätze angewendet werden, da damit eine erhebliche höhere Messgenauigkeit und Reproduzierbarkeit erreicht wird (3).

Unterschiedliche Sequenzen erlauben es, Myokardveränderungen voneinander zu differenzieren. Als Beispiele seien angeführt: myokardiale Ödeme, Fettinfiltrationen, fibrotische, inflammatorische Prozesse und Perfusionsveränderungen (2, 5).

kurzgefasst: **Die MRT erlaubt durch den Einsatz verschiedener Techniken eine nicht invasive Myokardcharakterisierung ohne Strahlenbelastung.**

Dilatative Kardiomyopathie

Die häufigste Fragestellung bei einer dilatativen Kardiomyopathie (DCM) betrifft die Quantifizierung von Volumina und Masse im Rahmen von Verlaufsbeobachtungen. In klinischen Studien kann die bessere Reproduzierbarkeit zu einer Kostenersparnis führen, da die Gruppengrößen deutlich reduziert werden können (19).

Neue Möglichkeiten eröffnen sich durch den Einsatz der kontrastverstärkten MRT (**Abb. 1**). McCrohon et.al. (11) zeigten, dass bei Patienten mit einer eingeschränkten linksventrikulären Funktion die Darstellung der Lokalisation der Kontrastmittel-Anreicherung zur Differentialdiagnose zwischen ischämischer und dilatativer Kardiomyopathie beitragen kann. Bei zugrunde liegender koronarer Herzkrankheit waren immer subendokardial lokalisierte Kontrastmittelanreicherung nachweisbar .

Eine mögliche Ursache einer DCM ist eine Myokarditis, deren Ätiologie vielschichtig sein kann (z.B. virale Infektionen, toxische Reaktionen, myokardiale Mitbeteiligung bei Systemerkrankungen). Die MRT kann zwar nicht das auslösende Agens diagnostizieren, aber es ist möglich, den Myokardschaden akut und im Verlauf darzustellen, somit könnte man nach weiterer Validierung der Methode den Krankheitsverlauf nicht invasiv dokumentieren (**Abb. 2**).

Myokardiale Ödeme konnten im Verlauf über 2 – 4 Wochen nach Krankheitsbeginn nachgewiesen werden (7). Die vermehrte kapilläre Permeabilität und die verstärkte Durchblutung bei Inflammation führen zu einer veränderten Kontrastmittelauswaschung. Mittels kontrastverstärkter T_1-gewichteter Techniken kann die Kontrastmittelanreicherung (Enhancement) dargestellt werden. Wenn auch unterschiedliche Ansätze der kontrastverstärkten MRT verwendet wurden, gelang es mehreren Arbeitsgruppen, inflammatorische Prozesse zu verschiedenen Zeitpunkten nach Beginn der Erkrankung darzustellen (6). Mahrholdt et al. konnten ihre Ergebnisse mittels Biopsie validieren (9).

Institut
Abteilung Kardiologie, Franz Volhard Klinik, Charité Campus Buch, Helios-Klinikum Berlin

Korrespondenz
Dr. Jeanette Schulz-Menger · Franz-Volhard-Klinik · Wiltbergstraße 50 · 13125 Berlin · Tel.: 030/94172593 · Fax: 030/9492560 · E-Mail: schulzmenger@fvk-berlin.de

eingereicht: 7.6.2004 · **akzeptiert:** 21.9.2004

Bibliografie
DOI: 10.1055/s-2004-831862
Dtsch Med Wochenschr 2004; 129: 2183–2186 · © Georg Thieme Verlag Stuttgart · New York · ISSN 0012-0472

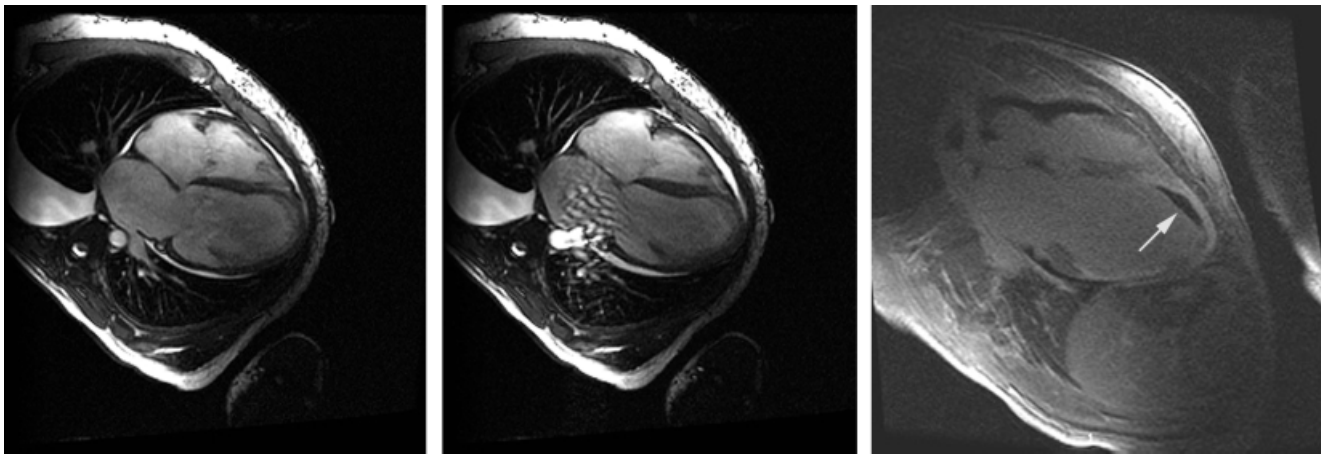

Abb.**1** Frage an das MRT: Hinweis für eine Myokarditis? **Links und Mitte:** Gradientenechosesequenz: links Diastole, Mitte Systole (LVEF 10%), Nebenbefund: Pleura- und Perikarderguss. **Rechts:** Kontrastverstärkte T_1-gewichtete Sequenz: ausgeprägte transmurale Fibrosierung (helles Signal) mit Darstellung eines Thrombus (Signalauslöschung – Pfeil). **MR-Diagnose:** Bild einer schweren ischämisch bedingten Kardiomyopathie.

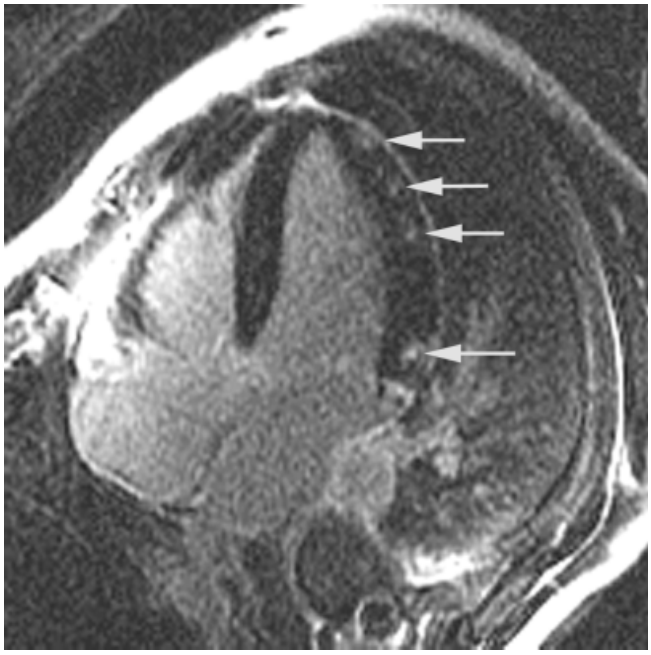

Abb.**2** MR-Bild eines 17-jährigen Patienten mit Infektanamnese, EKG: ST-Strecken-Hebungen in den lateralen EKG-Ableitungen, sowie CK-Erhöhung bei koronarographisch unauffälligen Koronarien. Im MRT Zeichen der Inflammation und darüberhinaus fokale KM-Anreicherungen in den Spätaufnahmen (delayed Enhancement) in der mittleren Myokardschicht (Pfeile) als Hinweis auf Nekrosen.

Auch bei der Darstellung einer myokardialen Beteiligung bei einer Sarkoidose erscheint die kontrastverstärkte MRT vielversprechend, da fokale und/oder globale Kontrastmittelanreicherungen nachweisbar sind (15), die in einer ersten Studie unter Glukokortikoidtherapie (17) rückläufig waren.

kurzgefasst: **Bei der DCM erscheint es möglich, durch den Einsatz kontrastverstärkter Techniken Hinweise auf die Genese der Einschränkung der linksventrikulären Funktion zu erhalten.**

Hypertrophische Kardiomyopathie

Als Screeningmethode wird die Echokardiografie weiterhin im Vordergrund stehen, aber eine genaue Erfassung von atypischen und sehr umschriebenen Hypertrophien ist häufig nur mittels MRT möglich (14). Dies trifft insbesondere auf apikale Hypertrophien zu (20), bei denen Veränderungen der Hypertrophielokalisation im Verlauf gezeigt werden konnten (**Abb.3**).

Der turbulente Fluss im Bereich von Obstruktionen führt zu Signalauslöschungen, die eine Lokalisation der Obstruktion ermöglichen. Eine Alternative zur Quantifizierung der sehr variablen Obstruktion des linksventrikulären Ausflusstraktes bietet die MRT durch die Planimetrie der hämodynamisch relevanten kleinsten systolischen Fläche. Kontrastverstärkte Techniken werden zur Darstellung des therapeutisch induzierten Infarktes nach Septumablation genutzt (16) (**Abb.4**).

Dagegen scheinen fokale Kontrastmittelanreicherungen ohne vorangegangene Intervention eine Gruppe von Patienten mit höherem Risiko zu charakterisieren (13). Dies betrifft sowohl die Ausprägung einer späteren systolischen Herzinsuffizienz, als auch das Risiko einen plötzlichen Herztod zu erleiden. Diese Daten müssen allerdings noch in prospektiven Studien validiert werden (13).

kurzgefasst: **Bei der hypertrophen Kardiomyopathie können auch atypisch lokalisierte Myokardverdickungen dargestellt werden. Die Darstellung von Gewebeveränderungen ermöglicht vielleicht in naher Zukunft, zur Risikostratifizierung beizutragen.**

Arrhythmogene rechtsventrikuläre Kardiomyopathie

Die Diagnose einer arrhythmogenen rechtsventrikulären Kardiomyopathie (ARVC) beruht auf Haupt- und Nebenkriterien (12). Die typischen funktionellen Veränderungen, beispielsweise globale oder regionale Kinetikstörungen der rechtsventrikulären Kinetik, lassen sich ebenso wie morphologische Veränderungen mittels MRT exakt erfassen.

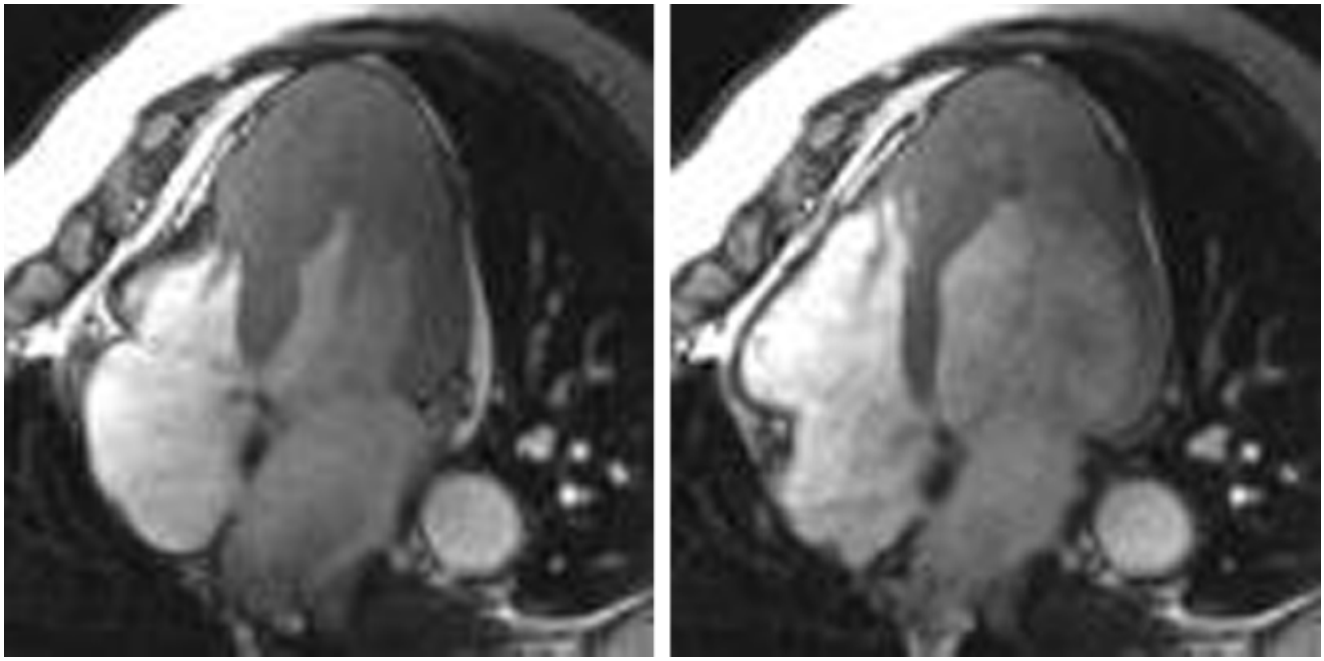

Abb. **3** Gradientenechosequenz bei einem 25-jährigen Patienten mit einer ausgeprägten Form einer apikalen hypertrophischen Kardiomyopathie (HCM).

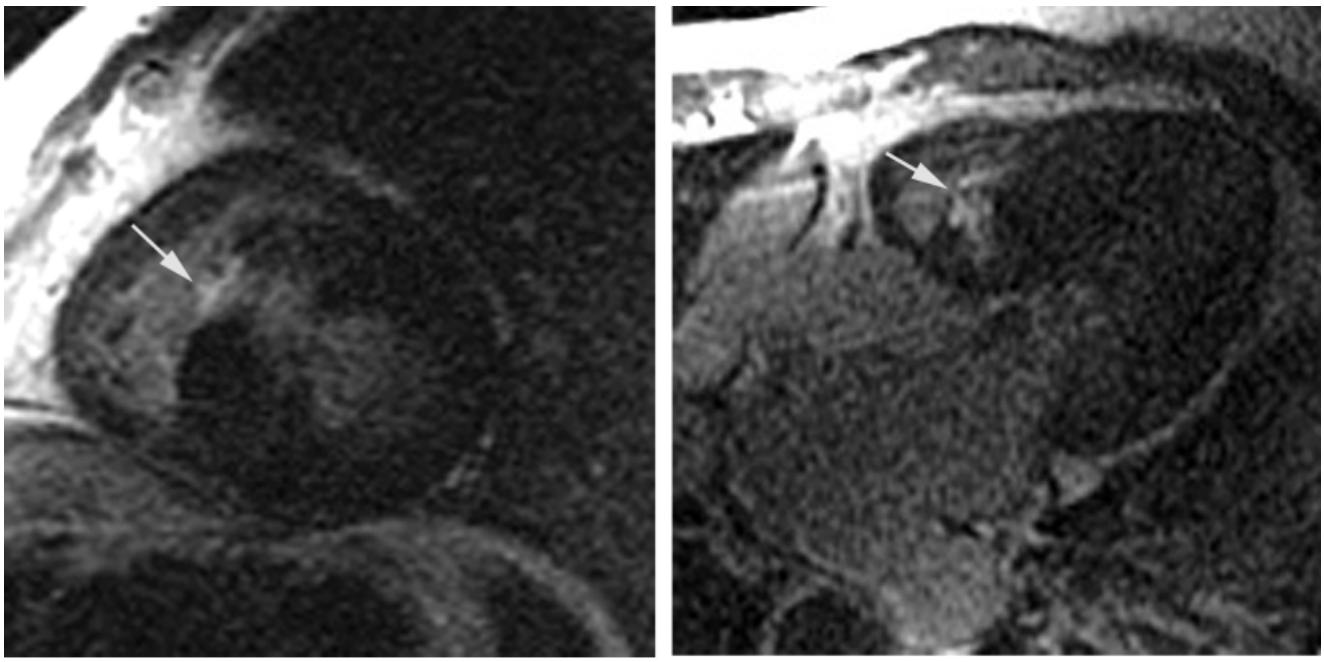

Abb. **4** MRT-Bild eines 41-jährigen Patient 3 Monate nach erfolgreicher Septumarterienembolisation bei hypertrophischer obstruktiver Kardiomyopathie (HOCM). Kontrastverstärkte T_1-gewichtete Sequenz: Das helle Signal (Pfeil) stellt den induzierten Infarkt dar.

Ein anderes Hauptkriterium ist der Ersatz rechtsventrikulärer Myokardanteile durch Fettgewebe. Wenn auch die MR diese Veränderungen unkompliziert mittels T_1-gewichteter Spinecho-Sequenzen darstellen kann, werden diese Gewebeveränderungen gegenwärtig im Rahmen der Kriterien nur als gesichert akzeptiert, wenn sie bioptisch bestätigt wurden. Es gibt erste Hinweise darauf, dass im MRT erfasste morphologische Veränderungen eine prognostische Bedeutung für das Arrhythmie-freie Überleben haben (8). Wenn auch die Darstellung der ARVC zu den bereits lange akzeptierten Indikationen für die Kardio-MRT gehören, gibt es doch eine Reihe unterschiedlicher Protokolle und Interpretationen, die potenziell zu Qualitätsverlusten führen können. Ursächlich ist ein unterschiedlicher Erfahrungsschatz, aber auch das sehr Zeit aufwändige Protokoll.

kurzgefasst: **Die morphologischen Veränderungen bei ARVC sind mittels MRT sehr genau erfassbar, es bedarf aber einer großen Erfahrung bei erheblichem zeitlichen Aufwand.**

Restriktive Kardiomyopathie (Differentialdiagnose konstriktive Perikarditis)

Die isolierte restriktive Kardiomyopathie (RCM) ist sehr selten, ein klassisches Beispiel sind die Speichererkrankungen. Relevant ist die Fragestellung der RCM aber meist in der Differenzialdiagnose zu perikardialen Erkrankungen.

Zum Ausschluss einer relevanten Konstriktion ist die Darstellung eines nicht verdickten Perikards erforderlich. Eine Perikarddicke von mehr als 4mm ist verdächtig (18). Durch nicht invasive Diagnostik kann es gelingen, eine chirurgische Exploration des Perikards zu vermeiden. Es sind allerdings Fälle mit konstriktiver Physiologie ohne Perikardverdickung berichtet worden, bei denen eine ausgeprägte Fibrosierung vorlag (1). Zur hämodynamischen Beurteilung sollte auch eine Gradientenechosequenz im Vierkammerblick hinzugezogen werden (4). So lässt sich die Relaxation des rechten Ventrikels und eine Dilatation der Vorhöfe zumindest qualitativ beurteilen.

Im Fall einer akuten Perikarditis kann ein Perikarderguss dargestellt werden und das Perikard erscheint hyperintens im T_2-gewichteten Bild (18). Eine sichere Darstellung verkalkter Anteile ist allerdings nicht möglich.

In den kürzlich veröffentlichten Guidelines zur Diagnose der Perikarditis wird die kardiale MRT als alternatives Verfahren empfohlen, wenn die konventionelle klinische Diagnostik einschließlich Echokardiografie nicht zu schlüssigen Ergebnissen führt (10).

kurzgefasst: **Im MRT gelingt eine Darstellung auch umschriebener perikardialer Veränderungen, zur sicheren Darstellung von Verkalkungen sollte die Computertomographie hinzugezogen werden.**

Fazit

Durch den Einsatz der MRT kann die kardiale Funktion mit hoher Genauigkeit quantifiziert werden, darüber hinaus sind umschriebene pathologische Veränderungen erfassbar. Dies kann und sollte gezielt für die Diagnose der verschiedenen Kardiomyopathieformen eingesetzt werden. Im Rahmen klinischer Studien können deutliche Reduktionen der Gruppengröße erreicht werden und somit potenzielle therapeutische Ansätze schneller und kosteneffektiver überprüft werden. Ein besonderes Potenzial der Methode besteht in der Möglichkeit der Differenzierung von Myokardschäden und Perikardveränderungen. Kontrastmittelanreicherungen scheinen einen prädiktiven Wert bei einzelnen Erkrankungen zu besitzen, es ist jedoch noch eine Validierung in multizentrischen Studien erforderlich.

In den nächsten Jahren ist aufgrund der rasanten technischen Entwicklungen ein ständiger Informationszuwachs im Verständnis der myo- und perikardialen Erkrankungen zu erwarten.

Danksagung: Ich möchte mich bei Herrn PD Dr. Matthias G. Friedrich und Herrn Dr. Olaf Schulz für die kritische Durchsicht des Manuskripts bedanken.

Autorenerklärung: Die Autorin erklärt, dass sie keine finanziellen Verbindungen mit einer Firma hat, deren Produkt in diesem Artikel eine Rolle spielt (oder mit einer Firma, die ein Konkurrenzprodukt vertreibt).

Literatur

1 Arcasoy SM, Christie JD, Pochettino A et al. Characteristics and outcomes of patients with sarcoidosis listed for lung transplantation. Chest 2001; 120: 873–880
2 Barkhausen J, Ebert W, Debatin JF, Weinmann HJ. Imaging of myocardial infarction: comparison of magnevist and gadophrin-3 in rabbits. J Am Coll Cardiol 2002; 39: 1392–1398
3 Bellenger NG, Davies LC, Francis JM, Coats AJ, Pennell DJ. Reduction in sample size for studies of remodeling in heart failure by the use of cardiovascular magnetic resonance. J Cardiovasc Magn Reson 2000; 2: 271–278
4 Breen JF. Imaging of the pericardium. J Thorac Imaging 2001; 16: 47–54
5 Dymarkowski S, Ni Y, Miao Y, Bogaert J, Rademakers F, Bosmans H, Marchal G. Value of t2-weighted magnetic resonance imaging early after myocardial infarction in dogs: comparison with bis-gadolinium-mesoporphyrin enhanced T1-weighted magnetic resonance imaging and functional data from cine magnetic resonance imaging. Invest Radiol 2002; 37: 77–85
6 Friedrich MG, Strohm O, Schulz Menger J, Marciniak H, Luft FC, Dietz R. Contrast media-enhanced magnetic resonance imaging visualizes myocardial changes in the course of viral myocarditis. Circulation 1998; 97: 1802–1809
7 Gagliardi M, Poletta B, Di Renzi P. MRI for the diagnosis and follow up of myocarditis (letter). Circulation 1999; 99: 458–459
8 Keller DI, Osswald S, Bremerich J et al. Arrhythmogenic right ventricular cardiomyopathy: diagnostic and prognostic value of the cardiac MRI in relation to arrhyzmia-free survival. Int J Cardiovascular Imaging 2003; 19: 537–543
9 Mahrholdt H, Goedecke C, Wagner A et al. Cardiovascular magnetic resonance assessment of human myocarditis: a comparison to histology and molecular pathology. Circulation 2004; 109: 1250–1258
10 Maisch B, Seferovic PM, Ristic AD et al. Guidelines on the diagnosis and management of pericardial diseases executive summary: The Task force on the diagnosis and management of pericardial diseases of the European society of cardiology. Eur Heart J 2004; 25: 587–610
11 McCrohon JA, Moon JC, Prasad SK et al. Differentiation of heart failure related to dilated cardiomyopathy and coronary artery disease using gadolinium-enhanced cardiovascular magnetic resonance. Circulation 2003; 108: 54–59
12 McKenna WJ, Thiene G, Nava A et al. Diagnosis of arrhythmogenic right ventricular dysplasia/cardiomyopathy. Task Force of the Working Group Myocardial and Pericardial Disease of the European Society of Cardiology and of the Scientific Council on Cardiomyopathies of the International Society and Federation of Cardiology. Br Heart J 1994; 71: 215–218
13 Moon JC, McKenna WJ, McCrohon JA et al. Toward clinical risk assessment in hypertrophic cardiomyopathy with gadolinium cardiovascular magnetic resonance. J Am Coll Cardiol 2003; 41: 1561–1567
14 Pons Llado G, Carreras F, Borras X, Palmer J, Llauger J, Bayes de Luna A. Comparison of morphologic assessment of hypertrophic cardiomyopathy by magnetic resonance versus echocardiographic imaging. Am-J-Cardiol, 1997; 79: 1651–1656
15 Schulz-Menger J, Strohm O, Dietz R, Friedrich MG. Visualization of cardiac involvement in patients with systemic sarcoidosis applying contrast-enhanced magnetic resonance imaging. Magma 2000; 11: 82–83
16 Schulz-Menger J, Strohm O, Waigand J, Uhlich F, Dietz R, Friedrich MG. The value of magnetic resonance imaging of the left ventricular outflow tract in patients with hypertrophic obstructive cardiomyopathy after septal artery embolization. Circulation 2000; 101: 1764–1766
17 Shimada T, Shimada K, Sakane T et al. Diagnosis of cardiac sarcoidosis and evaluation of the effects of steroid therapy by gadolinium-DTPA-enhanced magnetic resonance imaging. Am J Med 2001; 110: 520–527
18 Smith WH, Beacock DJ, Goddard AJ, Bloomer TN, Ridgway JP, Sivananthan UM. Magnetic resonance evaluation of the pericardium. Br J Radiol 2001; 74: 384–392
19 Strohm O, Schulz-Menger J, Pilz B, Osterziel KJ, Dietz R, Friedrich MG. Measurement of left ventricular dimensions and function in patients with dilated cardiomyopathy. J Magn Reson Imaging 2001; 13: 367–371
20 Suzuki J, Shimamato R, Nishikawa J et al. Morphological onset and early diagnosis in apical hypertrophic cardiomyopathy: a long term analysis with nuclear magnetic resonance imaging. J Am Coll Cardiol 1999; 33: 146–151

1. Hypertrophische Kardiomyopathie

Um den Effekt einer Septumablation auf die Obstruktion des Ausflusstraktes bei der HOCM evaluieren zu können, planimetrierten wir die hämodynamisch relevante kleinste systolische Fläche des LVOT und stellten die induzierten gezielten Infarkte mit kontrastverstärkten Techniken dar. Die dreidimensionale Quantifizierung der Obstruktion vor und im Verlauf nach der Intervention zeigte nicht nur eine gute Übereinstimmung mit der klinischen Verbesserung der Patienten, sondern wies auch erstmals auf eine Verzögerung des Remodelling nach perkutaner transluminaler septaler Myokardablation (PTSMA) hin. Im Jahre 2000 konnten wir diese Arbeit im Journal Circulation veröffentlichen.[51] Ursächlich für das verzögerte Remodelling ist mit hoher Wahrscheinlichkeit das infarktassoziierte Ödem, dessen Rückbildung invers mit der Verminderung der Obstruktion korreliert. Bemerkenswerterweise blieb die Ausflusstraktfläche ab dem Zeitpunkt stabil, da kein Ödem mehr nachweisbar war. (American Heart Association 2004, Abstrakt) Es ist vorstellbar, dass die Darstellung des Ödemes mit T2-gewichteten Sequenzen in Zukunft hilfreich sein könnte bei der Planung von Reinterventionen.

Bei der PTSMA, die in unserem Hause mit Schaumstoffpartikeln durchgeführt wird[52], konnten wir bereits innerhalb der ersten Stunde eine Nekrose nachweisen, während die sichere Darstellung des Ödemes erst später gelang.[53]

Während die Quantifizierung von Funktion, Volumina, Masse und die Darstellung lokalisierter Hypertrophien nebst Flussbeschleunigungen bereits zur klinischen MRT-Routine gehören, ist dies für die exakte Einschätzung der Obstruktion noch nicht der Fall. Um die Quantifizierung der LVOT-Obstruktion weiter verbreiten zu

können, wurden nicht nur die methodischen Details publiziert, sondern Grenzwerte bei Probanden und HCM-Patienten validiert. Die ROC-Analysen ergaben, dass mit einer LVOT-Fläche von 3,7 cm^2 Patienten mit einer HCM von Gesunden differenziert werden können (Sensitivität 83%, Spezifizität 100%, positiver bzw. negativer prädiktiver Wert 100% und 70%). Interessanterweise zeigte sich, dass die MRT-Methode bereits in Ruheuntersuchungen die Diagnose einer Obstruktion bei der Gruppe der latent obstruktiven Patienten gestattet.[54]

Eine Pilotstudie weist darauf hin, dass die bekannte hämodynamisch bedingte Variabilität des in der Echokardiographie ermittelten Druckgradienten bei der im MR quantifizierten Fläche des LVOT keine Rolle zu spielen scheint. Die unter Applikation von Glyceroltrinitrat sublingual ermittelten echokardiographischen Druckgradienten unterschieden sich signifikant von den Ausgangswerten, während die LVOT-Fläche stabil blieb. Dieses Ergebnis wurde im Jahre 2004 als Abstrakt bei der Jahrestagung der American Heart Association vorgestellt. Ursächlich ist wahrscheinlich der dreidimensionale Ansatz der Planimetrie im Gegensatz zu einem kalkulierten Druckgradienten, der auf Geschwindigkeitsmessungen beruht. Geschwindigkeitserhöhungen sind auch an kleinen Strukturen bekannt, ohne dass eine Obstruktion vorliegt. Einen zusätzlichen Einfluß haben aktuelle Füllungsbedingungen des Herzens z.B. durch variablen Flüssigkeitshaushalt des Patienten. Hier sind Experimente mit Strömungsphysikern geplant, da eine verlässliche Quantifizierung der Obstruktion zu einer klinisch bedeutsamen Sicherheit in der Diagnose führen würde.

Anhand der gemessenen Grenzwerte konnte bei Patienten mit Septumablation gezeigt werden, dass es postinterventionell zu einer deutlichen Zunahme der

Öffnungsfläche, nicht aber zu einer Normalisierung kommt. Die untersuchten Patienten zeigten klinisch eine deutliche Verbesserung und die ermittelte Öffnungsfläche entsprach den Patienten mit nichtobstruktiver HCM. Diese neuen Ergebnisse werden 2006 im Rahmen des jährlichen Treffens der Arbeitsgruppe Cardiovascular Magnetic Resonance der European Society of Cardiology vorgestellt.

Bei der HCM sind mittels kontrastverstärkter MRT auch unabhängig von einer Intervention Fibrosen nachweisbar. Um diese Veränderungen bei der Differenzierung nichtischämischer Herzerkrankung nutzen zu können, haben wir einen Algorithmus eingeführt, der eine systematische Evaluation gestattet. Bei 29 HCM Patienten mit LHE konnte gezeigt werden, dass die Fibrose im Gegensatz zu anderen myokardialen Erkrankungen insbesondere im Bereich der RV-Insertion lokalisiert ist und sich häufig diffus darstellt.[42]

The Value of Magnetic Resonance Imaging of the Left Ventricular Outflow Tract in Patients With Hypertrophic Obstructive Cardiomyopathy After Septal Artery Embolization

Jeanette Schulz-Menger, MD; Oliver Strohm, MD; Jürgen Waigand, MD; Frank Uhlich, MD; Rainer Dietz, MD; Matthias G. Friedrich, MD

Background—We tested the value of magnetic resonance imaging (MRI) in the follow-up of patients with hypertrophic obstructive cardiomyopathy after septal artery embolization. MRI provides a noninvasive visualization of transplanar turbulent flow in order to quantify left ventricular outflow tract obstruction.

Methods and Results—We followed 10 patients who were treated with septal artery embolization for 12 months. We used gradient echo sequences to document continuous improvement of the outflow tract area and T1- and T2-weighted spin echo sequences to visualize myocardial infarction. A continuous, but not linear, improvement of the outflow tract area occurred after septal artery embolization during the 12-month follow-up period. The improvement of the outflow tract area correlated well with the amelioration of symptoms ($r^2=0.86$).

Conclusions—We conclude that MRI reliably detects the degree of obstruction in patients with hypertrophic obstructive cardiomyopathy. This modality may be especially useful for follow-up after septal artery embolization. **(*Circulation*. 2000;101:1764-1766.)**

Key Words: hypertrophy ■ cardiomyopathy ■ magnetic resonance imaging ■ embolism ■ ventricular outflow obstruction

The hemodynamic relevance of hypertrophic obstructive cardiomyopathy (HOCM) is determined by the degree of left ventricular outflow tract (LVOT) obstruction. The pressure gradient serves as a follow-up parameter and is generally estimated by transthoracic echocardiography. Pressure gradients can be calculated by a modified Bernoulli formula,[1] according to which maximal flow velocities across a stenosis reflect the severity of obstruction. Pressure gradients calculated by echocardiography may be overestimated compared with those measured invasively. However, a significant number of patients have an impaired acoustic window, thereby contributing to the disappointing reproducibility of echocardiographic pressure gradients.[2,3] Cardiac catheterization allows for the comparison of simultaneous pressures proximal and distal to the obstruction. However, this technique is invasive and is also susceptible to variations of preload, afterload, and contractility, as well as to poststenotic pressure recovery.[4] A reliable noninvasive technique to assess the hemodynamic relevance of LVOT obstruction in HOCM would be highly useful. Such a method should provide information on the degree of the anatomical obstruction rather than on blood flow velocities or pressure gradients. Dall Agata et al[5] reported their initial experience with semi-invasive 3D echocardiography in describing LVOT obstruction in 13 patients with congenital LVOT obstruction.

The advent of septal artery infarction[6] to decrease LVOT obstruction in HOCM patients mandates objective monitoring.[7] Recent series have included up to 114 patients.[8–10] Gradient echo sequences with magnetic resonance imaging (MRI) permit the visualization of transplanar turbulent flow. When adequate echo times are used, a signal void is generated by turbulent blood flow due to the dispersion of spin magnetization. We capitalized on the turbulent flow crossing the imaging plane to estimate the degree of LVOT obstruction in HOCM patients undergoing septal artery embolization.

Methods

We investigated 10 patients (7 men and 3 women) with HOCM who were undergoing septal artery embolization. Their mean age was 66±22 years. The intervention was performed when patients had a status of New York Heart Association (NYHA) class III or IV (mean 3.2±0.2) and when maximal medical treatment was no longer helpful. One patient sequentially underwent the embolization of 2 septal arteries. MRI was performed before embolization and 3, 7, 14, 28, 90, 180, and 360 days after the intervention.

MRI was performed using a standard clinical system (Magnetom Expert/1.0T, Siemens AG). We assessed left ventricular morphology

Received December 16, 1999; revision received February 2, 2000; accepted February 28, 2000.
From Franz-Volhard-Klinik am Max-Delbrück-Centrum Berlin-Buch, Humboldt-Universität Berlin, Germany.
Correspondence to Jeanette Schulz-Menger, MD, Franz-Volhard-Klinik, Wiltbergstr 50, D-13125 Berlin, Germany. E-mail schulzmenger@fvk-berlin.de

Circulation **is available at http://www.circulationaha.org**

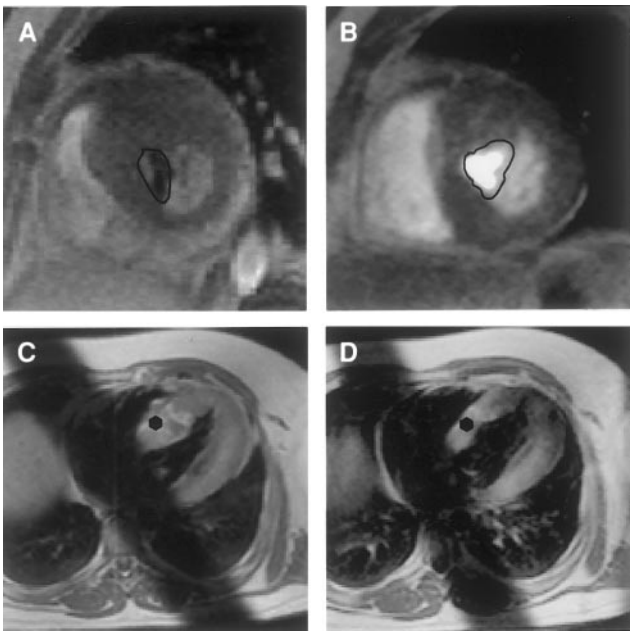

Figure 1. During follow-up, the initially thickened septum shows a significant reduction of its mass, thereby decreasing LVOT obstruction. A, Gradient echo sequence with turbulent flow through the LOVT 7 days after intervention using the region of interest for planimetry. B, Increased LVOT area 6 months after intervention; image shows partially laminar flow through the LVOT. C, Contrast-media–enhanced T1-weighted axial view of the septum on day 7. The thickened septum and its infarcted zone are clearly visible. D, Axial view using the same technique and position after 6 months. A substantial shrinkage of the septum has occurred in the area of the occluded septal artery.

and function by standard gradient echo sequences (2D fast imaging steady-state pression [FISP]; echo time [TE], 6.1 ms; repetition time [TR], 70 ms; flip angle, 30°). Measurements included LV mass and volume, as well as wall thickness. For MRI planimetry of the LVOT area, we first determined the time of peak systolic flow using a flow quantification sequence (phase contrast; TR, 28 ms). We then visualized the turbulent flow in the long axis of the LVOT by a flow-sensitive gradient echo sequence (2D FISP). Finally, we placed a multiplanar series (slice thickness, 5 mm) perpendicular to the base of the turbulent jet ("vena contracta") at the time of peak systolic flow. From the resulting image set, the image with the smallest area of turbulent flow (narrowest part of the obstruction) was selected for evaluation.

The area of the proximal vena contracta (perpendicular to this slice) was then quantified by simple planimetry (Figure 1, A and B). After embolization, the resulting myocardial infarction was assessed by T1-weighted multislice spin echo sequence images (4 to 6 acquisitions; TE, 30 ms, TR, 480 to 725 ms) before and 20 minutes after the application of contrast media (0.1 mmol/kg gadolinium-DTPA, Magnevist; Schering AG) into the antecubital vein (Figure 1, C and D). The diameters of the left ventricle were measured, and the left ventricular ejection fraction was calculated in a biplanar fashion.

Results

Total measuring time generally required ≈45 minutes. No complications occurred, and image quality was sufficient for evaluation in all patients. Septal artery embolization was successful, as defined by a rapid onset of regional septal hypokinesia resulting in an immediate decrease of the pressure gradient from 88±10 mm Hg to 31±11 mm Hg ($P<0.001$), which was measured during the catheter procedure. No significant correlation existed between the initial decrease in the pressure gradient and the clinical outcome after 12 months ($r=0.03$; $P<0.9$). During the intervention, 5 patients reported chest pain, and 2 developed nausea and vomiting. All patients recovered quickly and uneventfully. Creatine kinase levels increased to 624±214 mmol/L within the first 24 hours after the intervention. In 3 patients, the ECG revealed signs of septal infarction, as defined by ST segment elevation (>0.1 mV) in ≥2 adjacent chest leads (V2 to V4). Transient third-degree atrioventricular block occurred in 2 patients. The temporary pacemakers were removed 6 to 48 hours after the intervention. All patients left the hospital ≈1 week after undergoing the treatment.

The clinical status of all patients improved: NYHA class improved from grade 3.3±0.1 to grade 1.3±0.3. The diameter of the septum at the site of the obstruction was reduced from 24±2 to 19.2±1.0 mm (23.9%) within 12 months. No significant change occurred in posterior wall thickness (from 15.1±2.1 to 13.7±1.8 mm) or the ejection fraction (from 70±5% to 71±4%).

Three independent cardiologists experienced in cardiac MRI, who were not aware of the each other's results or the patients' symptoms, performed LVOT planimetry in 11 typical cases (of the 80 performed MRIs) using images with varying quality. The resulting intraobserver variability was 10.7%. The interobserver variability was 12.8%. The LVOT area increased from 1.3±0.1 cm^2 to 3.5±0.6 cm^2, which represents a 128±12% (range, 100% to 156%) improvement. A close relationship existed between the increase in LVOT area and the decrease in septal wall thickness ($r=0.93$; $P<0.018$; $r^2=0.86$). Remarkably, the increase in LVOT orifice area was not complete within the first weeks after embolization. Instead, most patients reached maximum improvement no earlier than 3 months after the intervention (Figure 2A). The LVOT increase paralleled the degree of clinical (NYHA class) improvement (Figure 2B). A close relationship ($P<0.0001$; $r^2=0.95$) between LVOT orifice area and NYHA class was identified.

Discussion

Our study documents the usefulness of MRI in following HOCM patients treated with septal artery embolization. The LVOT orifice area determined by the planimetry of the transplanar flow with MRI proved to be a suitable parameter to characterize patients with HOCM, both initially and during follow-up. In contrast to parameters routinely used in echocardiography, MRI is relatively free of interobserver variability and variable imaging conditions. Other investigators have measured interobserver variability with MRI and found such variability to be negligible for both estimates of mass and diameter.[11,12] In contrast to cardiac catheterization, MRI is noninvasive and free of radiation.

MRI was successful in visualizing the extent of myocardial infarction after septal artery embolization and the relationship of the lesion to the outflow tract. Thus, MRI served as a tool to evaluate the morphological and functional changes due to interventional or medical therapy. The time course of the decrease in LVOT obstruction after septal embolization varied. The initial pressure gradient decrease was not a good predictor of long-term outcome after 12 months. The systolic

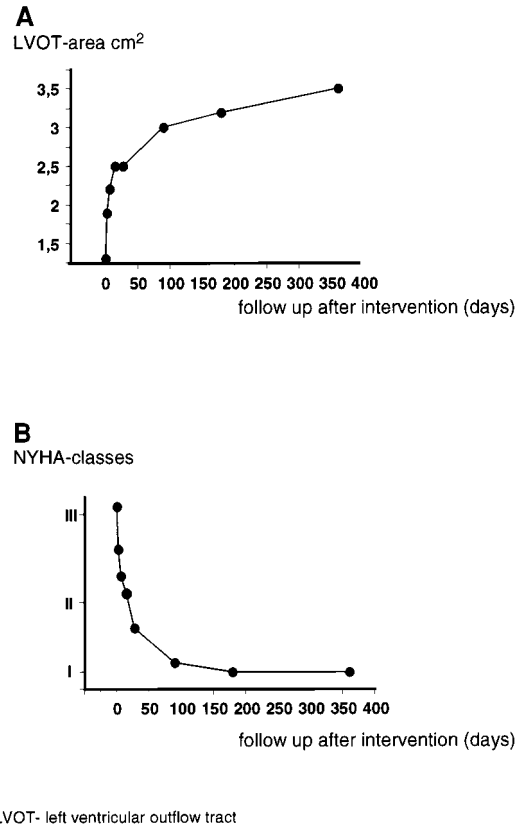

Figure 2. A, Increase of LVOT area in follow-up investigations after intervention. B, Improvement of clinical outcome after intervention.

pressure gradient decrease was mainly related to the loss of systolic septal contraction. The total increase in LVOT area during follow-up did include the fibrotic involution of the infarcted septum. The decrease of the septal wall largely determined the increase in the LVOT area. Thus, the impact of septal artery ablation on morphology and function followed a biphasic pattern. Posterior wall thickness was not influenced by the intervention, and left ventricular function remained unaltered. The maximum patient benefit could only be evaluated 4 months after the intervention, and it was stable for the remainder of the observation.

Septal artery embolization is gaining popularity as a treatment for refractory HOCM. Our experience documents the utility of MRI in following these patients. We suggest that MRI provides major advantages and will become the diagnostic tool of choice.

Acknowledgments

The authors thank Dankward Hänlein for technical assistance and Angela Weiss for assistance with MRI.

References

1. Levine RA, Cape EG, Jimoh A, et al. Pressure recovery distal to a stenosis: potential cause of gradient "overestimation" by Doppler echocardiography. *J Am Coll Cardiol.* 1989;13:706–715.
2. Fischer JL, Haberer T, Dickson D, et al. Comparison of Doppler echocardiographic methods with heart catheterization in assessing aortic valve area in 100 patients with aortic stenosis. *Br Heart J.* 1995;73:293–298.
3. Maron BJ, Gottdiener JS, Arce J, et al. Dynamic subaortic obstruction in hypertrophic cardiomyopathy: analysis by pulsed Doppler echocardiography. *J Am Coll Cardiol.* 1985;6:1–18.
4. Cape EG, Jones SM, Yamada I, et al. Turbulent/viscous interactions control doppler/catheter pressure discrepancies in aortic stenosis: the role of the Reynolds number. *Circulation.* 1996;94:2975–2981.
5. Dall Agata A, Cromme-Dijkhuis AH, Meijboom FJ, et al. Use of three-dimensional echocardiography for analysis of outflow obstruction in congenital heart disease. *Am J Cardiol.* 1999;83:921–925.
6. Sigwart U. Non-surgical myocardial reduction for hypertrophic obstructive cardiomyopathy. *Lancet.* 1995;346:211–214.
7. Spirito P, Maron BJ. Perspectives on the role of new treatment strategies in hypertrophic obstructive cardiomyopathy. *J Am Coll Cardiol.* 1999; 33:1071–1075.
8. Seggewiss H, Faber L, Gleichmann U. Percutaneous transluminal septal ablation in hypertrophic obstructive cardiomyopathy. *Thorac Cardiovasc Surg.* 1999;47:94–100.
9. Knight C, Sigwart U. Non-surgical ablation of the ventricular septum for the treatment of hypertrophic cardiomyopathy. *Heart.* 1996;76:92. Letter.
10. Kuhn HJ. Induced septal infarction/nonsurgical septal reduction for hypertrophic obstructive cardiomyopathy. *Circulation.* 1998;97: 708–709. Letter.
11. Dulce MC, Mostbeck GH, Higgins CB, et al. Magnetic resonance tomography (MRT) in the evaluation of heart disease: quantitative determination of aortic regurgitation volume. *Rontgenpraxis.* 1994;47:65–69.
12. Allison JD, Flickinger FW, Wright JC, et al. Measurement of left ventricular mass in hypertrophic cardiomyopathy using MRI: comparison with echocardiography. *Magn Reson Imaging.* 1993;11:329–334.

Left Ventricular Outflow Tract Planimetry by Cardiovascular Magnetic Resonance Differentiates Obstructive from Non-obstructive Hypertrophic Cardiomyopathy

Journal Cardiovascular Magnetic Resonance in press

Jeanette Schulz-Menger[1*] MD, Hassan Abdel-Aty MD[1,2*], Andreas Busjahn PhD[3], Ralf Wassmuth MD[1], Bernhard Pilz MD[1], Rainer Dietz MD[1] and Matthias G. Friedrich MD F.E.S.C.[1,2]

[1]Franz-Volhard-Klinik, Helios-Klinikum Berlin, Kardiologie, Charité Campus Berlin-Buch, Humboldt-Universität zu Berlin; Berlin, Germany; [2] Stephenson CMR Centre, Department of Cardiac Sciences, University of Calgary, Canada, [3]HealthTwiSt GmbH Berlin, Germany

[*] *Both authors contributed equally to this work*

Suggested running head: LVOT-planimetry in hypertrophic cardiomyopathy

Corresponding author

Jeanette Schulz-Menger MD

Franz-Volhard-KlinikCharité-Campus-Buch, Kardiologie

Universitätsmedizin Berlin, Helios-Klinikum Berlin;

Wiltbergstr. 50, D-13125

Berlin, Germany

Tel: +49 30 9417-2593/2552

Fax: +49 30 9417-2560

Email: schulzmenger@fvk-berlin.de

Word count:

Words including title page, abstracts, text, references and figure legends: 3132

The authors do not have a financial or conflict of interest to disclose.

Abstract:

The relation to the pressure gradient as assessed by Echo and the CMR-derived planimetry of the LVOT is not known, no values for the differentiation of obstruction exist. We studied 37 patients with hypertrophic cardiomyopathy and 14 healthy controls using standard sequences with 3D coverage of the left ventricular outflow tract. A cutoff value of 2.7 cm^2 identified obstruction as defined by echocardiography with 100% accuracy. CMR planimetry at rest is a promising tool to evaluate patients with hypertrophic cardiomyopathy.

Key words

Hypertrophic Cardiomyopathy

Cardiovascular Magnetic Resonance

Left Ventricular Outflow Tract

Echocardiography

Introduction

A crucial step in the diagnostic work-up of patients with hypertrophic cardiomyopathy (HCM) is to differentiate between obstructive and non-obstructive forms of the disease. In patients with obstruction of the left ventricular outflow tract (LVOT) the Doppler echocardiography-derived pressure gradient (PG) is currently the accepted approach (1,2); however, it is limited by the variability of the measurements (3) and the need to apply stress to detect the 'latent' obstruction (4). Furthermore, PG measurements vary significantly in relation to hemodynamic conditions (5,6). More than 20 years ago Spirito et al.(7) introduced the planimetry of LVOT-area by transthoracic echocardiography. The method however was not applicable in clinical routine due to technical limitations of available ultrasound technique. Recently, 3D echocardiography partly overcame this limitation (8), yet complex image processing is needed (9) and a significant fraction of patients may not be evaluated due to poor image quality(8). Transesophageal 3D-echocardiography was also used to measure the LVOT in HCM patients before and after myectomy (10). However the technique is relatively invasive, frequently requires sedation and is not very well tolerated by many patients. Finally, in all echocardiographic approaches, the actual position of the obtained views cannot be easily controlled for accuracy.

A unique feature of CMR is the ability to provide noninvasive, reproducible and direct planimetric quantification of complex-shaped structures such as stenotic valves (11-13). We have shown the feasibility and relevance of LVOT

planimetry using CMR (14). The results correlate well with the clinical severity of the disease both before and after septal artery embolization.

Yet, there are no reports using CMR or 3D echocardiography that attempted to assess the LVOT area in the full scale of HCM i.e. obstructive, latent obstructive and non obstructive HCM. Furthermore there are neither CMR-LVOT area measurements from healthy subjects available nor a validation against the well-established PG measurements in HCM patients. CMR assessment of the LVOT area would allow for relating obstruction to tissue changes such as edema or focal fibrosis.

This study was designed to measure LVOT area by CMR in different forms of HCM and healthy subjects in comparison to pressure gradient measurements as the standard technique.

Methods

Patients:

Thirty-seven HCM patients were consecutively enrolled. HCM was defined based on the echocardiographic demonstration of a hypertrophied (wall thickness of 15 mm or more), non-dilated left ventricle in the absence of another related cardiac or systemic disorder. The clinical status of the patients was classified depending on the degree of dyspnea following the classification of the New York Heart Association (NYHA). Exclusion criteria were atrial fibrillation with large RR-interval-variations, contraindications to CMR and poor ultrasound imaging conditions.

Control group:

Fourteen healthy subjects (10 males, 28±10 years) with no current or previous cardiovascular disorders and with normal ECG served as our control group. Those subjects underwent only CMR but not Doppler echocardiography.

Echocardiography:

Echocardiographic examinations were performed on a commercially available instrument (Acuson Sequoia C256, Siemens Medical Solutions, Erlangen, Germany) with a 3.2 MHz transducer. Left-ventricular dimensions, ejection fraction and wall thickness of the anteroseptal and posterior wall were measured in the parasternal long axis according to the guidelines of the American Society of Echocardiography. Maximum thickness of the septal wall was measured in the apical four-chamber view using 2D-echocardiography. The maximum velocity within the LVOT was measured at rest and after Valsalva maneuver in the five-chamber view, applying multiple PW- and CW-Doppler-measurements. We cautiously tried to avoid contamination of the Doppler-signal by flow from mitral

regurgitation or flow through the aortic valve. The maximum PG was calculated from velocity measurements.

Patients were divided into 3 groups based on their PG: a) Non-obstructive HCM (HNCM) (PG<30 at rest and after provocation, n= 12), b) Latent obstructive HCM (LHOCM) (PG<30 at rest and >30 after provocation, n=8),) and c) Obstructive HCM (HOCM) (PG>30 at rest, n= 17).

CMR

CMR studies were performed in a 1.5 Tesla system (Signa CV/*i*, GE medical systems, Milwaukee) using a four-element phased array coil with the patient in the supine position. Breath-hold, real-time scout images and a subsequent series of breath-hold gradient-echo images (SSFP/steady-state free precession, TR 4.5 ms, TE 1.8 ms, matrix: 256 x 192, FOV: 32x32-38x38 cm, number of phases: 20-30) were used for localization of the LVOT (figure 1). Based on long-axis views of the LVOT, a stack of cross-sectional views was obtained to cover the whole LVOT (cine mode, 6-8 slices, slice thickness 5mm, no gap). The LVOT in HCM was defined as the whole region bounded by the anterior mitral valve leaflet and the septal wall. The smallest LVOT area obtained in theses slices was measured during systole, including the effect of the systolic anterior movement of the anterior mitral valve leaflet. The smallest area during systole was accepted as hemodynamic relevant and was documented. A reader blinded to other subject-related data manually traced the LVOT area using the anterior mitral valve leaflet and the septum as anatomical borders.

Figure 2 shows the LVOT in different forms of disease.

Statistics

All statistical tests were performed using a commercially available statistical program (SPSS 11 for Macintosh). Data are presented as mean ± one standard deviation. Continuous variables were compared using ANOVA. Correlations between continuous variables were tested using linear regression and the Pearson correlation coefficient. A p value of less than 0.05 was considered significant. Non-parametric data were compared by Mann Whitney U-Test, Receiver operated curves were used to define the cutoff values of LVOT area to differentiate patients from controls as well as obstructive from non-obstructive HCM. As the gradient measure showed a non-linear relation to area, we applied a cubic root transformation prior to correlation analysis.

Results

Table 1 summarizes the patients' characteristics. The mean duration between echocardiography and CMR was 5±6 days. 43% of the patients however underwent both examinations on the same day. LVOT was evaluable in all but one patient. CMR assessment of myocardial mass and volume could not be performed in 4 patients, due to incomplete coverage of the left ventricle.

LVOT area by CMR:

Figure 3 shows the relation of the size of the LVOT area to the presence or absence of the pressure-gradient-defined obstruction. Compared to volunteers with a mean LVOT area of 4.8±0.8 cm^2, the area was significantly smaller in patients with HNCM (3.6±1.1 cm^2, $p<0.004$), LHOCM (2.2±1.5 cm^2, $p<0.002$.) and HOCM (1.6±0.6 cm^2, $p<0.0001$) respectively. Patients with HNCM had significantly larger LVOT than latent ($p = 0.013$) or HOCM ($p < 0.0001$) respectively. When the latent obstructive and obstructive forms were considered together as obstructive HCM, significant differences in LVOT still existed between the obstructive and non-obstructive (1.8 cm^2±1.0 vs. 3.6±1.1 cm^2, $p<0.0001$) forms of the disease. No significant difference was found between the LVOT in LHOCM and HOCM ($p = 0.478$). (figure 3) The comparison of the mean values (Bland-Altman plots) in a representative sample showed an excellent agreement between readers (correlation = 0.97). Based on ROC analysis, a cutoff value of 3.7 cm^2 could be shown to differentiate patients from controls (sensitivity 83%, specificity 100%, positive and negative predictive values 100% and 70%, respectively). On the other

hand, a cutoff value of 2.7 cm^2 was able to differentiate HOCM from HNCM with a sensitivity and specificity of 100%.

Correlation between PG and LVOT:

There was no significant relation of area or gradient with height and weight. Age showed a significant inverse correlation to area (r=-0.68), even after restricting the analysis to patients only (r=-0.50). There was no significant correlation between age and gradient (r=0.22). The correlation between area and gradient was -0.67 and remained significant after correction for age (partial correlation r=-0.68). (figure 4)

Discussion

This is the first report describing CMR planimetry of the LVOT in different forms of HCM compared to healthy subjects. We could verify the step-wise reduction of the LVOT area from HNCM, LHOCM to HOCM, as expected by the disease definition. These findings can be explained by the inverse relation between flow velocity and the size of the anatomic structure, mainly described by the smallest systolic LVOT area. Based on this theory, however one would expect a linear correlation between LVOT area and PG which was not the case neither in ours nor in previous reports using 3D echocardiography (8,10). This is likely related to two factors: First, the susceptibility of PG measurements to minor changes in loading conditions (6) and/or the variability of PG measurement from day to day (3). This is especially true for LVOT areas with borderline hemodynamic relevance at rest. Second: Based on simple considerations on flow dynamics in obstructed vessels, the linearity between flow velocity and a narrowed LVOT is expected to get lost once a 'critical' LVOT area range is reached. In such a case (likely to be accompanied by symptoms in HCM patients), small changes as induced by preload variations may lead to a significant increase of resistance and thus of measure pressure gradients.

The finding that the LVOT area was significantly reduced in apparently non-obstructive at rest forms of HCM (LHOCM and HNCM) deserves special attention. Panza et al. (15) found that a reduction of the LVOT diameter in children with HNCM was predictive of the future development of SAM and significant obstruction. Although extrapolation of these results to adult patients should be

taken with care, it seems conceivable that a mild obstruction although not yet hemodynamically overt will have a relevant predictive value.

A LVOT cutoff value of 3.7 cm^2 appears to offer a promising screening tool to rule out the disease whereas a LVOT value of 2.7 cm^2 has an accuracy of 100% to differentiate obstructive from non-obstructive HCM.

This value is larger than the 2.0 cm^2 identified by Qin et al (8) using 3D echocardiography. The reason of this difference is most likely related to the PG cutoff value to define obstructive HCM. Whereas we used a value of 30 mmHg (1), Qin et al. defined obstruction as values above 50 mmHg.

Clinical implications

An emerging role of CMR to evaluate HCM is being shaped with unique features to assess tissue structure and ventricular function (16-20). Planimetry of the LVOT area provides relevant additional information and may have an important role within a comprehensive CMR exam of HCM patients.

Limitations and technical considerations

The major limitation of this study is the limited number of patients in the subgroups. The aim however was to validate the concept that LVOT is related to the degree of obstruction. Future studies in larger patient cohorts are definitely warranted. Due to the known day-to-day variation in PG measurements it would have been ideal to perform both Doppler and CMR on the same day. For logistical reasons, this demand was fulfilled in only 43% of our patients. Yet, the correlation between PG and LVOT area measurement remained significant even after correcting for the inter-study duration.

Conclusion

CMR planimetry of the LVOT accurately differentiates obstructive from non-obstructive HCM without the need for hemodynamic provocation.

Abbreviations list

CMR: cardiovascular magnetic resonance

HCM: hypertrophic cardiomyopathy

HOCM: hypertrophic obstructive cardiomyopathy

HNCM: hypertrophic non-obstructive cardiomyopathy

LHOCM: latent hypertrophic obstructive cardiomyopathy

LVOT: left ventricular outflow tract

PG: pressure gradient

Echo: echocardiography

Acknowledgments

We would like to thank Kerstin Kretschel, Evelyn Polzin and Ursula Wagner for their technical assistance and Melanie Bochmann for her help in recruiting patients.

We also thank Andreas Kumar, Anja Zagrossek and Philipp Boye for their help in scanning the patients.

References

1. Maron BJ, McKenna WJ, Danielson GK, et al. American College of Cardiology/European Society of Cardiology clinical expert consensus document on hypertrophic cardiomyopathy. A report of the American College of Cardiology Foundation Task Force on Clinical Expert Consensus Documents and the European Society of Cardiology Committee for Practice Guidelines. J Am Coll Cardiol 2003;42:1687-713.
2. Maron MS, Olivotto I, Betocchi S, et al. Effect of left ventricular outflow tract obstruction on clinical outcome in hypertrophic cardiomyopathy. N Engl J Med 2003;348:295-303.
3. Kizilbash AM, Heinle SK, Grayburn PA. Spontaneous variability of left ventricular outflow tract gradient in hypertrophic obstructive cardiomyopathy. Circulation 1998;97:461-6.
4. Marwick TH, Nakatani S, Haluska B, Thomas JD, Lever HM. Provocation of latent left ventricular outflow tract gradients with amyl nitrite and exercise in hypertrophic cardiomyopathy. Am J Cardiol 1995;75:805-9.
5. Klues HG, Leuner C, Kuhn H. Left ventricular outflow tract obstruction in patients with hypertrophic cardiomyopathy: increase in gradient after exercise [see comments]. J-Am-Coll-Cardiol 1992;19:527-33.
6. Paz R, Jortner R, Tunick PA, et al. The effect of the ingestion of ethanol on obstruction of the left ventricular outflow tract in hypertrophic cardiomyopathy. N Engl J Med 1996;335:938-41.

7. Spirito P, Maron BJ. Significance of left ventricular outflow tract cross-sectional area in hypertrophic cardiomyopathy: a two-dimensional echocardiographic assessment. Circulation 1983;67:1100-8.

8. Qin JX, Shiota T, Lever HM, et al. Impact of left ventricular outflow tract area on systolic outflow velocity in hypertrophic cardiomyopathy: a real-time three-dimensional echocardiographic study. J Am Coll Cardiol 2002;39:308-14.

9. Salustri A, Kofflard MJ, Roelandt JR, et al. Assessment of left ventricular outflow in hypertrophic cardiomyopathy using anyplane and paraplane analysis of three-dimensional echocardiography. Am J Cardiol 1996;78:462-8.

10. Franke A, Schondube FA, Kuhl HP, et al. Quantitative assessment of the operative results after extended myectomy and surgical reconstruction of the subvalvular mitral apparatus in hypertrophic obstructive cardiomyopathy using dynamic three-dimensional transesophageal echocardiography. J-Am-Coll-Cardiol 1998;31:1641-9.

11. John AS, Dill T, Brandt RR, et al. Magnetic resonance to assess the aortic valve area in aortic stenosis: how does it compare to current diagnostic standards? J Am Coll Cardiol 2003;42:519-26.

12. Friedrich MG, Schulz-Menger J, Poetsch T, Pilz B, Uhlich F, Dietz R. Quantification of valvular aortic stenosis by magnetic resonance imaging. Am Heart J 2002;144:329-34.

13. Strohm O, Schulz-Menger J, Hanlein D, Dietz R, Friedrich MG. Magnetic resonance planimetry of the vena contracta as a new approach to

assessment of stenotic heart valves: an in vitro study. J Magn Reson Imaging 2001;14:31-4.

14. Schulz-Menger J, Strohm O, Waigand J, Uhlich F, Dietz R, Friedrich MG. The value of magnetic resonance imaging of the left ventricular outflow tract in patients with hypertrophic obstructive cardiomyopathy after septal artery embolization. Circulation 2000;101:1764-6.

15. Panza JA, Maris TJ, Maron BJ. Development and determinants of dynamic obstruction to left ventricular outflow in young patients with hypertrophic cardiomyopathy. Circulation 1992;85:1398-405.

16. Choudhury L, Mahrholdt H, Wagner A, et al. Myocardial scarring in asymptomatic or mildly symptomatic patients with hypertrophic cardiomyopathy. J Am Coll Cardiol 2002;40:2156-64.

17. Moon JC, McKenna WJ, McCrohon JA, Elliott PM, Smith GC, Pennell DJ. Toward clinical risk assessment in hypertrophic cardiomyopathy with gadolinium cardiovascular magnetic resonance. J Am Coll Cardiol 2003;41:1561-7.

18. van Dockum WG, ten Cate FJ, ten Berg JM, et al. Myocardial infarction after percutaneous transluminal septal myocardial ablation in hypertrophic obstructive cardiomyopathy: evaluation by contrast-enhanced magnetic resonance imaging. J Am Coll Cardiol 2004;43:27-34.

19. Ennis DB, Epstein FH, Kellman P, Fananapazir L, McVeigh ER, Arai AE. Assessment of regional systolic and diastolic dysfunction in familial hypertrophic cardiomyopathy using MR tagging. Magn Reson Med 2003;50:638-42.

20. Dong SJ, MacGregor JH, Crawley AP, et al. Left ventricular wall thickness and regional systolic function in patients with hypertrophic cardiomyopathy. A three-dimensional tagged magnetic resonance imaging study. Circulation 1994;90:1200-9.

Table 1: Characteristics of the study's patient population

	Non-obstructive	Latent obstructive	Obstructive
Number of subjects	12	8	17
EF	71±9%	76±10%	79±10%*
LVM	197±51 g	207±25 g	249±78 g
LVM/height	1.2±0.3 g/cm	1.2±0.2 g/cm	1.5±0.7 g/cm
Age	48±15	57±14	61±12*
Male gender	67%	50%	53%

*$p<0.05$

EF: ejection fraction

LVM: left ventricular mass

Figure legends

Figure 1:

Localization and planimetry of the left ventricular outflow tract -

Stepwise localization of LVOT

Left: LVOT defined by the interventricular septal wall and the anterior leaflet of the mitral valve with lines visualizing the slices for coverage of the LVOT. It is demonstrated in a patient with HNCM

Middle: short axis through the LVOT

Right: short axis through the LVOT with region of interest giving the quantified area of the LVOT

Figure 2:

Alteration in size of the LVOT area in patients with obstructive forms of hypertrophic cardiomyopathy:

Top: HOCM signal void to obstruction in the whole LVOT (area = 1.0cm^2)

Bottom: LHOCM signal void is also assessable (area = 1.9cm^2)

In both:

left: long axis view of the LVOT

right: short axis view of the LVOT

Figure 3:

Step-wise reduction in the LVOT-area from controls, non-obstructive to obstructive HCM

Figure 4:

Inverse nonlinear relation between the LVOT area and pressure gradient in Doppler echocardiography

figure 1 Localization and planimetry of the LVOT

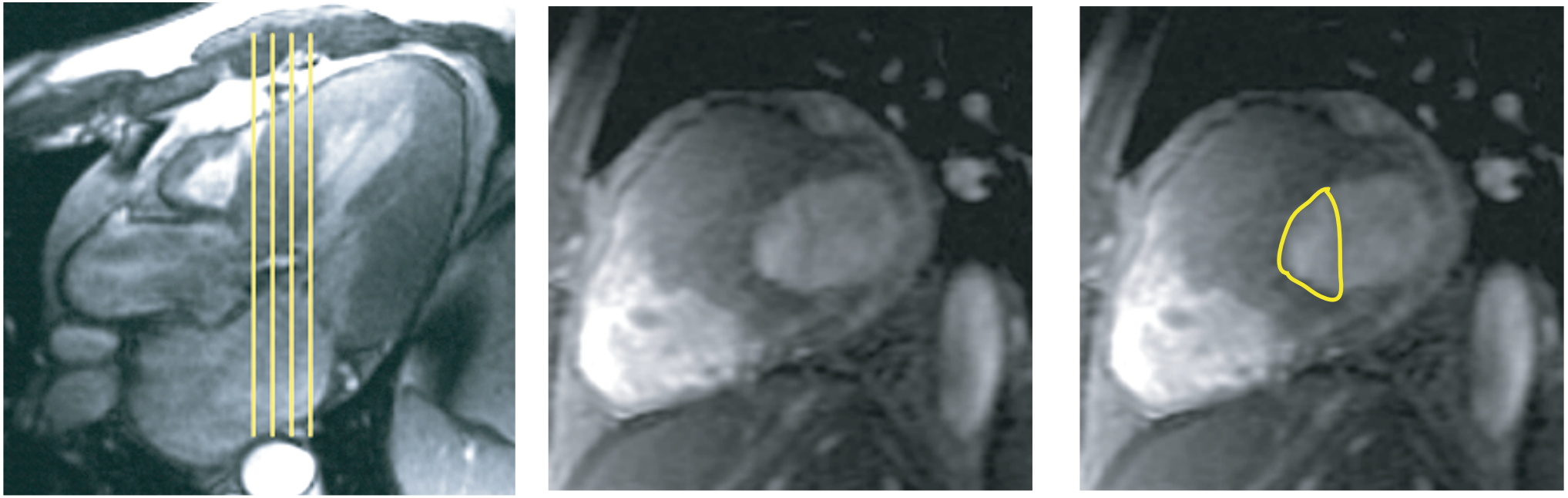

Figute 2
Alteration in the size of the LVOT area

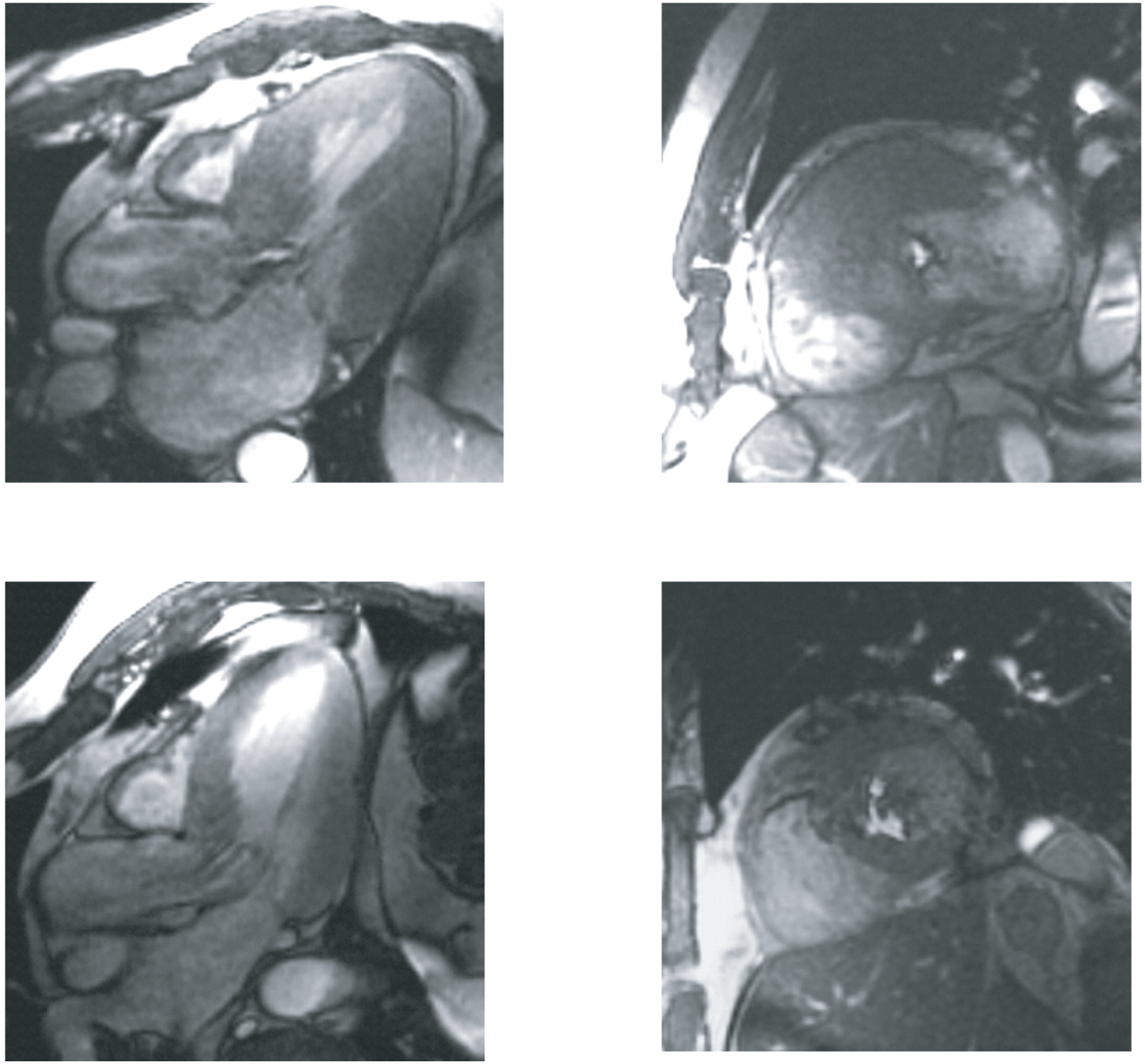

figure 3

Step-wise reduction in the LVOT-area from controls, non-obstructive to obstructive HCM

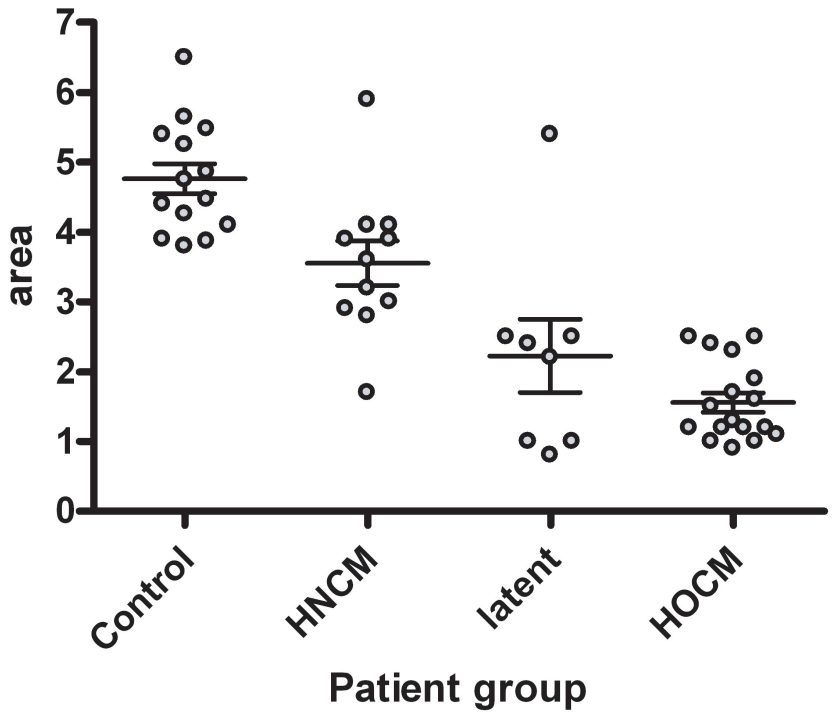

figure 4

Inverse nonlinear relation between the LVOT area and pressure gradient in Doppler echocardiography

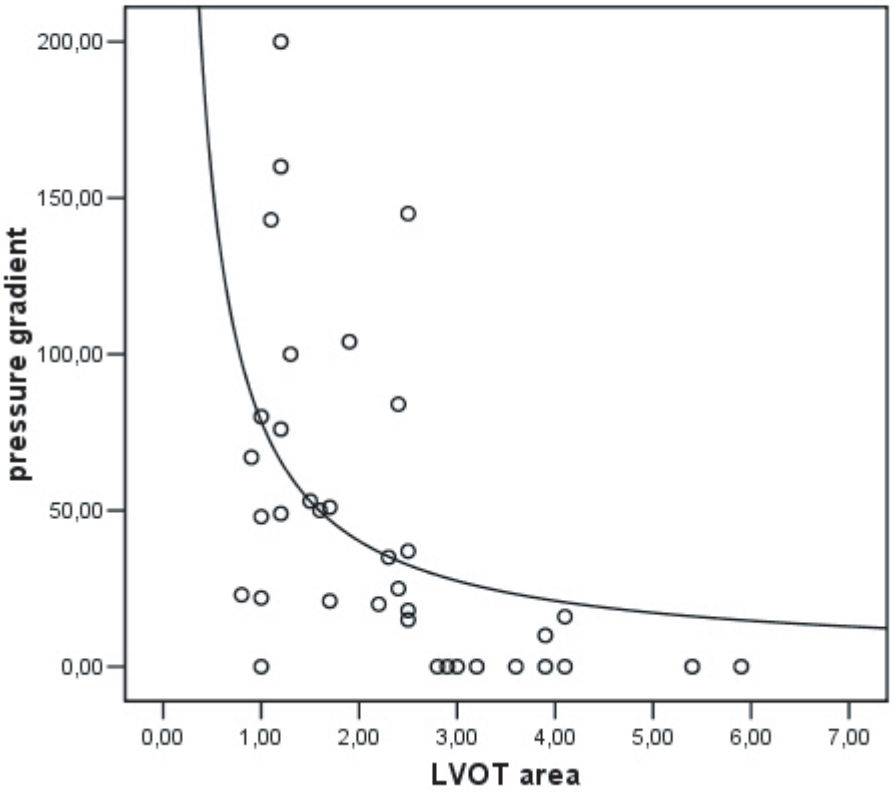

2 Myokardschaden bei sekundären myokardialen Erkrankungen

2.1. Myokarditis

Im Jahre 1998 konnte unsere Arbeitsgruppe den Einsatz der kardialen MRT bei Myokarditis erstveröffentlichen.[40] Da aus kardiologischer Sicht die Diagnose einer Myokarditis häufig schwierig erscheint, ist dies unverändert einer unserer Forschungsschwerpunkte. Sowohl die bei uns eingesetzten T_2-gewichteten Sequenzen, als auch die kontrastverstärkten T_1-gewichteten Gradientenechosequenzen mit Inversionspuls ließen erwarten, dass sich pathologische Veränderungen besser differenzieren lassen. Der dann verwendete quantitative multi-sequenzielle Ansatz (Kapitel II 3.2; Seite 18) führte zu einer deutlich höheren diagnostischen Sicherheit bei der akuten Myokarditis im Vergleich zur Einzelanwendung von Sequenzen.[55] Die gesamte durch uns eingeführte MRT-basierte Myokarditisdiagnostik findet zunehmend Akzeptanz in internationalen Übersichtsarbeiten zur Myokarditis.[12] Erfreulicherweise erlaubt dieses Wissen auch eine rege wissenschaftliche Diskussion, die sich unter anderem im schriftlichen wissenschaftlichen Austausch wieder findet.[56] Erste Verlaufsuntersuchungen weisen darauf hin, dass es unser Ansatz gestattet, bereits primär reversible von irrereversiblen Veränderungen zu unterscheiden. Während die durch LHE darstellbaren Läsionen auch im Verlauf nachweisbar waren, zeigte sich sowohl eine Verbesserung der linksventrikulären Funktion, als auch eine Normalisierung der T_2-Ratio und der frühen KM-Anreicherung. [57]

Journal of the American College of Cardiology
Vol. 45, No. 11, 2005
ISSN 0735-1097/05/$30.00
doi:10.1016/j.jacc.2004.11.069

Published by Elsevier Inc.

Diagnostic Performance of Cardiovascular Magnetic Resonance in Patients With Suspected Acute Myocarditis

Comparison of Different Approaches

Hassan Abdel-Aty, MD,* Philipp Boyé, MD,* Anja Zagrosek, MD,* Ralf Wassmuth, MD,* Andreas Kumar, MD,* Daniel Messroghli, MD,* Petra Bock, MD,* Rainer Dietz, MD,* Matthias G. Friedrich, MD, FESC,*† Jeanette Schulz-Menger, MD*

Berlin, Germany; and Calgary, Alberta, Canada

OBJECTIVES The aim of this research was to identify the diagnostic performance of gadolinium-enhanced and T2-weighted cardiovascular magnetic resonance (CMR) in suspected acute myocarditis.

BACKGROUND Acute myocarditis is difficult to diagnose; CMR provides various means to visualize myocardial inflammatory changes. A CMR approach with clear-cut diagnostic criteria would be desirable.

METHODS We investigated 25 patients with suspected acute myocarditis (18 males, 44 ± 17 years) and 23 healthy controls (13 males, 29 ± 10 years). Cardiovascular magnetic resonance studies included the following sequences: 1) T2-weighted triple inversion recovery; 2) T1-weighted spin echo before and over 4 min after gadolinium injection; and 3) inversion recovery-gradient echo 10 min after gadolinium injection. Qualitative and quantitative image analysis was performed for: 1) focal and global T2 signal intensity (SI); 2) myocardial global relative enhancement (gRE); and 3) areas of late gadolinium enhancement (LGE).

RESULTS Both global T2 SI and gRE were higher in patients than in controls (T2: 2.3 ± 0.4 vs. 1.7 ± 0.4; $p < 0.0001$, gRE: 6.8 ± 4.0 vs. 3.7 ± 2.3; $p < 0.001$). The sensitivity, specificity, and diagnostic accuracy for T2 (cutoff value of 1.9) were 84%, 74%, and 79%, respectively; gRE: (cutoff value of 4.0) 80%, 68%, and 74.5% respectively; LGE: 44%, 100%, and 71%, respectively. The best diagnostic performance was obtained when "any-two" of the three sequences were positive in the same patient yielding a 76% sensitivity, 95.5% specificity, and 85% diagnostic accuracy.

CONCLUSIONS A combined CMR approach using T2-weighted imaging, early and late gadolinium enhancement, provides a high diagnostic accuracy and is a useful tool in the diagnosis and assessment of patients with suspected acute myocarditis. (J Am Coll Cardiol 2005;45: 1815–22) © 2005 by the American College of Cardiology Foundation

Identifying patients with acute myocarditis is a challenging task. Clinical presentations often mimic other disorders and may vary from flu-like symptoms or subclinical disease to acute heart failure and sudden cardiac death (1). Of the imaging approaches utilized to diagnose the disease, cardiovascular magnetic resonance (CMR) has emerged as an important tool. The two relevant gadolinium-enhanced CMR approaches described so far depend on the measurement of myocardial global (early) relative enhancement (gRE) (2) or the visualization of late gadolinium enhancement (LGE) (3). Each of these approaches monitors a different aspect of myocardial injury in myocarditis. Whereas gRE likely reflects myocardial hyperemia and increased capillary permeability as features of present inflammation, LGE mostly indicates irreversible myocardial injury. Another interesting and yet inadequately studied noncontrast CMR approach in myocarditis is T2-weighted imaging, which almost exclusively depends on the detection of myocardial edema. It has been shown to be of diagnostic value (4), but experience has been reported only sparsely. The diagnostic performance of these techniques to identify myocarditis is not well-defined. For example, the reported sensitivity of LGE to detect acute myocarditis varies from 44% to 88% (3,5). Furthermore, a comprehensive CMR protocol combining data obtained from each approach has not reached the clinical arena and yet appears promising for two reasons: first, the spectrum of myocardial injury caused by the disease is diverse, ranging from mild inflammation with hyperemia or edema to frank necrosis (6). One would then expect that an imaging approach designed to detect only one of these injuries would lack sufficient sensitivity. Second, providing information on the various myocarditis-induced injuries could help identify patients with a severe form of the disease or those with a potentially unfavorable prognosis.

See page 1823

METHODS

Patients. Inclusion criteria:

1) Symptoms and signs suggestive of cardiac disease (angina pectoris, dyspnea, palpitations).

From the *Franz-Volhard-Klinik, Charité Campus Buch, Universität Medizin Berlin, Berlin, Germany; and the †Stephenson CMR Centre, Departments of Cardiac Sciences and Radiology, University of Calgary, Calgary, Alberta, Canada.

Manuscript received September 1, 2004; revised manuscript received November 3, 2004, accepted November 11, 2004.

JACC Vol. 45, No. 11, 2005
June 7, 2005:1815–22

Abbreviations and Acronyms

CK = creatine kinase
CMR = cardiovascular magnetic resonance
gRE = global relative enhancement
LGE = late gadolinium enhancement
SI = signal intensity

2) Evidence for myocardial injury as defined by electrocardiogram (ECG) changes (ST-segment changes, conduction defects) and elevated serum markers (creatine kinase [CK], troponin T or I).
3) Exclusion of coronary artery disease by angiographic and/or clinical criteria.

Criteria of exclusion were previous myocardial infarction, evidence of chronic myocarditis, and known contraindications to CMR.

Control group. Twenty-three healthy volunteers (13 males, age 29.3 ± 10 years) with no current or past evidence of cardiovascular disorders served as our control group.

A written informed consent was obtained from each subject, and the local ethics committee approved the study.

CMR. Cardiovascular magnetic resonance studies were performed in a 1.5-T system (Signa CV/*i*, GE Medical Systems, Milwaukee, Wisconsin). Localization was performed using breath-hold real time and steady-state free precession images of true anatomical axes of the heart. For the T2- and T1-weighted spin echo sequences, which were used for a quantitative evaluation, the body coil was used. We applied a breath-hold, black-blood, T2-weighted, triple inversion recovery sequence (TR 2 × RR, TE 65 ms, TI 140 ms) in three (basal, midventricular, and apical) short-axis slices (slice thickness 15 mm, gap 5 mm, field of vision 34 to 38 cm, matrix: 256 × 256). Breath-hold steady-state free precession images (TR 3.8 ms, TE 1.6 ms) were acquired in two- and four-chamber views to assess global ventricular function. We then applied a free breathing spin echo sequence in four identical axial slices both before and after (without any change in parameters in between) intravascular injection of 0.1 mmol gadolinium-diethylenetriaminepentaacetate (DTPA) (Magnevist, Schering, Germany) using an automated injector (Medrad, Indianola, Pennsylvania). The sequence was started immediately after injection and lasted 3 to 4 min; thus, the images reflect gadolinium enhancement at a mean of 2 min. After the acquisition of spin echo images, an additional dose (0.1 mmol) of gadolinium-DTPA was injected, and a breath-hold contrast-enhanced inversion-recovery gradient-echo sequence (TR 5.5 ms, TE 1.4 ms, TI 225 to 275 ms as individually optimized to null myocardial signal, matrix 256 × 192, slice thickness/gap 15/5 mm) was applied after a delay of 10 min in three short- and three long- (two-, three-, and four-chamber views, respectively) axis slices.

Coronary angiography. Coronary angiography was performed on a standard angiography suite (Hicor, Siemens, Erlangen, Germany) in 21 patients to exclude the presence of significant coronary artery disease (>70% stenosis).

Clinical analysis. Two observers (A.Z. and P.B.), who were blinded to CMR data, assessed the clinical course of the patients during their hospital stay.

Image analysis. SPIN ECHO IMAGES. Regions of interest covering the left ventricular myocardium as well as within a skeletal muscle (erector spinae or lattisimus dorsi) in the same slice were manually drawn in the precontrast images and were copied to the postcontrast images (Fig. 1), and gRE was calculated as previously described (2).

T2-WEIGHTED IMAGES. Quantitative analysis: regions of interest were drawn covering the left ventricular myocardium and within a skeletal muscle in the same slice. The myocardial signal intensity (SI) was related to that of the skeletal muscle:

$$\text{Relative myocardial T2 SI} = SI_{myocardium} / SI_{skeletal\ muscle}$$

Endocardial and epicardial contours were manually drawn, and focal areas of high T2 SI (those with SI more than the normal myocardium plus two standard deviations) were identified (MASS 6, Medis, Leiden, the Netherlands).

QUALITATIVE ANALYSIS. This was performed by the consensus agreement of two observers (J.S-M. and H.A-A.) who were blinded to the patients' clinical data. Images were evaluated for the presence or absence of focal or segmental areas of high T2 SI.

LGE. QUALITATIVE ANALYSIS. This was done for the presence, number, and transmurality of LGE areas.

QUANTITATIVE ANALYSIS. Areas of LGE (those with SI more than the normal myocardium plus two standard deviations) were delineated similar to that in T2 imaging. Regions of interest were also drawn within background air. The contrast-to-noise ratio (CNR) and the signal-to-noise ratio (SNR) of LGE were then calculated as follows:

$$CNR = (SI_{LGE} - SI_{myocardium}) / SI_{noise}$$

$$SNR = SI_{LGE} / SI_{noise}$$

Foci of high signal in delayed enhancement and T2 images were traced, and their volume expressed as a percentage of the total myocardial slice volume.

Statistics. All statistical tests were performed using a commercially available statistical program (SPSS 11 for Macintosh, SPSS Gmbh Software, Munich, Germany). Data are presented as mean ± SD. Continuous variables were compared using the Mann-Whitney *U* test and noncontinuous data using the chi-square test. Data were correlated using the Spearman correlation coeffecient. Reciever operating charcteristic curves were used to identify the cutoff values of gRE and global T2 signal changes. A p value <0.05 was considered significant.

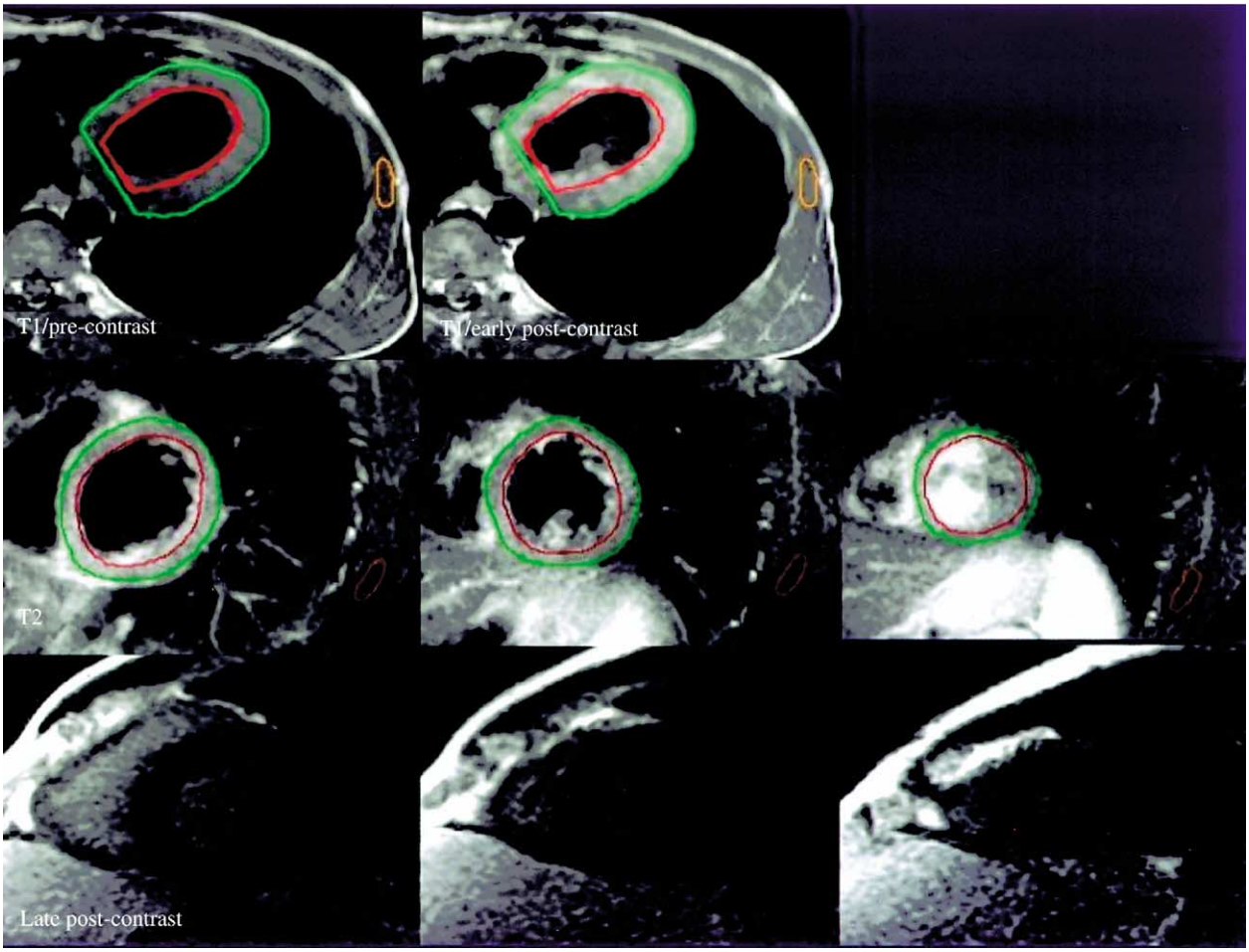

Figure 1. Cardiovascular magnetic resonance images from Patient #6. **(Top)** Pre- and postcontrast axial T1-weighted spin echo images of the same slice. Global relative enhancement was elevated (4.6). Regions of interest are drawn around the myocardium and within the skeletal muscle. **(Middle)** Short-axis T2-weighted images: no focal areas of high T2 signal, yet the higher global myocardial T2 signal in relation to the skeletal muscle is visibly appreciable (exact value = 2.5). **(Bottom)** Corresponding late enhancement images: no evidence of late gadolinium enhancement.

RESULTS

Table 1 provides the characteristics of the study patient population. The average duration between the onset of cardiac symptoms and CMR was 5.6 ± 4.2 days. Patients had significantly lower ejection fraction than controls (57.1 ± 12.6% vs. 64.2 ± 5.2%, $p = 0.013$). Biopsy was performed in two patients (Patients #5 and #25) and showed acute giant cell myocarditis with round cell infiltration and multiple necrotic foci in Patient #5 and diffuse fibrosis, myocardial hypertrophy, regional inflammatory cell infiltration, and fresh erythrocyte extravasation in Patient #25.

gRE. Global relative enhancement was significantly higher in patients compared to controls (6.8 ± 4.0 vs. 3.7 ± 2.3; $p < 0.001$). Figures 1 and 2 show representative images from two patients with increased gRE. Figure 3 shows the receiver operating characteristic curve of gRE to identify myocarditis. A cutoff value of 4.0 had a sensitivity, specificity, and diagnostic accuracy of 80%, 68%, and 74.5%, respectively; gRE did not significantly correlate with ejection fraction ($p = 0.350$) or hospital stay ($p = 0.320$).

T2-weighted imaging. The global myocardial T2 SI ratio was significantly higher in patients than in controls (2.3 ± 0.4 vs. 1.7 ± 0.4; $p < 0.0001$). Figure 3 shows the receiver operating characteristic curve of global myocardial T2 SI to identify myocarditis. A cutoff value of 1.9 had a sensitivity of 84%, specificity of 74%, and a diagnostic accuracy of 79%; T2-SI ratio was not related to gRE ($p = 0.462$). Moderate (0.42) significant correlation was found between T2-SI ratio and troponin levels ($p = 0.035$). Eight patients showed focal areas of high T2 SI, which were either transmural or subepicardial (Fig. 4) but never confined to the subendocardium. These eight patients had significantly higher peak CK (781.6 ± 695.4 vs. 254.5 ± 173.1; $p = 0.014$). Corresponding areas of LGE were noted in seven of these eight patients with a spatial extent significantly smaller than areas of high T2 SI (13.8 ± 8.2% vs. 21.6 ± 5.8%; $p = 0.018$).

LGE. The sensitivity, specificity, and diagnostic accuracy of LGE were 44%, 100%, and 71%, respectively. Posterolateral and inferior segments were most likely to be affected (73%) followed by anterior (36%) and septal (27%) seg-

JACC Vol. 45, No. 11, 2005
June 7, 2005:1815–22

Table 1. Characteristics of Myocarditis Patients

Patient #	Age (yrs)	Gender	Symptoms	EF	ECG	CA	CK*	TnT/I†	gRE	T2	LGE
1	38	M	ACP	56	ST-segment elevation: II, III, aVF T-negative: I, II	yes	2,267	3.6	3.8	2.0	yes
2	50	F	ACP	47	T-negative: I, II, aVL, aVF, V_2–V_6	yes	51	1.3	2.8	2.5	no
3	35	M	ACP	70	ST-segment elevation: I, II, aVF, V_5, V_6	yes	166	0.2	2.3	2.7	no
4	63	F	ACP, D	49	ST-segment elevation: I, II, aVL; T-negative: III	yes	429	70.1	10.1	2.3	no
5	39	F	D	26	ST-segment elevation: V_2–V_4 ST-segment depression: V_5, V_6 T-negative: I, aVL, V_1–V_3	yes	246	274	11.0	3.3	yes
6	26	M	ACP	65	ST-segment elevation: I, II, aVF, V_4–V_6	np	8.5	2.0	4.6	2.5	no
7	36	F	D, ACP	51	T-negative: III, aVF	yes	407	8.5	2.5	2.2	no
8	18	M	ACP	61	ST-segment elevation: II, III, aVF, V_5–V_6 T-negative: II, III, aVF, V_5–V_6	yes	168	41.0	4.4	3.0	yes
9	39	M	ACP	66	ST-segment elevation: V_4–V_6	yes	292	29.0	9.3	1.6	yes
10	38	M	ACP	63	ST-segment elevation: II, III, aVF, V_5–V_6	yes	213	15.7	9.0	2.2	no
11	37	M	ACP	63	ST-segment elevation: I, II, aVL, V_4–V_6	yes	1,100	103	5.1	2.9	yes
12	50	M	ACP, D	56	ST-segment elevation: I, II, aVF, V_5–V_6	yes	609	70.0	2.8	2.9	yes
13	66	F	ACP	63	T-negative: I, II, aVL, V_2–V_6	yes	547	1.8	4.4	2.2	no
14	29	M	P	42	Atrial fibrillation and J-point elevation: I, II, aVF, V_2–V_6	np	84	0.4	21.0	2.0	yes
15	17	M	ACP	62	ST-segment elevation: II, III, aVF, V_3–V_5 T-negative: I, aVL	np	443	39.0	9.3	2.0	no
16	23	M	P	57	ST-segment elevation: I, II, aVF T-negative: III	np	570	0.3	4.8	2.0	no
17	52	M	ACP	65	ST-segment elevation: V_1–V_6, II, III, aVF	yes	1,023	0.7	8.7	2.1	yes
18	84	F	ACP	74	T-negative: I, II, aVL, aVF, V_2–V_6 ST-segment elevation: V_1–V_2	yes	166	4.8	7.0	2.3	no
19	67	M	ACP, D	76	ST-segment elevation: II, III, aVF, V_4–V_6	yes	213	0.4	6.1	1.7	no
20	44	M	D	45	T-negative: II, III, aVF, V_5–V_6	yes	105	0.1	4.5	1.7	no
21	37	M	ACP	62	ST-segment elevation: II, III, aVF T-negative: II, III, aVF, V_5–V_6	yes	200	1.4	4.1	1.8	no
22	51	M	ACP	67	ST-segment elevation: V_2–V_5 T-negative: III	yes	349	1.6	7.9	2.1	yes
23	40	M	ACP	62	ST-segment elevation: I, II, aVL, V_5–V_6 T-negative: III	yes	594	1.0	10.0	2.2	yes
24	52	M	ACP	54	ST-segment elevation: II, III, aVF, V_2–V_6	yes	20	1.0	5.3	2.3	yes
25	67	F	ACP, D, P	26	Atrioventricular block III	yes	232	3.9	8.9	2.7	no

*Upper limit: 180 I/U; †Upper limit: <0.1 for TnT and <0.3 for TnI.

ACP = acute chest pain; CA = coronary angiography excluding significant coronary artery disease; CK = creatine kinase; D = dyspnea; EF = ejection fraction; gRE = global relative enhancement; LGE = late gadolinium enhancement; np = not performed; P = palpitation.

ments. One patient had LGE involving most of the right ventricular free wall as well. The number of these foci ranged from one to three (>1 in 64%); LGE was always located in the epicardial or midportion of the ventricular wall but never within the subendocardium (Fig. 4). Signal-to-noise ratio and contrast-to-noise ratio (in relation to normal myocardium) were 5.2 ± 2.3 and 3.5 ± 1.7, respectively. There was no significant difference between patients with and those without LGE regarding age ($p = 0.805$), time from onset to CMR ($p = 0.579$), ejection fraction ($p = 0.742$), duration of hospital stay ($p = 0.977$), peak CK ($p = 0.154$), troponin levels ($p = 0.262$), or ST-segment elevation ($p = 0.122$).

Combined approach. The best diagnostic performance was obtained when any two of the criteria obtained by the three techniques were positive (T2: SI ratio 1.9; gRE: SI ratio 4.0; LGE: presence of visually detectable bright areas) in the same patient. This approach had 76% sensitivity, 95.5% specificity, and 85% diagnostic accuracy (Fig. 5). Specifically, gRE and T2 were positive in 64%, LGE and T2 in 40%, LGE and gRE in 36%. The three sequences were all positive in 32% of the patients and in none of the controls.

DISCUSSION

gRE. In agreement with previous reports (2,7), we found that myocarditis patients have an increased gRE. Tissue hyperemia is an integral component of the acute inflammatory reaction of the myocardium, which may explain this finding. Diffuse myocyte injury can also increase the volume of distribution and subsequently the extraction fraction of extracellular compounds like gadolinium-DTPA, resulting in abnormal myocardial enhancement. This concept is supported by the results of Almenar et al. (8) who found a significant correlation between gRE and the presence of

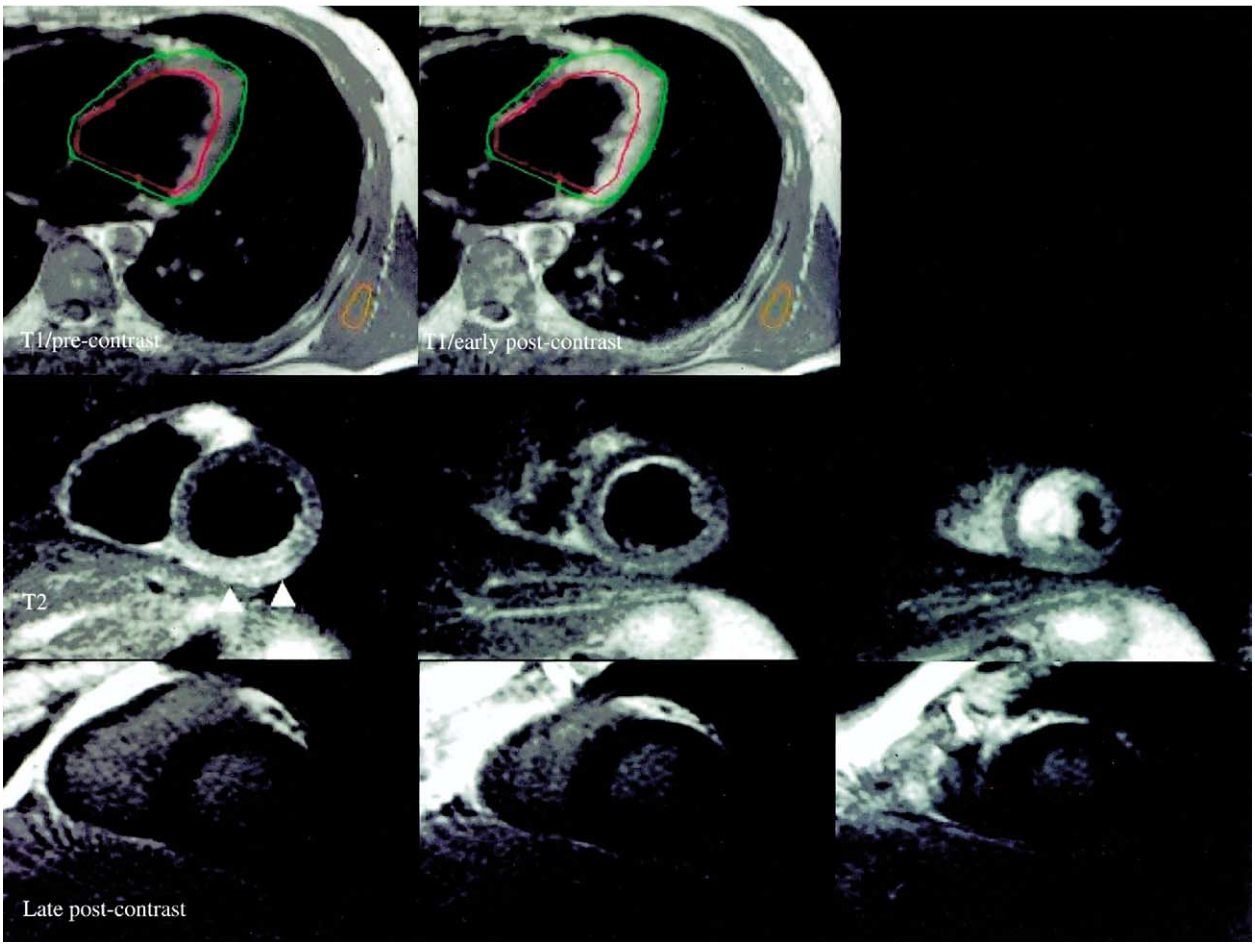

Figure 2. Cardiovascular magnetic resonance findings in Patient #21. **(Top)** Pre- and postcontrast axial T1-weighted spin echo images of the same slice. Global relative enhancement was elevated (4.1). **(Middle)** T2-weighted images in three short-axis slices. Note the posterolateral focal high T2 signal **(arrowheads)** in the basal slice with apparent focal increase in myocardial thickness. **(Bottom)** Corresponding late enhancement images: no evidence of late gadolinium enhancement.

myocyte injury after heart transplantation. The diagnostic performance of gRE to detect myocarditis in our series was lower than that previously reported (7). Two reasons may explain this finding: first gRE measurements depend on the assumption that the skeletal muscles exhibit a "normal" pattern of gadolinium enhancement. This assumption may not hold true in some cases when the inflammatory process extends to involve skeletal muscles as well (9). In such a case, gRE will be "pseudonormalized" even in the presence of abnormal myocardial enhancement. Indeed, patients with negative gRE showed abnormally increased skeletal muscle enhancement (22%). Second, early in the course of myocarditis, the inflammatory process is predominantly focal (10), which could result in a negative gRE. The fact that our patients were studied at an average of six days after the onset of cardiac symptoms supports this notion.

LGE. The exact pathophysiological grounds of LGE in myocarditis are still under investigation. Myocardial necrosis in the acute phase appears to play a major role, but also severe edema could sufficiently increase the volume of distribution of gadolinium to cause visually detectable SI changes. The absence of a significant correlation between LGE and troponin release is not surprising and may reflect one of two possibilities: first, it could be that—at least in some patients—these foci represent replacement fibrosis from previous subclinical episodes of myocarditis, which would then result in gadolinium accumulation similar to that in a chronic myocardial scar (11) in the absence of elevated troponin. Second, diffuse myocarditis could result in troponin release (12) without LGE.

The incidence of LGE in myocarditis is a controversial issue. The 44% incidence we observed is in perfect agreement with the 44% found by Rieker et al. (5). Kuhl et al. (13), using antimyosin scintigraphy, observed focal myocardial cell damage in 55%. Mahrholdt et al. (3), however, reported a much higher incidence of LGE (88%). The reason for discrepancy may be related to differences in patient populations or study designs. Whereas we and Rieker et al. (5) studied patients in the acute phase of the disease, Kuhl et al. (13) and Mahrholdt et al. (3) included a significant fraction of patients with "healed" myocarditis. Moreover, the pattern of myocardial injury is influenced by the virus type (14). This could partially explain differences between our results and those of Mahrholdt et al. (3) where

JACC Vol. 45, No. 11, 2005
June 7, 2005:1815–22

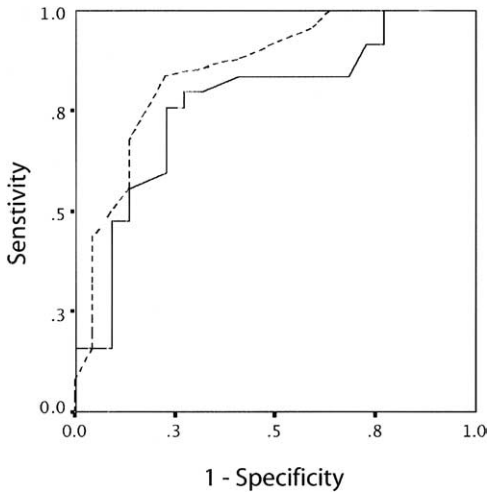

Figure 3. Receiver operating characteristic curves for global relative enhancement **(solid line)** and global relative T2 signal **(broken line)**.

parvovirus was identified as a causative agent in a significant fraction of patients. Parvovirus is unique in selectively injuring the endothelial cells resulting in microinfarcts (15), which may be detectable as LGE.

The classical pathological description of myocarditis, the so-called Dallas criteria (16), can also provide insight into the incidence of LGE in myocarditis. Active myocarditis is defined as inflammatory reaction with myocyte injury. This is expected to result in LGE secondary to the focal expansion of the extracellular space. In borderline myocarditis, however, myocyte injury is lacking, and it is in this group of patients that LGE may not be observed.

Finally, the clinical significance of LGE in myocarditis is yet to be defined. We did not find a significant correlation between LGE and markers of disease severity such as ejection fraction or duration of hospital stay. Nevertheless, the finding that there are two subgroups of myocarditis patients—those with and those without LGE—holds promise that LGE may provide additional significant prognostic information. Specifically, we propose two hypotheses which, if proven to be true, could define an exciting role of CMR to risk-stratify myocarditis patients. First, the link between myocarditis and the later development of dilated cardiomyopathy is well-established (17). Yet only a fraction of myocarditis patients progress to dilated cardiomyopathy. McCrohon et al. (18) found that a group of dilated cardiomyopathy patients exhibit a pattern of focal enhancement similar to the one we observed in myocarditis patients. It seems intriguing to postulate that those myocarditis patients with positive LGE may be more likely to develop dilated cardiomyopathy. Second, the border zone between scar tissue and healthy myocardium is a known substrate for electrical instability. The question of whether myocarditis

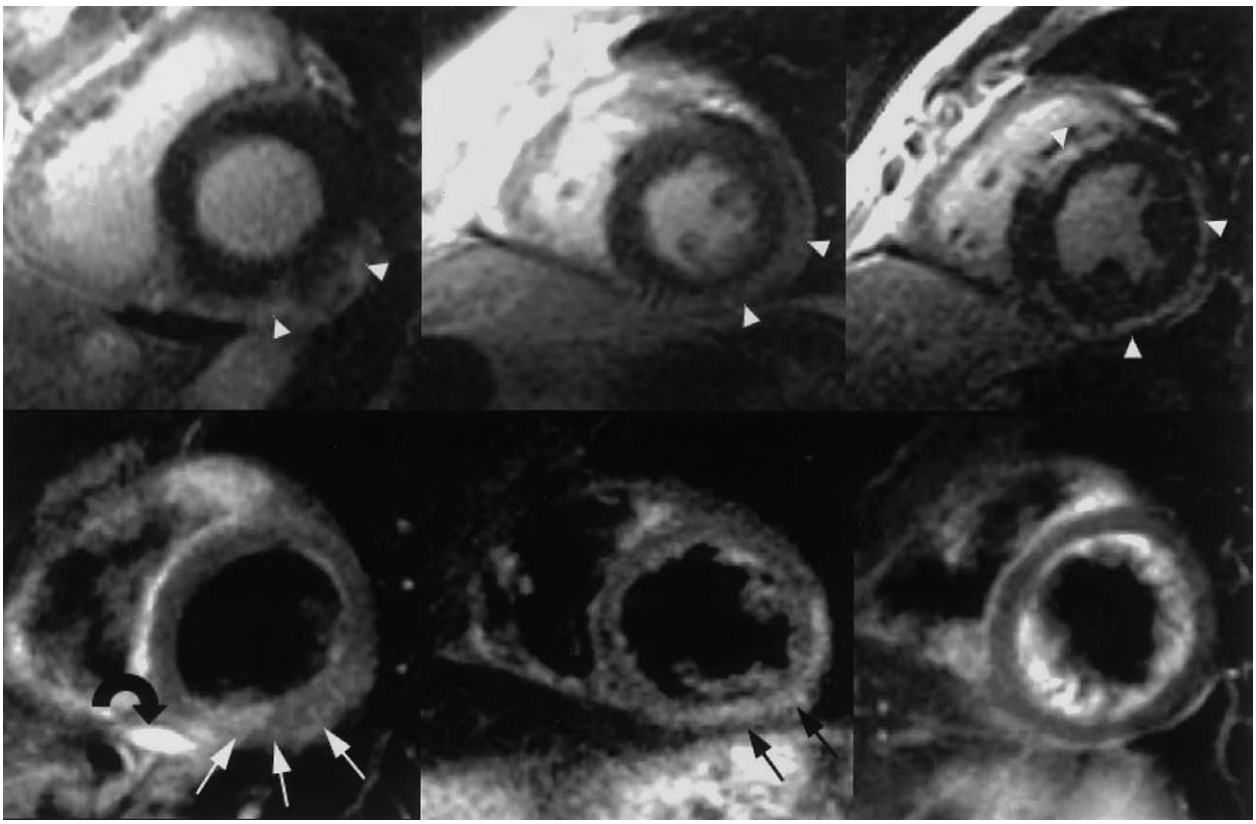

Figure 4. Representative images from 3 patients (#8, #12, and #14 from **left to right**, respectively). **(Top)** Late gadolinium enhancement (LGE). **(Bottom)** T2-weighted. Focal high T2 signal **(thin arrows)** corresponds to areas of LGE **(arrowheads)** in Patients #8 and #12 but not in Patient #14. Note the predominant epicardial distribution of high T2 signal in Patient #12. Small pericardial effusion is seen in Patient #8 **(thick curved arrow)**.

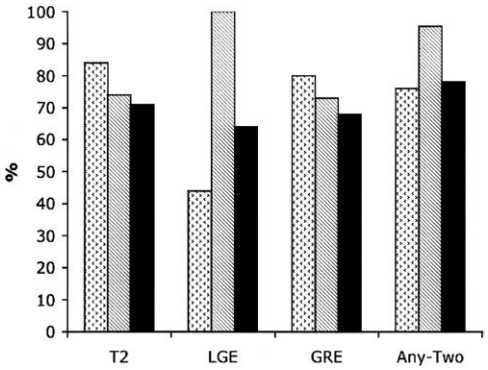

Figure 5. Diagnostic performance of T2, late gadolinium enhancement (LGE), and global relative enhancement (GRE) as compared to the "any-two" approach. **Spotted bars** = sensitivity; **diagonal striped bars** = specificity; **solid bars** = diagnostic accuracy.

patients with LGE would be, thus, more liable to develop ventricular arrhythmias deserves to be a research focus.

T2-weighted imaging. The most likely explanation for the T2 abnormalities we observed in myocarditis patients is the water-sensitive characteristics of this technique, which allows the detection of tissue edema, a substantial feature of the acute inflammatory reaction in the myocardium (19). Other than expected, a focal increase in T2 signal was not always associated with LGE. Although there was a significant correlation between the two findings, many patients had LGE or T2 abnormality only (Figs. 2 and 4). It seems that the evolution/resolution pattern of myocardial edema might be different from that of LGE. Accordingly, at a particular "time window" after the symptoms, only one of the two is detectable. One other possibility would be that focal edema marks a less severe form of myocardial injury, which then may or may not progress to actual necrosis in a cascade similar to that of acute ischemic injury (20). Another unexpected finding was the absence of a significant correlation between the global myocardial T2 signal and global myocardial enhancement. One would expect that tissue edema should increase both myocardial T2 SI as well as the volume of distribution of gadolinium-DTPA with subsequent increase in myocardial enhancement. It could be that global myocardial edema results in a degree of capillary compression hindering abnormal contrast enhancement (21), which then starts to increase with the resolution of edema. This differential time course is supported by the finding that only T2 abnormalities significantly correlated with laboratory markers of acute myocardial injury.

Clinical implications. The "any-two" approach has the potential to increase the diagnostic performance of CMR in the clinical setting as well as in multicenter trials. A significant fraction of acute myocarditis patients present with a clinical picture mimicking that of acute myocardial infarction representing a diagnostic challenge (22,23). Acute myocardial infarction is characterized by focal transmural high T2 signal and subendocardial or transmural LGE (24). This is different from the subepicardial LGE of myocarditis with no focal high T2 signal in the majority of cases.

Study limitations and technical considerations. The parameter that should be used as the "gold standard" to identify myocarditis remains a controversial issue. Some investigators used endomyocardial biopsy to identify the disease (6,22,25), and many others relied instead on a combination of clinical, laboratory, ECG, and angiographic findings (7,23,26,27). We have also relied on this later approach for the following reasons: first, the sensitivity of endomyocardial biopsy to identify myocarditis is limited possibly secondary to the focal nature of the disease (28). Using polymerase chain reaction to identify viral genomes in the myocardium, disagreement with the results of myocardial biopsy was noted in 50% of the cases (29). This likely explains the discrepancy between the low incidence of biopsy-identified myocarditis in many trials and the clinical or postmortem incidence of the disease (25,27,30). Second, the majority of our patients were young with an acute, often fairly unstable presentation; thus, we did not want to subject this group of patients to unnecessary invasive procedures.

Although there is a theoretical possibility that patients in our study suffered from undetectable coronary heart disease, the absence of any coronary stenosis makes an ischemic injury unlikely. In the four patients without catheter verification of the absence of coronary stenosis, neither the risk profile nor other clinical criteria or injury morphology indicated any evidence for coronary heart disease. But, more importantly, the pattern of either a complete lack of scarring or a focal injury distribution not attributable to epicardial coronary artery occlusion makes this very unlikely. Late gadolinium enhancement images were acquired using a slice thickness of 15 mm, which may have reduced the sensitivity to detect small lesions. This was chosen to match the slice thickness of T2 images to maximize the signal-to-noise ratio of this technique. To reduce the possibility of missing small lesions, we acquired additional LGE images in long-axis slices.

Conclusions. A combined CMR approach using T2-weighted imaging, early and LGE provides a high diagnostic accuracy and is a useful tool in the diagnosis and assessment of patients with suspected acute myocarditis.

Acknowledgments

The authors would like to thank Kerstin Kretschel, Evelyn Polzin, and Ursula Wagner for their technical assistance, and Melanie Bochmann for her help in recruiting patients.

Reprint requests and correspondence: Dr. Jeanette Schulz-Menger, Wiltbergstr. 50, D-13125, Berlin, Germany. E-mail: schulzmenger@fvk-berlin.de.

REFERENCES

1. Feldman AM, McNamara D. Myocarditis. N Engl J Med 2000;343: 1388–98.

2. Friedrich MG, Strohm O, Schulz-Menger J, Marciniak H, Luft FC, Dietz R. Contrast media-enhanced magnetic resonance imaging visualizes myocardial changes in the course of viral myocarditis. Circulation 1998;97:1802–9.
3. Mahrholdt H, Goedecke C, Wagner A, et al. Cardiovascular magnetic resonance assessment of human myocarditis: a comparison to histology and molecular pathology. Circulation 2004;109:1250–8.
4. Gagliardi MG, Bevilacqua M, Di Renzi P, Picardo S, Passariello R, Marcelletti C. Usefulness of magnetic resonance imaging for diagnosis of acute myocarditis in infants and children, and comparison with endomyocardial biopsy. Am J Cardiol 1991;68:1089–91.
5. Rieker O, Mohrs O, Oberholzer K, Kreitner KF, Thelen M. Cardiac MRI in suspected myocarditis (in German). Rofo Fortschr Geb Rontgenstr Neuen Bildgeb Verfahr 2002;174:1530–6.
6. Lieberman EB, Hutchins GM, Herskowitz A, Rose NR, Baughman KL. Clinicopathologic description of myocarditis. J Am Coll Cardiol 1991;18:1617–26.
7. Laissy JP, Messin B, Varenne O, et al. MRI of acute myocarditis: a comprehensive approach based on various imaging sequences. Chest 2002;122:1638–48.
8. Almenar L, Igual B, Martinez-Dolz L, et al. Utility of cardiac magnetic resonance imaging for the diagnosis of heart transplant rejection. Transplant Proc 2003;35:1962–4.
9. Greaves K, Oxford JS, Price CP, Clarke GH, Crake T. The prevalence of myocarditis and skeletal muscle injury during acute viral infection in adults: measurement of cardiac troponins I and T in 152 patients with acute influenza infection. Arch Intern Med 2003;163:165–8.
10. Herskowitz A, Wolfgram LJ, Rose NR, Beisel KW. Coxsackievirus B3 murine myocarditis: a pathologic spectrum of myocarditis in genetically defined inbred strains. J Am Coll Cardiol 1987;9:1311–9.
11. Wu E, Judd RM, Vargas JD, Klocke FJ, Bonow RO, Kim RJ. Visualisation of presence, location, and transmural extent of healed Q-wave and non–Q-wave myocardial infarction. Lancet 2001;357: 21–8.
12. Smith SC, Ladenson JH, Mason JW, Jaffe AS. Elevations of cardiac troponin I associated with myocarditis. Experimental and clinical correlates. Circulation 1997;95:163–8.
13. Kuhl U, Lauer B, Souvatzoglu M, Vosberg H, Schultheiss HP. Antimyosin scintigraphy and immunohistologic analysis of endomyocardial biopsy in patients with clinically suspected myocarditis—evidence of myocardial cell damage and inflammation in the absence of histologic signs of myocarditis. J Am Coll Cardiol 1998;32:1371–6.
14. Bowles NE, Ni J, Kearney DL, et al. Detection of viruses in myocardial tissues by polymerase chain reaction. Evidence of adenovirus as a common cause of myocarditis in children and adults. J Am Coll Cardiol 2003;42:466–72.
15. Bultmann BD, Klingel K, Sotlar K, et al. Fatal parvovirus B19-associated myocarditis clinically mimicking ischemic heart disease: an endothelial cell-mediated disease. Hum Pathol 2003;34:92–5.
16. Aretz HT, Billingham ME, Edwards WD, et al. Myocarditis. A histopathologic definition and classification. Am J Cardiovasc Pathol 1987;1:3–14.
17. Sole MJ, Liu P. Viral myocarditis: a paradigm for understanding the pathogenesis and treatment of dilated cardiomyopathy. J Am Coll Cardiol 1993;22:99A–105A.
18. McCrohon JA, Moon JC, Prasad SK, et al. Differentiation of heart failure related to dilated cardiomyopathy and coronary artery disease using gadolinium-enhanced cardiovascular magnetic resonance. Circulation 2003;108:54–9.
19. Sekiguchi M, Yu ZX, Hasumi M, Hiroe M, Morimoto S, Nishikawa T. Histopathologic and ultrastructural observations of acute and convalescent myocarditis: a serial endomyocardial biopsy study. Heart Vessels Suppl 1985;1:143–53.
20. Jennings RB, Schaper J, Hill ML, Steenbergen C, Jr., Reimer KA. Effect of reperfusion late in the phase of reversible ischemic injury. Changes in cell volume, electrolytes, metabolites, and ultrastructure. Circ Res 1985;56:262–78.
21. Manciet LH, Poole DC, McDonagh PF, Copeland JG, Mathieu-Costello O. Microvascular compression during myocardial ischemia: mechanistic basis for no-reflow phenomenon. Am J Physiol 1994;266: H1541–50.
22. Kuhl U, Pauschinger M, Bock T, et al. Parvovirus B19 infection mimicking acute myocardial infarction. Circulation 2003;108:945–50.
23. Sarda L, Colin P, Boccara F, et al. Myocarditis in patients with clinical presentation of myocardial infarction and normal coronary angiograms. J Am Coll Cardiol 2001;37:786–92.
24. Abdel-Aty H, Zagrosek A, Schulz-Menger J, et al. Delayed enhancement and T2-weighted cardiovascular magnetic resonance imaging differentiate acute from chronic myocardial infarction. Circulation 2004;109:2411–6.
25. Mason JW, O'Connell JB, Herskowitz A, et al. A clinical trial of immunosuppressive therapy for myocarditis. The Myocarditis Treatment Trial Investigators. N Engl J Med 1995;333:269–75.
26. Miklozek CL, Crumpacker CS, Royal HD, Come PC, Sullivan JL, Abelmann WH. Myocarditis presenting as acute myocardial infarction. Am Heart J 1988;115:768–76.
27. Karjalainen J, Heikkila J. Incidence of three presentations of acute myocarditis in young men in military service. A 20-year experience. Eur Heart J 1999;20:1120–5.
28. Chow LH, Radio SJ, Sears TD, McManus BM. Insensitivity of right ventricular endomyocardial biopsy in the diagnosis of myocarditis. J Am Coll Cardiol 1989;14:915–20.
29. Martin AB, Webber S, Fricker FJ, et al. Acute myocarditis. Rapid diagnosis by PCR in children. Circulation 1994;90:330–9.
30. Lie JT. Diagnostic histology of myocardial disease in endomyocardial biopsies and at autopsy. Pathol Annu 1989;24:255–93.

Correspondence

Letter Regarding Article by Sharkey et al, "Acute and Reversible Cardiomyopathy Provoked by Stress in Women From the United States"

To the Editor:

We read with interest the article by Sharkey et al[1] describing the clinical and cardiovascular magnetic resonance (CMR) features of the apical ballooning cardiomyopathy. We have a few concerns about the interpretation of the CMR findings in the article as well as in the related editorial.[2]

The authors suggest that the lack of mid-wall delayed enhancement in their series should exclude myocardial inflammation as a possible underlying mechanism explaining their findings. We have recently investigated the diagnostic performance of various CMR techniques to identify acute myocarditis[3] and found that delayed enhancement occurs in only 44% of these patients, whereas T_2-weighted abnormalities reflecting myocardial edema and early global enhancement are noted in >80% of the cases. For this reason, we believe that the CMR approach of the authors does not allow exclusion of myocardial inflammation in those cases with certainty.

The related editorial suggested that the lack of delayed enhancement excludes the presence of myocardial edema in these patients. We have shown in the same report[3] that global or focal myocardial edema is frequently observed in the absence of delayed enhancement. We have also previously shown that chronic myocardial scars exhibit delayed enhancement without myocardial edema.[4] Furthermore, we recently investigated a female patient with "taku-tsubo" cardiomyopathy and found overt regional high T_2 signal intensity without any evidence of delayed enhancement. Accordingly, we believe that no firm conclusion could be drawn about the presence or absence of myocardial edema in these patients in the absence of T_2-weighted imaging experiments.

The editorial also suggested that "gadolinium-enhanced MRI . . . failed to detect regional T_2 enhancement which has been shown to detect myocardial inflammation and necrosis." We have 2 concerns about this statement: First, the enhancement effect of gadolinium is mainly caused by its effect on T_1 relaxation time. Second, the article cited to support the statement[5] did not include any T_2-weighted imaging experiments.

Despite these concerns, we congratulate the authors on their report, which provides many new insights into this rare and yet clinically relevant and novel cardiomyopathy.

Hassan Abdel-Aty, MD
Rainer Dietz, MD
Jeanette Schulz-Menger, MD
Franz-Volhard-Klinik
Kardiologie
Universitätmedizin Berlin
Berlin, Germany

1. Sharkey SW, Lesser JR, Zenovich AG, Maron MS, Lindberg J, Longe TF, Maron BJ. Acute and reversible cardiomyopathy provoked by stress in women from the United States. *Circulation*. 2005;111:472–479.
2. Dec GW. Recognition of the apical ballooning syndrome in the United States. *Circulation*. 2005;111:388–390.
3. Abdel-Aty H, Boyé P, Zagrosek A, Wassmuth R, Kumar A, Messroghli D, Bock P, Dietz R, Friedrich MG, Schulz-Menger J. Diagnostic performance of cardiovascular magnetic resonance in patients with suspected acute myocarditis: comparison of different approaches. *J Am Coll Cardiol*. 2005;45:1815–1822.
4. Abdel-Aty H, Zagrosek A, Schulz-Menger J, Taylor AJ, Messroghli D, Kumar A, Gross M, Dietz R, Friedrich MG. Delayed enhancement and T2-weighted cardiovascular magnetic resonance imaging differentiate acute from chronic myocardial infarction. *Circulation*. 2004;109:2411–2416.
5. Mahrholdt H, Goedecke C, Wagner A, Meinhardt G, Athanasiadis A, Vogelsberg H, Fritz P, Klingel K, Kandolf R, Sechtem U. Cardiovascular magnetic resonance assessment of human myocarditis: a comparison to histology and molecular pathology. *Circulation*. 2004;109:1250–1258.

Response

We appreciate the interest of Dr Abdel-Aty and colleagues in our work.[1] These investigators raise the question of whether the absence of postgadolinium-delayed hyperenhancement with T_1-weighted cardiac MRI (CMR) reported in our patients with stress ("tako-tsubo") cardiomyopathy failed to exclude myocardial inflammation because T_2-weighted imaging data were not presented.[1]

For several reasons, we believe that is a highly unlikely scenario for myocarditis to be the undetected and underlying mechanism responsible for stress cardiomyopathy in such a sizeable patient cohort. T_1-weighted imaging is the preferred and established technique to assess myocardial viability and exclude infarction and necrosis,[2] which was in fact the priority in this particular study. Indeed, 21 of our 22 study patients showed myocardial viability without evidence of delayed hyperenhancement (the other patient had an apical infarct caused by a previous cardiac arrest).

In our group of severely symptomatic patients with stress cardiomyopathy, we did initially perform some T_2-weighted scans (in addition to T_1-weighted imaging), which are preferable for the interrogation of myocardial edema (consistent with myocarditis). Of the 22 patients, 9 had technically adequate T_2-weighted images, and 2 of these (22%) had T_2-weighted scans consistent with myocardial edema. We found no difference, however, in clinical profile (including premonitory vital infection and laboratory evidence of systemic inflammation) between the 2 patients with myocardial edema and the 7 patients without this finding; furthermore, 1 of the 2 patients with myocardial edema had a myocardial biopsy that was negative for myocardial inflammation. Finally, and perhaps most importantly, myocarditis is not particularly consistent with the clinical profile evident in each of our patients with stress cardiomyopathy (ie, rapidly reversible apical ballooning with hypercontractile base involving all 3 vascular territories). Therefore, although we appreciate the reasonable insights of Abdel-Aty et al, we do not believe there are any data to substantiate an important role for myocarditis in our patients with stress cardiomyopathy.*

*Original coauthor Dr Jana Lindberg did not participate in the drafting of this letter.

Scott W. Sharkey, MD
John R. Lesser, MD
Andrey G. Zenovich, MSc
Terrence F. Longe, MD
Barry J. Maron, MD
Minneapolis Heart Institute Foundation
Minneapolis, Minn

Martin S. Maron, MD
Tufts-New England Medical Center
Boston, Mass

1. Sharkey SW, Lesser JR, Zenovich AG, Maron MS, Lindberg J, Longe TF, Maron BJ. Acute and reversible cardiomyopathy provoked by stress in women from the United States. *Circulation*. 2005;111:472–479.
2. Kim RJ, Fieno DS, Parrish TB, Harris K, Chen EL, Simonetti O, Bundy J, Finn JP, Klocke FJ, Judd RM. Relationship of MRI delayed contrast enhancement to irreversible injury, infarct age, and contractile function. *Circulation*. 1999;100:1992–2002.

2.2. Myokardiale Mitbeteiligung bei Systemerkrankungen

Es war nahe liegend zu untersuchen, ob kontrastverstärkte Techniken auch bei myokardialen Mitbeteiligungen im Rahmen von Systemerkrankungen die Diagnose erleichtern können. Erste Untersuchungen bei Patienten mit gesicherter systemischer Sarkoidose konnten im Jahre 2000 veröffentlicht werden.[58] Da bei Patienten mit Sarkoidose eine myokardiale Mitbeteiligung die Prognose deutlich verschlechtert, insbesondere wenn dies bereits zu einer Einschränkung der linksventrikulären Funktion geführt hat, erschien es essentiell zu überprüfen, ob die Diagnose bei noch erhaltener Pumpfunktion gestellt werden kann. In einer kürzlich publizierten Studie konnten wir die frühe Kontrastmittelanreicherung bei Sarkoidosepatienten mit noch normaler Funktion zeigen. Eine Aufschlüsselung der untersuchten Parameter erbrachte, dass die Veränderung der linksventrikulären Ejektionsfraktion nur in 8% zur Diagnose geführt hätte, die frühe KM-Anreicherung dagegen in 83%, das LHE in 23%.[59]

Der Verdacht auf eine myokardialen Beteiligung bei Amyloidose wird im klinischen Alltag anhand des Vorliegens einer linksventrikulären Hypertrophie und einer auffälligen Myokardstruktur in der Echokardiographie (ein als „sparkling“ bezeichnetes Bildmuster) geäußert. Allerdings haben die genannten Parameter eine nicht zufriedenstellende Sensitivität und Spezifität. Unter Einsatz der kontrastverstärkten MRT wurde ein ungewöhnliches LHE beschrieben, das die nichtinvasive Diagnose deutlich erleichterte.[60] Dieses Muster stellt einen Teil unseres Ansatzes dar, der wiederum neben der funktionellen Beschreibung des linken Ventrikels einschließlich der Quantifizierung der linksventrikulären Hypertrophie auch die Analyse der myokardialen Textur umfasst. Dabei kam eine

Kombination aus T_2-gwichteten und T_1-gewichteten Sequenzen zur Anwendung, die sowohl die frühe als auch die späte KM-Anreicherung erfasste. Auffällig war weiterhin das gehäufte Auftreten eines Perikardergusses, dagegen konnte die in der Literatur allerdings mit älteren Techniken beschriebene Verdickung der Vorhofwände nicht nachvollzogen werden. Diese Ergebnisse wurden 2006 als Abstrakt im Journal for Cardiovascular Magnetic Resonance veröffentlicht.[61] Wir gehen davon aus, dass der vorgestellte Ansatz die Sicherheit in der Diagnose verbessern wird. Dies muss in prospektiven Studien überprüft werden.

ELSEVIER

Magnetic Resonance Materials in Physics, Biology and Medicine 11 (2000) 82–83

MAGMA

Magnetic Resonance Materials in Physics, Biology and Medicine

www.elsevier.com/locate/magma

Visualization of cardiac involvement in patients with systemic sarcoidosis applying contrast-enhanced magnetic resonance imaging

Jeanette Schulz-Menger *, Oliver Strohm, Rainer Dietz, Matthias G. Friedrich

Franz-Volhard-Klinik, Working Group 'Cardiac MRI' Charite Campus Buch, Wiltbergstrasse 50, 13125 Berlin, Germany

Received 4 August 2000; accepted 4 August 2000

Keywords: Cardiac; Sarcoidosis; Magnetic resonance imaging

1. Background

The diagnosis of the cardiac involvement in patients with known systemic sarcoidosis is difficult because of the low sensitivity of myocardial biopsy. Applying contrast-enhanced Magnetic resonance imaging (MRI), it is possible to detect tissue changes associated with inflammation.

2. Patients and methods

We applied contrast-enhanced MRI in six patients with proven systemic sarcoidois and suspected cardiac involvement as defined by the presence of typical symptoms (dyspnea, fatigue) and arrhythmias documented by ECG.Figs. 1 and 2

We performed the MRI-studies on conventional MRI systems (1.0 T; Siemens-Expert; Siemens AG, Erlangen, Germany and 1.5 T Signa CV/i; GE; Milwaukee, USA, respectively) using a body coil. We used standard T1-weighted multislice spin-echo sequences (TE 30 ms; TR 480-725 ms; slice thickness 6 mm) in an axial and short-axis orientation before and after application of 0.1 mmol/kg Gd-DTPA (Magnevist®, Schering AG; Berlin, Germany). The relative contrast enhancement was calculated using the signal intensity changes of the myocardium and the skeletal muscle.

Results were compared with eight patients with proven systemic sarcoidois but without cardiac symptoms or arrhythmias, and to nine healthy volunteers.

3. Results

We detected a patchy accumulation of contrast media in the hearts of the patients with evidence for cardiac involvement, but not in others. The focal relative signal enhancement was significantly higher in patients with suspected myocardial involvement (7.0 ± 1.7) than in patients without any clinical evidence for cardiac involvement (2.2 ± 0.3, $P < 0.01$). Furthermore, the global myocardial contrast enhancement was also significantly higher (6.3 ± 2.0) than in

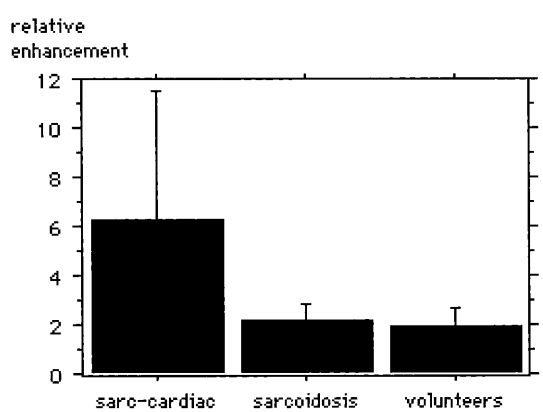

Fig. 1. Mean values of the relative enhancement in patients with proven sarcoidosis with (sarccardiac) and without (sarcoidosis) evidence for cardiac involovement as compared with volunteers.

* Corresponding author. Tel.: +49-30-94172593; fax: +49-30-94172560.

E-mail address: schulzmenger@fvk-berlin.de (J. Schulz-Menger).

PII: S1352-8661(00)00123-X

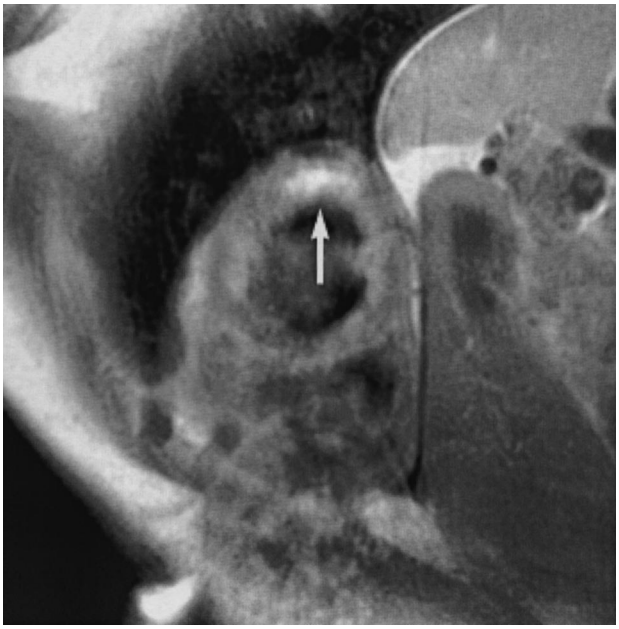

Fig. 2. Short axis view T1-weighted spin echo sequence after contrast-application with a visualization of the localized contrast enhancement.

patients without any clinical evidence for cardiac involvement (2.2 ± 0.3, $P < 0.01$). The difference of patients without cardiac involvement to controls (1.9 ± 0.2) was not significant.

Follow-up studies over 2 years (after 1, 6, 12 and 24 months) showed a normalization of the relative enhancement in five of six affected patients undergoing steroid medication. In one patient there were changing enhancement patterns closely related to the clinical picture with ongoing symptoms.

4. Discussion

Magnetic Resonance Imaging reveals an increased accumulation of contrast media in patients with systemic sarcoidosis and clinical evidence for cardiac involvement. This was present in focal areas, but also when quantified for the whole myocardium.

Thus, MRI may be helpful for guiding antiinflammatory therapy. Further studies in larger patient groups are necessary to assess the clinical applicability in patients with sarcoidosis.

5. Summary

Contrast-enhanced MRI may serve as a sensitive noninvasive tool for the detection and follow-up of myocardial involvement in patients with systemic sarcoidosis.

SCIENTIFIC LETTER

Patterns of myocardial inflammation and scarring in sarcoidosis as assessed by cardiovascular magnetic resonance

J Schulz-Menger, R Wassmuth, H Abdel-Aty, I Siegel, A Franke, R Dietz, M G Friedrich

Heart 2006;**92**:399–400. doi: 10.1136/hrt.2004.058016

Sarcoidosis is a multisystemic disease. Cardiac involvement has a strong impact on the patient's prognosis but is difficult to detect in vivo. This is reflected by the high rate of unexpected cardiac sarcoidosis in postmortem studies. In a study of patients with necropsy proven cardiac sarcoidosis, it was established or suspected before death in only 45%, with cardiac involvement being fatal in 67%.[1] Cardiac sarcoidosis is mostly identified by impaired systolic left ventricular (LV) function, a feature of more advanced disease.

Cardiovascular magnetic resonance (CMR) detects tissue inflammation and fibrosis. The focus of our study was to identify cardiac tissue changes in patients with systemic sarcoidosis by using CMR.

PATIENTS AND METHODS

Between 1999 and 2003, we studied 31 patients with proven systemic sarcoidosis (mean (SD) age 46 (2) years; 19 men). Twelve patients (48 (4) years; 10 men) had evidence for cardiac involvement as defined by typical symptoms and documented arrhythmias. In eight patients with chest pain, risk factors for coronary artery disease, or age above 30 years, coronary artery disease was excluded by coronary angiography. The remaining four patients were three men and one woman (25, 30, 29, and 30 years old, respectively). All of them were non-smokers, had a normal serum lipid profile, and had no family history of coronary artery disease. We also investigated 19 patients with sarcoidosis and without cardiac symptoms (45 (3) years; 15 men). Sarcoidosis was confirmed by biopsy in all cases, taken from either the lungs (n = 27) or the skin (n = 4).

Nine healthy subjects served as controls (38 (8) years, seven men).

We used a dedicated cardiovascular MRI system (Signa CV/*i*, 1.5 T; GE Medical Systems, Milwaukee, Wisconsin, USA) with a four element phased array coil or with a body coil. To visualise inflammatory myocardial tissue changes, we assessed global and focal myocardial contrast enhancement in T1 weighted multislice fast spin echo images obtained before and within the first four minutes after application of 0.1 mmol/kg gadolinium-diethylenetriaminepentaacetic acid (Gd-DTPA) (Magnevist; Schering AG, Berlin, Germany), as described elsewhere.[2]

For the detection of scar tissue, we assessed delayed contrast accumulation with a multislice T1 weighted inversion recovery prepared gradient echo sequence (short axis, inversion time individually optimised, repetition time 5.5 ms, echo time 1.4 ms, slice thickness 10 mm, and no gap) 15 minutes after an additional administration of 0.1 mmol/kg body weight Gd-DTPA.

We studied cardiac function with a steady state free precession gradient echo cine sequence (contiguous set of short axis images, slice thickness 10 mm, no gap, and three long axis images). CMR was performed at baseline and in the patients with suspected cardiac involvement after six and 12 months.

Global and focal early relative enhancement was quantified as previously described[2]. Focal scar lesions were identified by visual assessment. LV volumes, mass, and function were quantified by manually tracing the LV endocardial and epicardial borders at end diastole and end systole.

All values are presented as mean (SD). A probability value of $p < 0.05$ was considered significant. Data were analysed with the *t* test by standard software (StatView 4.5; Abacus Concepts, Berkeley, California, USA).

RESULTS

As defined by the inclusion criteria, all patients with sarcoidosis with suspected cardiac involvement had ventricular arrhythmias (bigeminy, trigeminy, or both); eight had atrial arrhythmias (two with atrioventricular bundle brunch block), five had atrial fibrillation or atrial flutter, and one had atrial tachycardia) and dyspnoea (six were in New York Heart Association functional class II, five in class III, and one in class IV).

Functional analysis showed normal values in all patients. No significant difference in the preserved LV ejection fraction between all groups was observed. We detected wall motion abnormalities in two patients and a posterior aneurysm in one patient. Global relative enhancement did not differ between volunteers and sarcoidosis patients without suspected cardiac involvement (1.9 (0.3) *v* 2.5 (0.2), not significant) but was significantly increased in patients with suspected cardiac involvement compared with patients without cardiac involvement (5.5 (1.0) *v* 2.5 (0.2), $p < 0.0002$). Focal areas of relative enhancement were detected in eight patients with suspected cardiac involvement (9.2 (2.8) *v* 3.0 (0.3) in volunteers, $p < 0.002$).

Follow up after six and 12 months in 12 patients showed a normalisation of relative enhancement during steroid treatment in 10 patients, according to an improvement of the clinical status in these patients. Focal delayed enhancement was present in three patients. In two of them the LV ejection fraction did not normalise and a clinical worsening was recognised during tapering off of steroids. Figure 1 shows the incidence of each pathological finding.

DISCUSSION

We showed that CMR can visualise myocardial contrast enhancement in patients with sarcoidosis and preserved LV function. This study confirms earlier reports on early contrast enhancement in myocardial inflammation and in patients with sarcoidosis.[2–5] Global relative enhancement was not altered in patients with proven sarcoidosis but without evidence for cardiac involvement but was significantly higher in patients with evidence for cardiac involvement. The incidence of delayed enhancement was low.

Our results extend the existing knowledge on CMR in sarcoidosis by three new aspects: firstly, we used quantitative global relative enhancement data to reduce investigator dependent bias. Secondly, we included patients with preserved

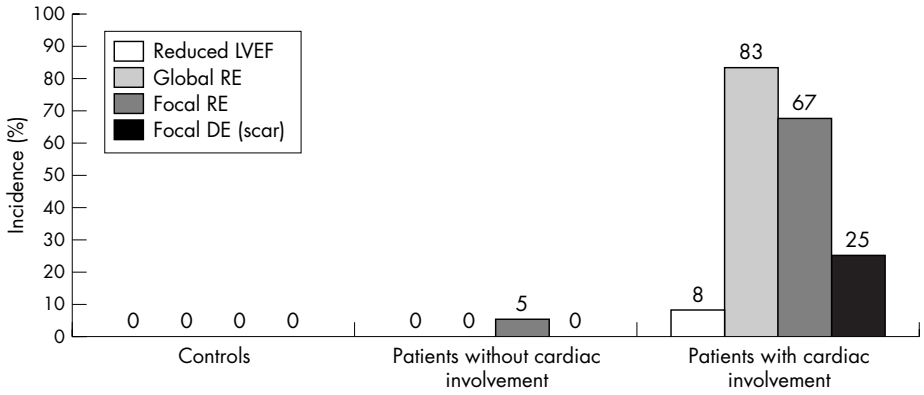

Figure 1 Incidence of pathological findings. DE, delayed enhancement; LVEF, left ventricular ejection fraction; RE, relative enhancement.

LV function. Thirdly, we assessed the incidence of late enhancement. Remarkably, patients with delayed enhancement had an impaired prognosis—that is, worsening of the ejection fraction over time and symptoms during tapering off of steroids.

In summary, the presented method potentially improves the diagnostic capabilities for early assessment of myocardial sarcoidosis. It has the potential to identify the type of myocardial injury (inflammation or fibrosis) and thus provide means for earlier detection and better understanding of the disease.

ACKNOWLEDGEMENTS

We thank Kerstin Kretschel, Evelyn Polzin, Ursula Wagner, and Melanie Bochmann for their technical assistance; Philipp Boye, Dr Andreas Kumar, and Dr Anja Zagrosek for their participation in scanning the patients and fruitful discussion; and Dr Andrew Taylor for careful revision of the manuscript.

Authors' affiliations

J Schulz-Menger, R Wassmuth, H Abdel-Aty*, I Siegel, R Dietz, M G Friedrich*, Franz-Volhard-Klinik, Helios-Klinikum Berlin, Kardiologie, Charité Campus Berlin-Buch, Humboldt-Universität zu Berlin, Berlin, Germany
A Franke, Fachkrankenhaus für Lungenheilkunde und Thoraxchirurgie, Berlin-Buch, Germany

*Also the Stephenson CMR Centre, Department of Cardiac Sciences and Radiology, University of Calgary, Calgary, Alberta, Canada

Correspondence to: Dr Jeanette Schulz-Menger, Franz-Volhard-Klinik, Charité Campus Buch, Wiltbergstrasse 50, D-13125 Berlin, Germany; schulzmenger@fvk-berlin.de

Accepted 30 June 2005

REFERENCES

1 **Perry A**, Vuitch F. Causes of death in patients with sarcoidosis: a morphologic study of 38 autopsies with clinicopathologic correlations. *Arch Pathol Lab Med* 1995;**119**:167–72.
2 **Friedrich MG**, Strohm O, Schulz Menger J, *et al.* Contrast media-enhanced magnetic resonance imaging visualizes myocardial changes in the course of viral myocarditis. *Circulation* 1998;**97**:1802–9.
3 **Mahrholdt H**, Goedecke C, Wagner A, *et al.* Cardiovascular magnetic resonance assessment of human myocarditis: a comparison to histology and molecular pathology. *Circulation* 2004;**109**:1250–8.
4 **Schulz-Menger J**, Strohm O, Dietz R, *et al.* Visualization of cardiac involvement in patients with systemic sarcoidosis applying contrast-enhanced magnetic resonance imaging. *Magma* 2000;**11**:82–3.
5 **Vignaux O**, Dhote R, Duboc D, *et al.* Detection of myocardial involvement in patients with sarcoidosis applying T2-weighted, contrast-enhanced, and cine magnetic resonance imaging: initial results of a prospective study. *J Comput Assist Tomogr* 2002;**26**:762–7.

WEB TOP 10

www.heartjnl.com
These articles scored the most hits on *Heart*'s website during December 2005

1 JBS 2: Joint British Societies' guidelines on prevention of cardiovascular disease in clinical practice
December 2005;**91**(suppl V):1–52. (Supplement)
2 The normal ECG in childhood and adolescence
DF Dickinson
December 2005;**91**:1626–30. (Education in Heart)
3 Dark chocolate improves endothelial and platelet function
F Hermann, LE Spieker, F Ruschitzka, I Sudano, M Hermann, C Binggeli, TF Lüscher, W Riesen, G Noll, R Corti
January 2006;**92**:119–20. (Scientific letter)
4 Should primary angioplasty be available for all patients with an ST elevation myocardial infarction?
A de Belder
December 2005;**91**:1509–11. (Editorial)
5 Origin of symptoms in chronic heart failure
AL Clark
January 2006;**92**:12–16. (Heart review)
6 Management of infective endocarditis
G Habib
January 2006;**92**:124–30. (Education in Heart)
7 Aortic stenosis: medical and surgical management
H Baumgartner
November 2005;**91**:1483–8. (Education in Heart)
8 Five year outcome after primary coronary intervention for acute ST elevation myocardial infarction: results from a single centre experience
G Parodi, G Memisha, R Valenti, M Trapani, A Migliorini, G M Santoro, D Antoniucci
December 2005;**91**:1541–4. (Cardiovascular medicine)
9 Percutaneous coronary intervention: recommendations for good practice and training
December 2005;**91**(suppl VI):1–27 (Supplement)
10 Diabetes and cardiovascular disease: the road to cardioprotection
P Monteiro, L Gonçalves, LA Providência
December 2005;**91**:1621–5. (Education in Heart)

Visit the *Heart* website for hyperlinks to these articles, by clicking on ''Top 10 papers''
www.heartjnl.com

2.3. Andere nicht-ischämischen Herzerkrankungen

Ohne Zweifel kann man davon ausgehen, dass auch bei anderen nicht-ischämischen Herzerkrankungen (NHID) eine Myokarddifferenzierung möglich ist. Insbesondere Ansätze zur Fibrosedarstellung erscheinen vielversprechend. Mit der Entwicklung eines Algorithmus zur Quantifizierung und systematischen Beschreibung der Qualität und Quantität einer Fibrose ist aus unserer Sicht ein wichtiger Schritt vollzogen worden, um Daten vergleichbar zu machen. Dieser Weg wurde bei insgesamt 156 retrospektiv analysierten Patienten angewendet. Diese nach einem einheitlichen Protokoll untersuchten Patienten wurden nach folgenden Kriterien rekrutiert: Ausschluss einer Koronaren Herzkrankheit und positives LHE aus einer Datenbank von 8237 Untersuchungen. Es wurden 2618 Segmente analysiert. Auf Grundlage dieser Arbeit konnten wir erstmals den nichtinvasiven Nachweis von Fibrosierungen bei Aortenstenosen beschreiben. Interessant erscheint weiterhin, dass bei einigen Erkrankungen (HCM, DCM, Myokarditis und Vaskulitis) charakteristische Muster detektiert werden konnten. Neben dem bereits im Kapitel III 1 auf der Seite 28 beschriebenen HCM-Muster, fiel bei der DCM eine Häufung von mitventrikulären Anreicherungen auf (mid-wall-sign). Interessant erscheint, dass bei der Myokarditis das LHE insbesondere supepikardial posterolateral nachweisbar ist, während die Fibrosen bei Vaskulitiden vorwiegend subendokardial, aber nicht assoziiert mit dem Versorgungsgebiet einer großen epikardialen Koronararterie, nachweisbar sind.

Unsere Untersuchungen zur Myokarditis und Sarkoidose lassen erkennen, dass insbesondere in aktiven Stadien eines Krankheitsbildes die Darstellung eines LHE allein nicht ausreichend ist. In unseren Arbeiten war das LHE bei der Myokarditis

in 40% der Patienten und bei Sarkoidose in 23% nachweisbar.[55, 59] Es ist aber anzunehmen, dass das Auftreten von Fibrosierungen zumindest bei bestimmten Entitäten mit einem höheren Schweregrad und vermutlich sogar einem höherem Risiko für die Entwicklung von Herzrhythmusstörungen und/oder einer Herzinsuffizienz einhergehen.

2.4. Entwicklung alternativer Techniken (T1-Mapping)

In dem Bewusstsein, dass die kontrastverstärkte MRT eine wesentliche Rolle bei der myokardialen Differenzierung spielt, erscheint es wesentlich, technische Optimierung vorzunehmen, welche die Potenz haben, auch diffuse Fibrosierung zu erfassen. Da eine Methode ideal wäre, welche die rasche Quantifizierung der Gewebeparameter, eventuell sogar kontrastmittelfrei gestattet, wurde die weitere Implementierung des T1-Mappings forciert. Daniel Messroghli aus unserer Arbeitsgruppe hatte bereits 2003 die erste Anwendung in einer damals noch suboptimalen Technik bei Patienten mit akutem Myokardinfarkt beschrieben.[62] Während seines Forschungsaufenthaltes in Leeds gelang es ihm, die Sequenz zu optimieren. Nach dem die Implementierung an unserem System gelang, wurden zur Erstellung von Normwerten, Probandenmessungen durchgeführt. Diese ersten Ergebnisse wurden 2006 als Abstrakt im Journal for Cardiovascular Magnetic Resonance publiziert und sind zur weiteren Veröffentlichung eingereicht.[63] Untersuchungen bei Patienten mit myokardialen Erkrankungen insbesondere akuter Myokarditis und linksventrikulärer Hypertrophie werden gegenwärtig durchgeführt.

3. **Koronare Herzkrankheit**

Im Mittelpunkt unserer Forschungsaktivitäten stand hier die Differenzierung von akuter und chronischer Schädigung.

3.1. Differenzierung der Schädigung der myokardialen Schädigung

Die Kombination von T_2-gewichteten Sequenzen zur Detektion eines potenziellen peri-infarziellen Ödemes in Kombination mit kontrastverstärkten T_1-gewichteten Techniken zur Fibrosedetektion ist prädestiniert für die Differenzierung von akuten und chronischen Infarkten. Unsere Arbeitsgruppe veröffentlichte dies bei 58 Patienten mit einer Spezifität von 96% im Jahre 2004.[32] Obwohl die einzelnen Anwendungen der Sequenzen schon lange bekannt sind, ist dies noch kein Allgemeingut, so dass wir uns im European Heart Journal an einer entsprechenden Diskussion beteiligten, um die Anwendung der T_2-Wichtung im akuten Infarkt zur Selbstverständlichkeit werden zu lassen.[64]

Wir nutzen das Modell einer klinisch indizierten PTSMA bei HOCM zur Untersuchung eines Myokardinfarktes. Die Durchführung unter Verwendung von Schaumstoffpartikeln entspricht einem plötzlichen Koronarverschluss, dies gestattete uns die myokardialen Veränderungen nach einem gezielt induzierten Infarkt zu untersuchen. Die Kontrolle der Patienten vor und zu definierten Zeitpunkten nach der Intervention zeigte, dass der Infarkt bereits nach einer Stunde mit kontrastverstärkten Techniken darstellbar war. Dies konnte im Jahre 2002 im Journal of American College of Cardiology publiziert werden.[53]

3.2. Optimierung und Validierung vorhandener Techniken

Die Implementierung einer neuen 3D-atemangehaltenen SSFP-Sequenz wurde genutzt, um die Anwendbarkeit bei der Darstellung von Koronararterien systematisch bei Probanden und Patienten zu untersuchen. Es konnte gezeigt werden, dass die Sequenz reproduzierbar nutzbar ist, allerdings brachte die Administration von Gd-DTPA insbesondere bei der rechten Koronararterie keinen Vorteil. Die Publikation erfolgte 2005 im Journal für Cardiovascular Magnetic Resonance.[65]

Ohne Zweifel wäre der Nachweis vulnerabler Plaques der reinen Stenosequantifizierung überlegen. Um uns dieser Fragestellung zu nähern, untersuchten wir am 1.5T MRT-Scanner Patienten mit Carotisstenosen und konnten in einem ersten Ansatz zeigen, dass ein multisequentieller MRT-Ansatz die im Ultraschall homogenen Plaques weiter differenzieren kann. Es wurden unter Verwendung einer Oberflächen-Carotis-Spule T_2-gewichtete, protonengewichtete und T_1- gewichtete Sequenz vor und nach Applikation von Gd-DTPA eingesetzt. Diese Ergebnisse wurden 2005 auf dem Treffen des American College of Cardiology vorgestellt.

Nach anfänglicher Euphorie in der Literatur wurden die Publikation zur First-Pass-Perfusion deutlich zurückhaltender, da die Spezifität bezogen auf den Stenosegrad in der ersten multizentrischen Studie geringer ausfiel als erwartet.[66] Ursächlich ist unter anderem die hohe räumliche Auflösung der Methode, die gut mit der PET vergleichbar ist und damit auch die durch primär intramyokardiale Minderperfusion bedingte Veränderungen erfasst.[30] Auf der anderen Seite gestattet dies aber, Perfusionsveränderungen auf myokardialer Ebene zu erfassen. So konnten wir

bereits nach elektiver erfolgreicher Koronarintervention Minderperfusionen nachweisen und zeigen, dass die Perfusionsveränderungen nach akuter Intervention bei Myokardinfarkt eine Bedeutung für spätere Veränderungen der linksventrikulären Funktion haben.[67, 68]

Leider besteht gegenwärtig noch keine Einigung über die optimale Sequenztechnik, Kontrastmitteldosis und -applikationsform. Da die Adenosin-First-Pass-Perfusion aber das Potenzial hat, eine Ischämie vor der Entstehung einer Wandbewegungsstörung innerhalb der Ischämiekaskade zu detektieren, setzten wir uns mit der Optimierung der Kontrastmitteldosis für die Doppelbolusapplikation bei speziell optimierten Sequenzen auseinander. Diese Technik wird uns die Möglichkeit eröffnen, die Myokardperfusion zu quantifizieren.

Diese Ergebnisse wurden 2006 als Abstrakt publiziert und sind zur weiteren Veröffentlichung eingereicht.[69]

Journal of the American College of Cardiology
Vol. 42, No. 3, 2003
ISSN 0735-1097/03/$30.00
doi:10.1016/S0735-1097(03)00717-4
Published by Elsevier Inc.

Cardiovascular Magnetic Resonance of Acute Myocardial Infarction at a Very Early Stage

Jeanette Schulz-Menger, MD, Michael Gross, MD, Daniel Messroghli, MD, Frank Uhlich, MD, Rainer Dietz, MD, Matthias G. Friedrich, MD

Berlin, Germany

OBJECTIVES Very early changes in myocardial tissue composition during acute myocardial infarction (AMI) are difficult to assess in vivo. Cardiovascular magnetic resonance (CMR) imaging provides techniques for visualizing tissue pathology.

BACKGROUND The diagnostic role of CMR in very acute stages of myocardial infarction is uncertain. We investigated signal intensity changes beginning within 60 min after acute coronary occlusion in patients undergoing therapeutic septal artery embolization.

METHODS We investigated eight patients with hypertrophic obstructive cardiomyopathy undergoing interventional septal artery embolization by applying microparticles to reduce left ventricular outflow tract obstruction. In a clinical 1.5-tesla (T) CMR system, we visualized infarct-related myocardial signal by T_1-weighted sequences before and 20 min after administration of contrast media (delayed enhancement) and edema-related signal by T_2-weighted spin-echo sequences before and 58 ± 14 min after the intervention as well as on days 1, 3, 7, 14, 28, 90, and 180 during follow-up.

RESULTS Infarct-related changes as defined by contrast enhancement were observed as early as 1 h after the intervention and during six months of follow-up. In contrast, infarct-related myocardial edema, as visualized by high signal intensity in T_2-weighted spin-echo sequences, was not consistently detectable 1 h after acute arterial occlusion; this was possible in all subsequent studies until day 28.

CONCLUSIONS Contrast-enhanced magnetic resonance imaging detected infarct-related signal changes as early as 1 h after AMI in humans, whereas the sensitivity of edema-related signal changes was not sufficient during this very early stage. (J Am Coll Cardiol 2003;42:513–8) © 2003 by the American College of Cardiology Foundation

The early and reliable diagnosis of acute myocardial infarction (AMI) has a strong impact on clinical outcomes (1). Current clinical routine is mostly based on medical history, physical status, the electrocardiogram (ECG), and serologic findings. Although the overall sensitivity of these parameters is good (2,3), it is less favorable early after the onset of ischemia (4). However, in the diagnosis of myocardial infarction (MI), speed is essential, and in selected patients with equivocal results, the knowledge of very early changes could be helpful in therapeutic decision-making.

Cardiovascular magnetic resonance (CMR) is able to differentiate infarcted from normal myocardium (5–7) and also detects myocardial edema by T_2-weighted pulse sequences (8,9). However, in most animal and human studies (10,11), the changes were assessed at least 24 h after the acute injury. We investigated the signal intensity changes in the very early stages of MI after acute occlusion of a coronary artery.

METHODS

Patients. We studied eight patients (5 men and 3 women; 41 to 78 years old) with hypertrophic obstructive cardiomyopathy scheduled for interventional septal artery embolization. All patients had severe symptoms with dyspnea (New York Heart Association [NYHA] functional class III or IV), despite optimized pharmacologic treatment, and fulfilled the accepted criteria for undergoing this intervention. Significant coronary artery disease was excluded by cardiac catheterization. All patients gave written, informed consent. One patient was embolized a second time three months after the first procedure because severe symptoms and a high pressure gradient persisted.

Septal artery embolization. The intervention was performed by infusion of a solution containing microparticles (Contour Emboli; Target, Boston Scientific Corp., Boston, Massachusetts) into the septal artery supplying the basal septum as identified by intra-procedural contrast-enhanced echocardiography. The infusion resulted in acute embolic occlusion of the artery with complete cessation of flow, thus closely matching the pathophysiology of thrombotic occlusion in atherosclerotic AMI.

CMR imaging. We used a dedicated CMR system (Signa CV/*i*; 1.5 T, GE Medical Systems, Milwaukee, Wisconsin) located close to the cardiac catheterization laboratory and intensive care unit. Patients were continuously monitored during the examination by ECG, repeated blood pressure measurements, and pulse oximetry.

We used a four-element, phased-array coil or body coil. A T_2-weighted spin-echo sequence (short T_1 inversion recovery [STIR], repetition time [TR] 2 RR interval, echo time [TE] 64 ms, slice thickness 10 mm, matrix 256 × 256, field

From the Franz Volhard Clinic at the Max Delbrück Center, Helios-Klinikum, Berlin-Buch, Medical Faculty of the Charité, Department Cardiology, Humboldt University of Berlin, Berlin, Germany.

Manuscript received April 29, 2002; revised manuscript received April 9, 2003, accepted April 17, 2003.

JACC Vol. 42, No. 3, 2003
August 6, 2003:513–8

Abbreviations and Acronyms

AMI	= acute myocardial infarction
CMR	= cardiovascular magnetic resonance
ECG	= electrocardiogram/electrocardiographic/ electrocardiography
MI	= myocardial infarction
MR	= magnetic resonance
NYHA	= New York Heart Association
STIR	= short T_1 inversion recovery
TE	= echo time
TI	= inversion time
TR	= repetition time

of view 34 × 34 or 36 × 36 mm) was used to visualize myocardial edema. Irreversible myocardial injury was visualized by T_1-weighted sequences (TE 23 ms, slice thickness 10 mm, matrix 256 × 160, field of view 36 × 36 cm) 20 min after intravenous application of 0.2 mmol/kg gadolinium–pentetic acid (Magnevist, Schering AG, Berlin, Germany). In three patients, we also assessed myocardial necrosis, as defined by "delayed enhancement," using a T_1-weighted, inversion-recovery prepared gradient echo sequence (TR 5.5 ms, TE 1.4 ms, inversion time [TI] 220 to 250 ms, slice thickness 10 mm).

We calculated the signal intensity ratio of the infarcted myocardium compared with remote myocardium and the proportion of the infarcted tissue related to the entire myocardium in the infarct-containing slice.

The left ventricular ejection fraction was quantified in a set of contiguous gradient-echo images (TE 4.8 to 6.1 ms, slice thickness 10 mm) in the true short-axis orientation.

Cardiovascular magnetic resonance was performed before and 58 ± 14 min after the intervention as well as on days 1, 3, 7, 14, 28, 90, and 180. One patient (who underwent 2 interventions) had an additional study 7 h after the intervention.

Care was taken to reproduce the same slice position in the follow-up studies, using anatomic landmarks.

Statistics. The infarct area during follow-up was compared with remote areas using an analysis of variance (Statview, SAS Inc., Cary, North Carolina) and as a post hoc analysis Fisher exact test.

RESULTS

All patients could be investigated without complications in a routine clinical setting.

Septal artery embolization procedure. All septal ablation procedures were successful, as defined by an immediate drop in the pressure gradient and subsequent enzyme release. No major complications occurred. Creatine kinase activity peaked at 570 ± 213 U/l (normal range <170 U/l for women and <200 U/l for men) after the intervention and normalized in all subjects within five days. In four patients, the ECG demonstrated signs of anteroseptal MI as defined by ST-segment elevations ≥0.2 mV in at least two adjacent chest wall leads (generally leads V_2 to V_4).

At the end of the follow-up period, the clinical status had improved in all patients (mean NYHA class 3.1 ± 0.1 vs. 1.3 ± 0.2, $p < 0.0001$).

T_2-weighted CMR. Before the intervention, the T_2-weighted images did not show any myocardial signal intensity abnormalities in the basal septal region. Also, within 1 h after the intervention, there were no relevant intramyocardial signal intensity changes in T_2-weighted images. In some patients it was necessary to differentiate intramyocardial signal from slow flow (Fig. 1). Therefore, a gradient-echo sequence was used to verify the endocardial border. Also, in the one patient with an additional CMR study 7 h after the intervention, no significant edema was detectable at that time point. However, 24 h after the intervention, a signal increase in the infarct area was visible in seven of eight patients. On days 3, 7, 14, and 28, these signal changes were visible in all patients, whereas after 90 and 180 days they had disappeared.

Contrast-enhanced CMR. The course of signal intensity changes in late contrast-enhanced T_1-weighted CMR images differed from that of T_2-weighted CMR images. The investigated regions had no contrast enhancement before the intervention. The signal intensity ratio between septal and remote myocardium increased from 1.01 ± 0.01 before the intervention to 1.84 ± 0.19 1 h after the intervention ($p < 0.05$). A localized enhancement persisted during the entire follow-up period (Figs. 1 and 2). The intensity and extent of the localized signal increase varied between the patients.

The area of the infarcted region during follow-up was significantly larger between days 1 and 14 than at all other time points ($p < 0.02$) in the late contrast-enhanced images. Furthermore, significant changes in the T_2-weighted CMR images were observed. The area of the increased STIR signal was larger than that of the late contrast-enhanced images, but this difference did not reach statistical significance (Fig. 2). After 180 days, the area of the signal increase in the late contrast-enhanced images appeared more sharply defined and smaller than on day 7.

Functional analysis. In all patients, a persisting regional hypokinesia in the infarcted region was observed, as quantified in gradient-echo CMR image series. The global left ventricular function did not change (ejection fraction: 68 ± 4% vs. 69 ± 4%, p = NS).

DISCUSSION

Our data show that contrast-enhanced CMR is able to visualize even small myocardial infarcts in vivo at a very early stage, whereas T_2-weighted CMR may not be sufficiently sensitive.

To our knowledge, this is the first report on CMR in patients early after an embolic event. There is a case report using CMR to visualize microvascular obstruction after

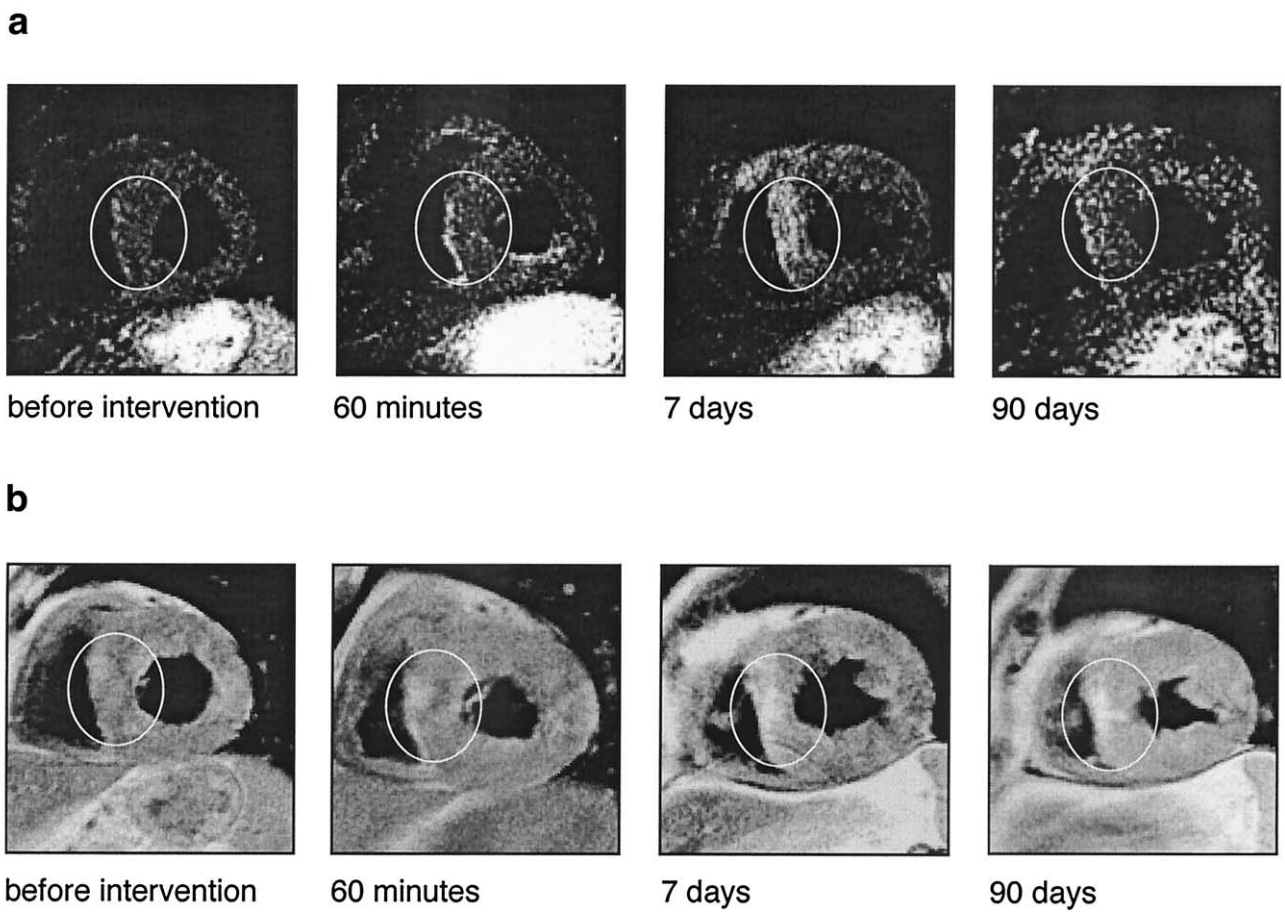

Figure 1. Signal changes in the septal myocardial infarction in a follow-up detected by magnetic resonance imaging. **(a)** T_2-weighted spin-echo sequences visualizing the edema. Sixty minutes after acute occlusion of the septal artery, there was no signal increase in the myocardium; the streaky artifacts visible adjacent to the septum and in the inferior parts in both ventricles are most likely due to slow flowing blood. **(b)** T_1-weighted spin-echo imaging after gadolinium. Enhancment was detectable within 60 min of infarction.

septal artery embolization (12). However, the ablation method in that case differed from ours by the use of alcohol.

Our findings of infarct-related contrast enhancement correspond to histologic evidence of the presence of myocardial necrosis as early as 40 min after arterial occlusion (13,14). The same studies showed that the infarct subsequently expands, a finding known as the "wave front phenomenon" (13). This is associated with the development of intracellular and interstitial myocardial edema.

In our approach, ablation of the septum was performed by applying micro-emboli consisting of foam gel, without any alcohol. Thus, an embolic event is created, providing a pathophysiology very similar to AMI. Thus, our model differs from classic infarcts by a more peripheral location of the occluding substrate and thus collateral flow. However, a better collateral flow, albeit reducing the infarct size, is unlikely to change the pathophysiology in the more central parts of the infarcted area. Thus, we are convinced that our model closely matches at least most parts of an atherosclerotic, but ultimately, no-flow infarction.

There are many studies on magnetic resonance (MR) findings in animal models of AMI. Although animal studies have provided significant insight into early ischemic myocardial injuries, studies in humans remain a necessity, considering the different profiles of myocardial ischemic injury in humans compared with other species. Our data may provide the information that is lacking by using a human model that closely matches the embolic event of AMI.

Magnetic resonance studies in animals showed an increase of T_1 and T_2 relaxation times 3 h after occlusion (15).

Higgins et al. (16) demonstrated in an animal model of AMI that the increase in T_2 signal of the infarcted regions reflects infarct-associated myocardial edema. Further studies on animal models confirmed the relationship between a high T_2 signal pattern and myocardial edema and further demonstrated that the spatial extent of myocardial edema exceeds that of irreversible myocardial injury (17). It was shown that diffusion-weighted MR imaging, but not T_2-weighted MR imaging, is sensitive to intracellular edema (18). Thus, it is very likely that the high signal intensity in our setting is reflective mainly of interstitial edema. In humans with subacute MI, Miller et al. (19) have shown that the function of myocardial segments showing a high STIR signal may recover, suggesting a mismatch between

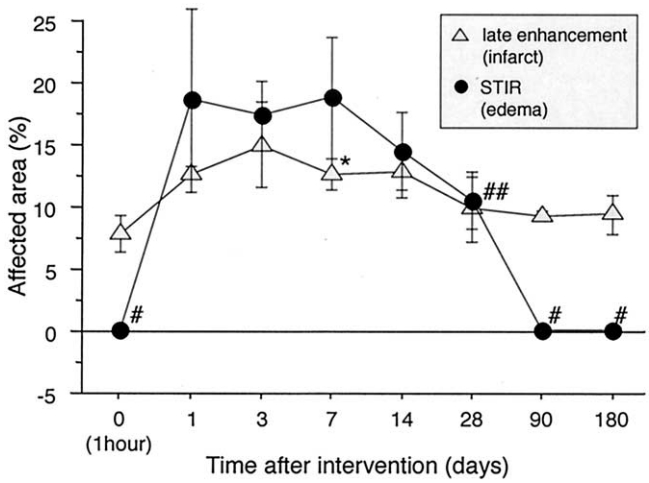

Figure 2. Changes over time in the infarcted and edematous areas. The affected area (%) = (area with signal abnormality/area of whole myocardium within slice) × 100. *Significant difference from day 0 (1 h after intervention) and days 28, 90, and 180 ($p < 0.05$). #Significant difference from days 1, 3, 7, 14, and 28 ($p < 0.05$). ##Significant difference from days 3 and 7 ($p < 0.05$). STIR = short T_1 inversion recovery.

myocardial edema and necrosis. Although myocardial edema occurs in irreversibly injured myocardium, it frequently also extends to reversibly injured myocardium and was shown to closely match the myocardial "area at risk" (9).

Our results indicate a differential time course of contrast enhancement, reflecting irreversible myocardial injury, and a high T_2 signal intensity, reflecting myocardial edema with a delay in the occurrence of T_2-related changes. Thus, for very early detection in a clinical setting, this approach does not seem to be sufficiently sensitive.

These results correspond to several animal studies showing that infarct-related myocardial edema was not detectable within the first hour before, but by 3 h after, occlusion (9,15,20). Different mechanisms may explain this. It is known that early in the course of ischemic injury myocardial edema is predominantly intracellular, and T_2-weighted CMR may not be able to detect bound water molecules in the case of intracellular edema.

Later on, however, a T_2-related high signal was consistently observed. There are no published in vivo human data on patients with edema in the very early stages of MI, but an increased signal intensity in T_2-weighted images was reported for infarcted regions three days after MI, which could be correlated with myocardial edema (21,22). We also found evidence of edema one day after AMI, consistent with these results. The edema persisted for at least one month but was not detectable after three months.

In contrast to T_2 changes, T_1 abnormalities due to MI are typically not visually detectable on MR images without using contrast agents.

On the other hand, CMR imaging late after administration of gadolinium (delayed enhancement) accurately reflects irreversible myocardial injury. In contrast to T_2-weighted images, only irreversibly damaged myocardium is enhanced. Thus, it is conceivable that the spatial extent of delayed enhancement would be less than that of STIR-determined myocardial edema.

Reperfusion injury early after experimental MI has been assessed by contrast-enhanced CMR (23,24), and there are numerous studies indicating that contrast-enhanced CMR is able to differentiate between infarcted and viable myocardium (6,25,26). The agreement of gadolinium accumulation with histologic parameters of myocardial necrosis was shown in animal CMR studies as early as 6 h after AMI (27,28).

The underlying pathophysiology of gadolinium accumulation in MI, however, has not been fully elucidated. Mechanisms under discussion include a prolonged wash-in/wash-out period in the infarcted tissue due to contrast media diffusion into necrotic cells, as well as a relative increase of interstitial space and interstitial edema (29,30). Thus, the contribution of edema, by comparison with necrosis or fibrosis, to the accumulation of gadolinium is difficult to estimate.

Interestingly, we observed a transient spatial increase of the enhancing area in the contrast-enhanced T_1-weighted images during the period with edema, as defined by high signal intensity areas in the T_2-weighted images, indicating a common underlying pathophysiology. Different mechanisms may explain this finding: it has been previously shown that in humans, the time needed for the infarct to reach its maximum size is about 6 to 12 h, compared with 3 to 4 h in dogs. Furthermore, gadolinium–pentetic acid also accumulates in edema (31), and thus our finding may simply reflect the involvement of infarct-associated edema. Finally, recent reports have underlined the role of apoptosis in the pathophysiologic cascade of irreversible ischemic injury. It is assumed that the apoptotic process achieves its final spatial extent a few days after the ischemic insult.

In patients with two infarctions, the more recent acute infarct revealed more blurred edges of the infarct-related necrosis than the chronic scar. Furthermore, signal intensity increased to a lesser extent. A clear discrimination of both infarcts, however, was possible only by the presence or absence of the infarct-associated edema (Fig. 3).

Thus, a delayed contrast enhancement without concomitant edema may be a marker of either necrosis during the first hours of infarction or chronic myocardial scar (after infarct-related inflammation has disappeared).

Clinical implications. Our results underscore the potential role of CMR in a number of clinical scenarios. Verifying the diagnosis of AMI is useful in the critical care setting, when conventional methods are inconclusive or contradictory and a therapeutic decision is urgently required. In addition, differentiation between acute and chronic infarcts is also possible. In the case of known infarcts, their age can be estimated: the finding of delayed enhancement in the absence of a corresponding high STIR signal intensity would exclude an acute event.

Finally, the unique ability of CMR to provide a non-invasive, reproducible means of assessing the temporal

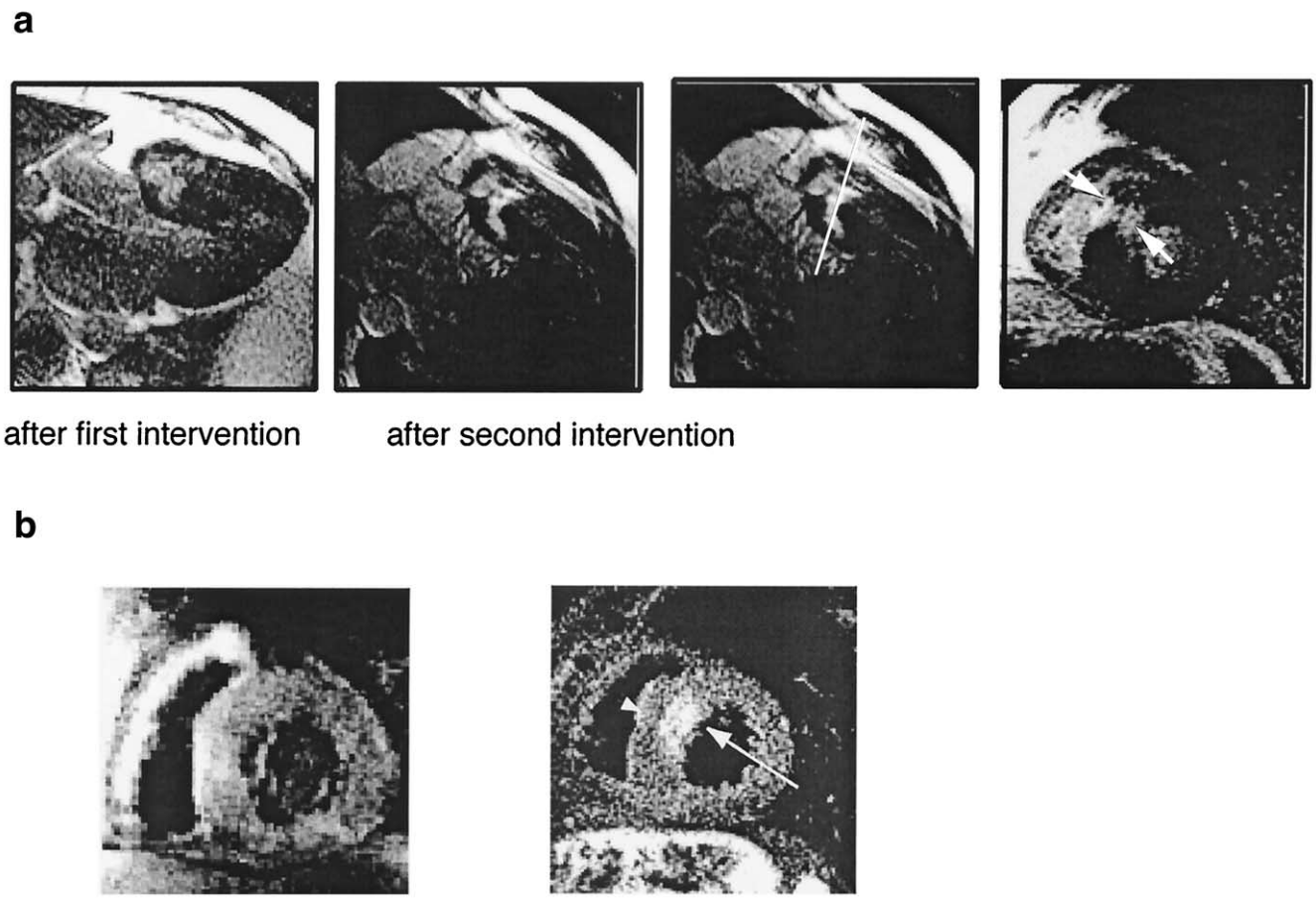

Figure 3. Contrast-enhanced CMR images. **(a)** First image = long-axis view after the first intervention; second image = long-axis view after the second intervention, with enlarged contrast accumulation; third image = long-axis view with planned short-axis orientation; fourth image = short-axis view showing a high signal intensity in the chronic infarction **(arrowhead)** and a lower, but still high, signal intensity in the acute infarction **(arrow)**. **(b)** T_2-weighted images: short-axis view after the first intervention **(left)** and short-axis view after the second intervention **(right)**. In contrast to the chronic infarction **(arrowhead)**, the acute infarction shows a very high signal **(arrow)**.

evolution and spatial extent of various myocardial ischemic injuries may justify its application as a tool for monitoring the effect of novel therapeutic approaches targeting these injuries.

Study limitations. Our study was performed on a specific patient population without chronic coronary artery disease. Although septal artery embolization produces an acute, non-reperfused MI, the injurious profile of this rather "controlled" myocardial insult may differ from the complex pathophysiology underlying clinical AMI.

We also did not register images, and despite our efforts to accurately reproduce the previous position with the help of anatomic landmarks, a slight shift of the position may have occurred.

Finally, because of the time we started our investigations, no inversion-prepared T_1-weighted gradient-echo sequence, as is usually used today for late enhancement CMR, was available. However, our experience with patients in whom both sequences were applied, did not reveal any significant differences between our and the newer techniques. Although newer techniques have a better contrast–noise relation, T_1-weighted sequences in general reveal the post-contrast signal changes we observed.

Conclusions. Contrast-enhanced T_1-weighted CMR is a sensitive method of detecting myocardial tissue damage even within 1 h after an acute embolic MI in humans, whereas T_2-weighted CMR was found to be not sufficiently sensitive at this early time point.

Acknowledgment

We are thankful to Hassan Abdel-Aty, MD, for helpful discussions and careful manuscript review.

Reprint requests and correspondence: Dr. Jeanette Schulz-Menger, Franz-Volhard-Klinik, Wiltbergstrasse 50, D-13125 Berlin, Germany. E-mail: schulzmenger@fvk-berlin.de.

REFERENCES

1. The First International Study of Infarct Survival Collaborative Group. Randomised trial of intravenous atenolol among 16,027 cases of suspected acute myocardial infarction: ISIS-1. Lancet 1986;2:57–66.
2. Wong GC, Morrow DA, Murphy S, et al. Elevations in troponin T and I are associated with abnormal tissue level perfusion: a

TACTICS-TIMI 18 substudy. Treat Angina with Aggrastat and Determine Cost of Therapy with an Invasive or Conservative Strategy-Thrombolysis in Myocardial Infarction. Circulation 2002;106:202–7.
3. Ooi SB, Lim YT, Lau TC, Chia BL, Pillai S, Liu T. Value of troponin-T rapid assay, cardiac enzymes, electrocardiogram and history of chest pain in the initial diagnosis of myocardial infarction in the emergency department. Eur J Emerg Med 2000;7:91–8.
4. Jernberg T, Lindahl B, James S, Ronquist G, Wallentin L. Comparison between strategies using creatine kinase-MB(mass), myoglobin, and troponin T in the early detection or exclusion of acute myocardial infarction in patients with chest pain and a nondiagnostic electrocardiogram. Am J Cardiol 2000;86:1367–71.
5. Tscholakoff D, Higgins CB, Sechtem U, Caputo G, Derugin N. MRI of reperfused myocardial infarct in dogs. Am J Roentgenol 1986;146: 925–30.
6. Kim RJ, Fieno DS, Parrish TB, et al. Relationship of MRI delayed contrast enhancement to irreversible injury, infarct age, and contractile function. Circulation 1999;100:1992–2002.
7. Eichstaedt HW, Felix R, Dougherty FC, Langer M, Rutsch W, Schmutzler H. Magnetic resonance imaging (MRI) in different stages of myocardial infarction using the contrast agent gadolinium-DTPA. Clin Cardiol 1986;9:527–35.
8. Simonetti OP, Finn JP, White RD, Laub G, Henry DA. 'Black blood' T_2-weighted inversion-recovery MR imaging of the heart. Radiology 1996;199:49–57.
9. Garcia-Dorado D, Oliveras J, Gili J, et al. Analysis of myocardial oedema by magnetic resonance imaging early after coronary artery occlusion with or without reperfusion. Cardiovasc Res 1993;27: 1462–9.
10. Judd RM, Lugo Olivieri CH, Arai M, et al. Physiological basis of myocardial contrast enhancement in fast magnetic resonance images of 2-day-old reperfused canine infarcts. Circulation 1995;92:1902–10.
11. Kramer CM, Rogers WJ, Geskin G, et al. Usefulness of magnetic resonance imaging early after acute myocardial infarction. Am J Cardiol 1997;80:690–5.
12. Wu KC, Heldman AW, Brinker JA, Hare JM, Lima JA. Microvascular obstruction after nonsurgical septal reduction for the treatment of hypertrophic cardiomyopathy. Circulation 2001;104:1868.
13. Reimer KA, Jennings B. The "wavefront phenomenon" of myocardial ischemic cell death. II. Transmural progression of necrosis within the framework of ischemic bed size (myocardium at risk) and collateral flow. Lab Invest 1979;40:633–44.
14. Schaper J, Schaper W. Time course of myocardial necrosis. Cardiovasc Drugs Ther 1988;2:17–25.
15. Johnston DL, Brady TJ, Ratner AV, et al. Assessment of myocardial ischemia with proton magnetic resonance: effects of a three hour coronary occlusion with and without reperfusion. Circulation 1985;71: 595–601.
16. Higgins CB, Herfkens R, Lipton MJ, et al. Nuclear magnetic resonance imaging of acute myocardial infarction in dogs: alterations in magnetic relaxation times. Am J Cardiol 1983;52:184–8.
17. Dymarkowski S, Ni Y, Miao Y, et al. Value of T_2-weighted magnetic resonance imaging early after myocardial infarction in dogs: comparison with bis-gadolinium-mesoporphyrin enhanced T_1-weighted magnetic resonance imaging and functional data from cine magnetic resonance imaging. Invest Radiol 2002;37:77–85.
18. Moseley ME, Cohen Y, Mintorovitch J, et al. Early detection of regional cerebral ischemia in cats: comparison of diffusion- and T_2-weighted MRI and spectroscopy. Magn Reson Med 1990;14:330–46.
19. Miller S, Helber U, Kramer U, et al. Subacute myocardial infarction: assessment by STIR T_2-weighted MR imaging in comparison to regional function. Magma 2001;13:8–14.
20. Jennings RB, Ganote CE. Structural changes in myocardium during acute ischemia. Circ Res 1974;34 and 35 Suppl III:154–68.
21. McNamara MT, Higgins CB. Magnetic resonance imaging of chronic myocardial infarcts in man. Am J Roentgenol 1986;146:315–20.
22. Lim TH, Hong MK, Lee JS, et al. Novel application of breath-hold turbo spin-echo T_2 MRI for detection of acute myocardial infarction. J Magn Reson Imaging 1997;7:996–1001.
23. Schaefer S, Malloy CR, Katz J, et al. Gadolinium-DTPA-enhanced nuclear magnetic resonance imaging of reperfused myocardium: identification of the myocardial bed of risk. J Am Coll Cardiol 1988;12: 1064–72.
24. Rochitte CE, Lima JA, Bluemke DA, et al. Magnitude and time course of microvascular obstruction and tissue injury after acute myocardial infarction. Circulation 1998;98:1006–14.
25. Rehr RB, Peshock RM, Malloy CR, et al. Improved in vivo magnetic resonance imaging of acute myocardial infarction after intravenous paramagnetic contrast agent administration. Am J Cardiol 1986;57: 864–8.
26. Saeed M, Bremerich J, Wendland MF, Wyttenbach R, Weinmann HJ, Higgins CB. Reperfused myocardial infarction as seen with use of necrosis-specific versus standard extracellular MR contrast media in rats. Radiology 1999;213:247–57.
27. Hillenbrand HB, Kim RJ, Parker MA, Fieno DS, Judd RM. Early assessment of myocardial salvage by contrast-enhanced magnetic resonance imaging. Circulation 2000;102:1678–83.
28. Kloner RA, Darsee JR, DeBoer LW, Carlson N. Early pathologic detection of acute myocardial infarction. Arch Pathol Lab Med 1981;105:403–6.
29. Saeed M, Wendland MF, Masui T, Higgins CB. Reperfused myocardial infarctions on T_1- and susceptibility-enhanced MRI: evidence for loss of compartmentalization of contrast media. Magn Reson Med 1994;31:31–9.
30. Choi SI, Jiang CZ, Lim KH, et al. Application of breath-hold T_2-weighted, first-pass perfusion and gadolinium-enhanced T_1-weighted MR imaging for assessment of myocardial viability in a pig model. J Magn Reson Imaging 2000;11:476–80.
31. Slutsky RA, Brown JJ, Peck WW, Stritch G, Andre M. Effects of transient coronary ischemia and reperfusion on myocardial edema formation and in vitro magnetic relaxation times. J Am Coll Cardiol 1984;3:1454–60.

Journal of Cardiovascular Magnetic Resonance (2005) **7**, 809–814

ISSN: 1097-6647 print / 1532-429X online
DOI: 10.1080/10976640500287786

Taylor & Francis
Taylor & Francis Group

ANGIOGRAPHY

MR coronary angiography using 3D-SSFP with and without contrast application

ANJA ZAGROSEK, M.D.,[1,*] RALPH NOESKE, PH.D.,[2] HASSAN ABDEL-ATY, M.D.,[1] MATTHIAS G. FRIEDRICH, M.D., F.E.S.C.,[1,3] RAINER DIETZ, M.D.,[1] and JEANETTE SCHULZ-MENGER, M.D.[1]

[1]*Franz-Volhard-Klinik, Helios-Klinikum Berlin, Kardiologie, Charité Campus Berlin-Buch, Humboldt-Universität zu Berlin, Berlin, Germany*
[2]*GE Healthcare, Berlin, Germany*
[3]*Department of Cardiac Sciences and Radiology, University of Calgary, Calgary, Alberta, Canada*

We compared the performance of a contrast-enhanced with a non-contrast breath-hold 3D-SSFP-sequence for Magnetic Resonance Coronary Angiography in seven healthy subjects and 14 patients. Visibility of coronary segments, vessel length, image quality and the influence of an extracellular contrast agent (Gadolinium-DTPA) were assessed. Overall, the performance of the sequence was better in healthy subjects than in patients. Although the application of Gadolinium-DTPA increased the contrast-to-noise-ratio of the right coronary artery, the overall performance was not significantly improved. We conclude that a 3D-SSFP-technique depicts extensive parts of the coronary arteries and does not require contrast application.

Key Words: Magnetic resonance coronary angiography; Coronary artery imaging; Breath-hold technique; Contrast media; Three-dimensional technique; SSFP-sequence

1. Introduction

Although Magnetic Resonance Coronary Angiography (MRCA) has been under development for more than a decade (1), there is still no agreement on the type of sequence and the need for contrast application. Main challenges for MRCA include the spatial resolution, motion artifacts, tortuosity of the vessels and the proximity of pericardial fat and cardiac chambers (2–4). To overcome these problems, three-dimensional (3D) breath-hold and free-breathing MRCA techniques (5–9) have been recently introduced. Among those, steady-state free precession (SSFP) sequences appear promising because of their short repetition and echo times and excellent contrast between blood and surrounding structures (10–15). In SSFP sequences applied for MRCA, however, data are acquired while the signal is in transience to steady state and thus SNR and CNR do not reach their maximal values. Since image contrast in SSFP is primarily based upon the ratio of tissue T2/T1 relaxation times, intravascular application of a T1-shortening contrast agent increases the signal intensity of blood, and should thus lead to higher SNR and CNR values of the coronary arteries. Moreover, the rather slow washout of the contrast agent would provide a relatively long temporal window (20–30 min) of optimal contrast impact, sufficient enough for image acquisition and evading the limitations of a first-pass angiography. So far, data are only available for peripheral angiography (16).

We assessed the performance and the clinical feasibility of a breath-hold 3D-SSFP sequence to visualize the coronary arteries with and without application of an extracellular contrast agent (Gadolinium-DTPA).

2. Materials and methods

Twenty-one individuals underwent MRCA, among them seven healthy subjects and 14 patients, 1 ± 3 days after conventional X-ray coronary angiography for clinical suspicion of coronary artery disease. All participants gave written informed consent before the examination and the study was approved by the institutions local ethics committee. Special exclusion criteria were prior coronary bypass grafts or cardiac surgery with implantation of metallic clips, coronary artery stenting, severe cardiac arrhythmia and pre-existing pulmonary disease. Patients with contraindications to MR imaging

Received 7 January 2004; accepted 29 July 2005.
*Address correspondence to Anja Zagrosek, M.D., Franz-Volhard-Klinik, Working Group Cardiac MRI, Helios-Klinikum Berlin, Charité, Campus Berlin-Buch, Humboldt-Universitaet zu Berlin, Wiltbergstr. 50, Berlin D-13125, Germany; Fax: +49-30-9417-2560; E-mail: zagrosek@fvk.charite-buch.de

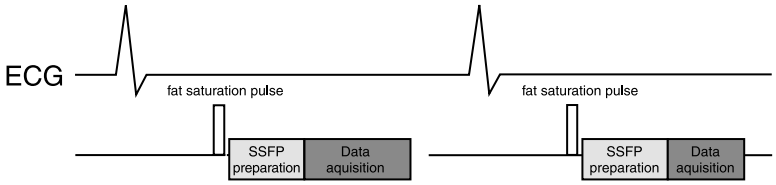

Figure 1. ECG-gated 3D-SSFP sequence (FIESTA) using the variable sampling in time approach (VAST): Each partition encoding set is acquired in two heartbeats: 32 lines are acquired in the first R-R interval and the rest in the second R-R interval (data acquisition). The spectrally selective inversion RF-pulse (fat saturation pulse) is followed by a half-alpha, half-TR preparation pulse and 6 dummy RF pulses to accelerate the approach to steady-state (SSFP preparation). The SSFP preparation phase is then followed by the data acquisition.

(automatic implantable defibrillators, pacemakers, intracranial aneurysm clip, etc) or contrast administration were excluded as well. All studies were performed on a 1.5- Tesla system (Signa CV/*i*, GE Healthcare Technologies, Milwaukee, Wisconsin, USA) with a high-performance gradient system (peak amplitude 40 mT/m, maximum slew rate 150 mT/m/ms).

2.1. *MR coronary angiography*

All subjects were examined in supine position. Data acquisition was electrocardiographically triggered and each imaging sequence was performed within one breath-hold in exspiration using a four-element, cardiac-optimized phased-array coil.

The imaging protocol for the investigational sequence consisted of two steps. First, two to three scout scans were acquired for coronary artery localization in transverse, sagittal and/or coronal orientation. For these scans an ECG-triggered multislice 2D segmented fast gradient echo sequence (TR=5.7 ms, TE=1.6 ms, matrix=256 × 160, FOV=34.0 × 25.5 mm, NEX=1, slice thickness=5 mm, no slice gap) was used, yielding 12–16 slices per breathhold. On these 2D scout images the position of the coronary arteries was determined and the double-oblique 3D-imaging planes were planned separately for the left anterior descending (LAD) coronary artery, the left circumflex (LCX) and the right coronary artery (RCA). Volume targeted breath-hold scans were then acquired in exspiration along the above-obtained orientations using the investigational 3D steady state free precession sequence (FIESTA, Fig. 1). Technical parameters were as follows: TR=4.4 ms, TE=1.8 ms, flip angle 65°, receiver bandwidth 125 kHz, NEX 0.5, matrix 256 × 192, FOV 26.0–28.0 cm, 2.2–2.6 cm slab thickness. Fat suppression was achieved by a spectrally selective inversion RF-pulse, which was played out prior to each data acquisition window. A half-alpha, half-TR preparation pulse followed by 6 dummy RF pulses was used to accelerate the approach to steady-state. The segmented data acquisition was distributed over 24 heartbeats, yielding 12 partitions. Each partition encoding set was acquired in two heartbeats using the variable sampling in time (VAST, Fig. 1) approach (17, 18). For each slice partition, the data acquisition consists of two non-equal temporal segments, which are placed at the same cardiac phase of two consecutive cardiac cycles. By acquiring the low-spatial-frequency data in a more compact acquisition window than the high-spatial-frequency k-space lines for each slice partition, cardiac motion related blurring can be reduced as compared to the standard symmetric approach. Using a matrix of 256 × 192, this leads to a VAST-ratio of 24:84, meaning that 24 k-space lines are acquired in the first and 84 k-space lines in the second RR-interval. Shimming of the magnetic field was performed prior to each scan. Trigger delays were adjusted to the subjects' heart rate so that the data acquisition was placed in middiastole between 60–80% of the RR-interval. If necessary, these scans were repeated and optimized for the vessels' exact courses. Images of the right or left coronary artery were obtained in a random order to decrease the influence of the examination's duration on image quality.

In 5 healthy subjects and in all of the patients a second scan for each coronary artery was applied with the investigational sequence after intravenous injection of Gadolinium-DTPA (Magnevist, Schering, Germany) using an automated injector (Medrad, PA). The contrast dose was 0.1–0.2 mmol/kg bodyweight of Gd-DTPA as a bolus, followed by 20 mL of normal saline. No particular imaging order of the coronary arteries was followed after application of Gd-DTPA.

Table 1. Visibility of coronary segments

Segment	Healthy subjects	Patients
LMCA	100.0% (7/7)	83.3% (10/12)
LAD1	100.0% (7/7)	83.3% (10/12)
LAD 2	100.0% (7/7)	75.0% (9/12)
LAD 3	71.4% (5/7)	25.0% (3/12)
LCX 1	83.3% (5/6)	100% (8/8)
LCX 2	0.0% (0/6)	37.5% (3/8)
LCX 3	0.0% (0/6)	0.0% (0/8)
RCA 1	100.0% (7/7)	100.0% (12/12)
RCA 2	100.0% (7/7)	91.7% (11/12)
RCA 3	100.0% (7/7)	66.6% (8/12)
Total	77.6% (52/67)	68.5% (74/108)

Segments of the coronary artery tree visualized in MRCA in patients and in healthy subjects.

Table 2. Length of the coronary arteries

Vessel	Healthy subjects	Patients	p value
LMCA	12 mm ± 3 (7–15 mm)	12 mm ± 1 (9–13 mm)	.96
LAD	75 mm ± 6 (68–82 mm)	51 mm ± 20 (29–90 mm)	.02
LCX	23 mm ± 7 (15–32 mm)	35 mm ± 12 (14–52 mm)	.10
RCA	106 mm ± 19 (79–135 mm)	84 mm ± 37 (12–134 mm)	.18

Length of the coronary arteries as visualized in MRCA, data are mean values ± SD, numbers in parentheses are ranges.

Table 3. Diameter of the coronary arteries

Vessel	Healthy subjects	Patients	p value
LMCA	3.1 mm ± 0.3 (3.1–3.5 mm)	3.8 mm ± 0.6 (3.0–4.7 mm)	.01
LAD	2.9 mm ± 0.5 (2.4–3.7 mm)	2.9 mm ± 0.4 (2.2–3.5 mm)	.89
LCX	2.5 mm ± 0.4 (1.9–3.0 mm)	2.9 mm ± 0.6 (2.2–3.2 mm)	.22
RCA	3.3 mm ± 0.5 (2.7–4.2 mm)	3.7 mm ± 0.7 (2.7–4.9 mm)	.19

Diameter of the coronary arteries as visualized in MRCA, data are mean values ± SD, numbers in parentheses are ranges.

2.2. *Image analysis*

Images were transferred to a commercially available workstation (Advantage Windows 4.0, GE Healthcare Technologies, Milwaukee, Wisconsin, USA). The image quality was determined by one observer blinded to the participants' data, based on the 2D original source data. The image quality was evaluated on a per-coronary basis and graded using a score from 1 to 4, depending on sharp vessel definition, visualization of side-branches and motion artefacts (1 = unreadable; 2 = moderate, vessel visible but not clearly demarcated from adjacent myocardium; 3 = good, vessel demarcated from adjacent myocardium; 4 = excellent, vessel borders clearly defined). The length of each coronary artery and its diameter 1 cm distal to the offspring were measured.

The coronary artery tree was subdivided into 10 segments with 3 segments of 3 cm length per coronary artery plus the left main stem, allowing for a quantification of visible segments. This approach avoids the use of side-branches to subdivide the coronary arteries (19).

2.3. *SNR and CNR measurements*

SNR and CNR were measured on images before and after the application of contrast agent in two identical slices of the source images. Blood signal (S_{Blood}) was measured in the lumen of the proximal to middle segments of the coronary arteries, with the region-of-interest (ROI) drawn within the boundaries of the vessels and then copied to the post-contrast images. The myocardial signal ($S_{Myocardium}$) was measured in close proximity to the coronaries. The standard deviation of noise was considered the mean signal intensity of air divided by a factor of 1.25 (10). SNR and CNR were then calculated as follows:

$$\mathrm{SNR} = \frac{S_{Blood} \times 1.25}{\text{Mean SI of air}} \quad (1)$$

$$\mathrm{CNR} = \frac{(S_{Blood} - S_{Myocardium}) \times 1.25}{\text{Mean SI of air}} \quad (2)$$

2.4. *Statistical analysis*

SNR and CNR values are presented as mean ± SD. A p value < .05 was considered statistically significant. Statistical analysis was performed using commercially available software (StatView 4.5, Abacus Concepts, Berkeley, California, USA). All statistical tests were 2 tailed. Continuous data were compared using the student t-test.

Table 4. Image quality

Vessel	Healthy subjects	Patients	p value
LMCA	3.9 ± 0.3	3.0 ± 0.6	< .05
LAD	3.0 ± 0.5	2.4 ± 0.6	< .05
LCX	1.7 ± 0.4	1.9 ± 0.5	.36
RCA	3.6 ± 0.3	3.1 ± 0.7	< .05
Overall	3.0 ± 0.3	2.4 ± 0.6	< .05

Image quality of MRCA in healthy subjects and in patients. Data are mean image quality scores ± SD (4=excellent, 3=good, 2=moderate, 1=unreadable).

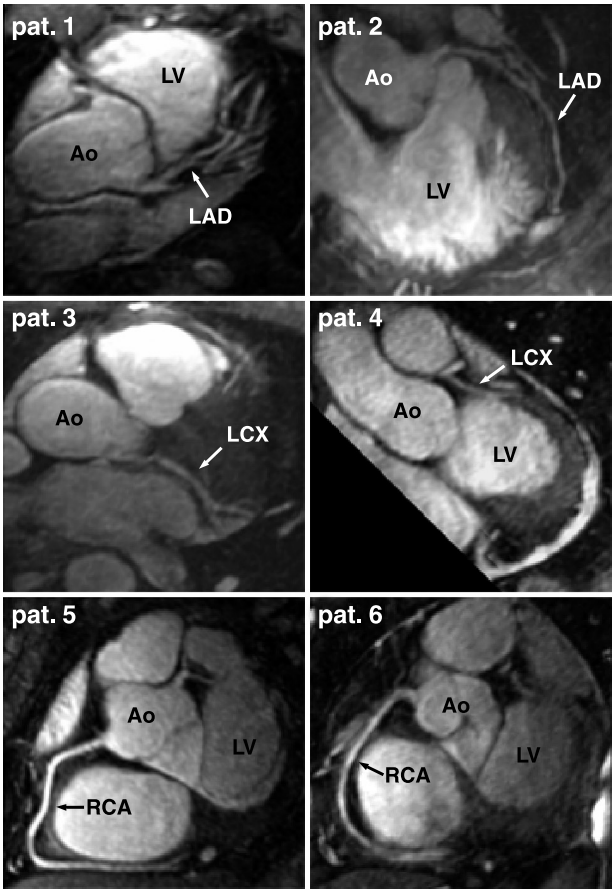

Figure 2. MIP-images of the left anterior descending coronary artery (LAD), the left circumflex coronary artery (LCX) and the right coronary artery (RCA) of 6 different patients after application of contrast agent (Gd-DTPA). Image quality of the patients, according to the score applied in this study: patients 1–4 = good (3), patients 5 and 6 = excellent (4). LV = left ventricle, Ao = Aorta.

3. Results

MRCA was completed in 7 healthy subjects (3 males) and 14 patients (8 males) without complications. All the participants were able to sustain the 24 heartbeats breath-hold. The mean age was 41 ± 14 years in healthy subjects and 67 ± 6 years in patients ($p < .05$). The mean heart rate during the breath-hold was 64.0 ± 5.3 in healthy subjects and 67.5 ± 10.2 ($p = .43$) in patients. The mean LVEF was 63.3 ± 7.4 in healthy subjects and 66.3 ± 5.1 ($p = .34$) in patients. Two patient studies revealed a non-diagnostic image quality excluding their images from further analysis.

The mean scan duration was 38 ± 14 min in healthy subjects and 44 ± 9 min in patients (p = n.s.), including localization of the heart, scout scans for coronary artery localization and accomplishment of the investigational MRCA-scans before and after application of contrast agent. The two healthy subjects not having received Gd-DTPA were excluded from the time calculations.

Seventy-two percent of the targeted vessel segments were eligible for evaluation. Imaging of the LMCA, the LAD and the RCA was accomplished in all of the participants, whereas scanning of the LCX was performed in only 6 (86%) of the healthy subjects and 8 (57%) of the patients. In summary, visualization of the targeted vessel segments was more successful in healthy subjects than in patients, although the difference did not reach statistical significance (Table 1). Generally, the more distal the vessels were, the lower the percentage of visible segments was. The RCA was the vessel to be visualized most reliably; the LCX was the most difficult vessel to assess.

The results of vessel length and diameter were strongly correlated to those of the visible coronary segments. In healthy subjects, we found an average vessel length of 12 ± 3 mm for the left main coronary artery (LMCA); 75 ± 6 mm for the LAD; 23 ± 7 mm for the LCX; and 106 ± 19 mm for the RCA. In patients, the average vessel length was 12 ± 1 mm for the LMCA; 51 ± 20 mm for the LAD; 35 ± 12 mm for the LCX; and 84 ± 37 mm for the RCA (Table 2). Except for the LAD, the differences in length between the two groups did not reach statistical significance, probably due to the substantial variability.

Data for the proximal diameters of the vessels are presented in Table 3. Although there appeared to be a distinct trend towards larger vessel calibres in patients, this difference did reach statistical significance only for the left main coronary artery.

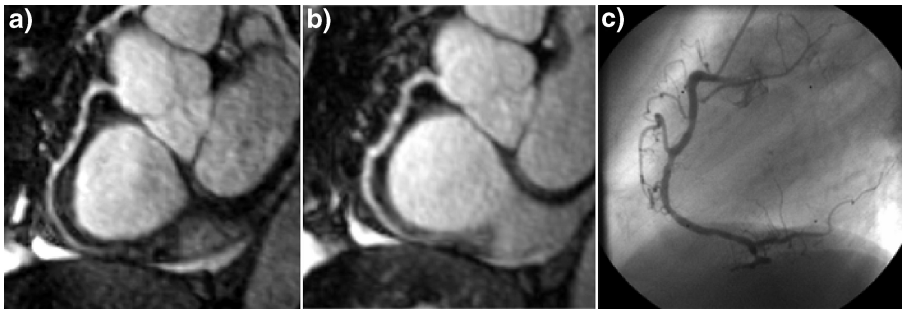

Figure 3. Comparison of MRCA and conventional X-ray angiography: a + b) MIP-images of the RCA before and after application of contrast agent (Gd-DTPA), demonstrating no significant change in image quality; c) corresponding conventional X-ray angiography.

Table 5. Influence of Gd-DTPA on SNR and CNR

		Pre-contrast	Post-contrast	p value
SNR	LAD	6.8 ± 3.1	8.8 ± 4.1	< .01
	LCX	7.6 ± 3.8	10.1 ± 2.7	< .01
	RCA	12.8 ± 5.1	17.2 ± 6.6	< .01
CNR	LAD	3.7 ± 1.5	3.8 ± 1.7	.38
	LCX	4.3 ± 2.8	4.6 ± 1.2	.36
	RCA	10.0 ± 4.5	12.7 ± 5.2	< .01

Signal-to-noise ratio (SNR) and contrast-to-noise ratio (CNR) of the left and right coronary artery (LAD, LCX and RCA) before and after application of Gd-DTPA. Data are mean signal intensity (SI).

Table 6. Overall image quality before and after application of contrast agent

Vessel	Before contrast	After contrast	p value
LMCA	3.3 ± 1.0	3.1 ± 0.9	.58
LAD	2.4 ± 1.1	2.3 ± 1.1	.64
LCX	1.8 ± 1.0	1.9 ± 1.1	.79
RCA	3.3 ± 1.0	3.4 ± 0.9	.63

Overall image quality of MRCA before and after application of contrast agent. Data are mean image quality scores ± SD (4=excellent, 3=good, 2=moderate, 1=unreadable).

Except for the LCX, the image quality was significantly better in healthy subjects than in patients (Table 4). Healthy subjects had an excellent image quality of the RCA and LMCA and a good image quality of the LAD, whereas patients presented with slightly lower values than the group of healthy subjects. Image quality of the LCX was poor with no significant differences between healthy subjects and patients. To demonstrate the image quality and the use of our 4-point-score, Fig. 2 shows MIP-images of the LAD, LCX and RCA.

3.1. *Application of contrast agent*

An extracellular contrast agent was applied in all patients and 5 healthy subjects. None of the participants experienced any adverse reaction to the contrast agent. SNR- and CNR-values were assessed before and after application of contrast agent for proximal LAD, proximal LCX and proximal RCA, separately. Table 5 summarizes the SNR- and CNR-data.

A single dose (0.1 mmol/kg) of Gd-DTPA was applied in 9 participants; a double dose of 0.2 mmol/kg was given to 10 participants. No significant differences in SNR and CNR were observed between the two groups.

In both vessels, SNR increased significantly after application of Gd-DTPA. The CNR of the RCA improved after application of this extracellular contrast agent, whereas it remained rather unchanged for LAD and LCX. The overall number of visible segments was not altered by the application of an extracellular contrast agent (71.0 ± 16.1% vs. 71.6 ± 16.3%, p = ns) nor was the image quality (Table 6, Fig. 3).

4. Discussion

In the present study, we assessed the impact of Gadolinium-DTPA on the performance of an ECG-gated, breath-hold 3D-SSFP sequence. We found that this technique allows for depiction of extensive parts of the coronary artery tree within an acceptable examination time. Despite an increase of SNR in all coronaries and an increase of CNR in the RCA, the application of an extravascular contrast agent did not significantly increase the number of visualized segments or the image quality.

Our results confirm earlier reports on a better visualization of the RCA as compared to LAD and LCX (6, 19, 20, 21), which can be explained by the location and shape of the vessels. Furthermore, our data underscore the fact that MRCA of patients is more difficult than in healthy subjects (22). In addition, we observed, that total examination times were shorter in healthy subjects (38 ± 14 min) than in patients (44 ± 9 min). This was mainly due to difficulties in holding their breath and more difficult vessel identification due to altered signal intensities.

SSFP-based sequences are known to be especially sensitive to magnetic field inhomogenities leading to off-resonance artefacts. Although careful magnetic field shimming was carried out prior to each scan in this study, a volume selective magnetic field shim of the heart was applied when severe artifacts occurred, and reduced this problem. Nevertheless, two patients had to be excluded from image analysis due to off-resonance artifacts. Another technical challenge for MRCA is coronary artery motion, which may reach a distance of up to 2 cm during the cardiac cycle. Cardiac motion is expected to be minimal in mid-diastole, although the timing of this period varies considerably between subjects (23).

We started data acquisition after a trigger delay of 60% of the RR-interval in mid-diastole. The individual optimization of the trigger delay (24) may have improved the image quality.

4.1. *Limitations*

In the present study, only feasibility has been tested; improvement of the investigational sequence has not been the aim of this work. Recently, newer technical approaches, such as the use of parallel imaging or different cardiac coils (18, 25), have been published and may be of additional value for this technique.

We did not intend to assess the diagnostic accuracy of the investigational technique and thus a careful investigation of the diagnostic performance in terms of sensitivity and specificity is required.

5. Conclusion

In conclusion, a 3D breath-hold SSFP technique may serve as a useful pulse sequence for MR Coronary Angiography. The application of an extracellular contrast agent (Gadolinium-DTPA) does not significantly improve visibility or image quality of the coronary arteries. Now that feasibility has been shown, the diagnostic performance of this technique should be tested in future studies.

6. Abbreviations

FIESTA	fast imaging employing steady-state acquisition
CNR	contrast-to-noise ratio
LAD	left anterior descending coronary artery
LCA	left coronary artery
LCX	left circumflex coronary artery
LMCA	left main coronary artery
MIP	maximum intensity projection
RCA	right coronary artery
SNR	signal-to-noise ratio
SSFP	steady state free precession

Acknowledgments

We are indebted to Kerstin Kretschel, Evelyn Polzin and Ursula Wagner for their technical assistance.

References

1. Manning WJ, Li W, Edelman RR. A preliminary report comparing magnetic resonance coronary angiography with conventional angiography. N Engl J Med 1993; 328:828–832.
2. Botnar RM, Stuber M, Danias PG, Kissinger KV, Manning WJ. Improved coronary artery definition with T2-weighted free-breathing three-dimensional coronary MRA. Circulation 1999; 99:3139–3148.
3. Boernert P, Stuber M, Botnar RM, Kissinger KV, Manning WJ. Comparison of fat suppression strategies in 3D spiral coronary magnetic resonance angiography. J Magn Reson Imaging 2002; 15:462–466.
4. Spuentrup E, Stuber M, Botnar RM, Kissinger KV, Manning WJ. Real-time motion correction in navigator-gated free-breathing double-oblique submillimeter 3D right coronary artery magnetic resonance angiography. Invest Radiol 2002; 37:632–636.
5. Stuber M, Botnar RM, Danias PG, Sodickson DK, Kissinger KV, Van Cauteren M, De Becker J, Manning WJ. Double-oblique free-breathing high resolution three-dimensional coronary magnetic resonance angiography. J Am Coll Cardiol 1999; 34:524–531.
6. Regenfus M, Ropers D, Achenbach S, Schlundt C, Kessler W, Laub G, Moshage W, Daniel WG. Comparison of contrast-enhanced breath-hold and free-breathing respiratory-gated imaging in three-dimensional magnetic resonance coronary angiography. Am J Cardiol 2002; 90:725–730.
7. Deshpande VS, Shea SM, Chung YC, McCarthy RM, Finn JP, Debiao L. Breath-hold three-dimensional true-FISP imaging of coronary arteries using asymmetric sampling. J Magn Reson Imaging 2002; 15:473–478.
8. Stuber M, Boernert P, Spuentrup E, Botnar RM, Manning WJ. Selective three-dimensional visualization of the coronary arterial lumen using arterial spin tagging. Magn Reson Med 2002; 47:322–329.
9. Wittlinger T, Voigtlander T, Rohr M, Meyer J, Thelen M, Kreitner KF, Kalden P. Magnetic resonance imaging of coronary artery occlusions in the navigator technique. Int J Cardiovasc Imaging 2002; 18:203–211.
10. Deshpande VS, Shea SM, Laub G, Simonetti OP, Finn JP, Li D. 3D magnetization-prepared trueFISP: a new technique for imaging coronary arteries. Magn Reson Med 2001; 46:494–502.
11. McCarthy RM, Shea SM, Deshpande VS, Green JD, Pereles FS, Carr JC, Finn JP, Li D. Coronary MR angiography: trueFISP imaging improved by prolonging breath holds with preoxygenation in healthy volunteers. Radiology 2003; 227:283–288.
12. Weber OM, Martin AJ, Higgins CB. Whole-heart steady-state free precession coronary artery magnetic resonance angiography. Magn Reson Med 2003; 50:1223–1228.
13. Giorgi B, Dymarkowski S, Maes F, Kouwenhoven M, Bogaert J. Improved visualization of coronary arteries using a new three-dimensional submillimeter MR coronary angiography sequence with balanced gradients. Am J Radiol 2002; 179:901–910.
14. Spuentrup E, Buecker A, Stuber M, Botnar R, Nguyen TH, Bornert P, Kolker C, Gunther RW. Navigator-gated coronary magnetic resonance angiography using steady-state free precession: comparison to standard T2-prepared gradient-echo and spiral imaging. Invest Radiol 2003; 38:263–268.
15. Barkhausen J, Ruehm SG, Goyen M, Buck T, Laub G, Debatin JF. MR evaluation of ventricular function: true fast imaging with steady-state precession versus fast low-angle shot cine MR imaging: feasibility study. Radiology 2001; 219:264–269.
16. Foo TK, Ho VB, Marcos HB, Hood MN, Choyke PL. MR angiography using steady-state free precession. Magn Reson Med 2002; 48:699–706.
17. Saranathan M, Rochitte CE, Foo TK. Fast, three-dimensional free-breathing MR imaging of myocardial infarction: a feasibility study. Magn Reson Med 2004; 51:1055–1060.
18. Niendorf T, Saranathan M, Lingamneni A, Pedrosa I, Spencer M, Cline H, Foo TK.F, Rofsky NM. Short breath-hold, volumetric coronary MR angiography employing steady-state free precession in conjunction with parallel imaging. Magn Reson Med 2005; 53:885–894.
19. Bogaert J, Kuzo R, Dymarkowski S, Beckers R, Piessens J, Rademakers FE. Coronary artery imaging with real-time navigator three-dimensional turbo-field-echo MR coronary angiography: initial experience. Radiology 2003; 226:707–716.
20. Kim WY, Danias PG, Stuber M, Flamm SD, Plein S, Nagel E, Langerak SE, Weber OM, Pedersen EM, Schmidt M, Botnar RM, Manning WJ. Coronary magnetic resonance angiography for the detection of coronary stenoses. N Engl J Med 2001; 345:1863–1869.
21. van Geuns RJ, Wielopolski PA, de Bruin HG, Rensing BJ, Hulshoff M, van Ooijen PM, de Feyter PJ, Oudkerk M. MR coronary angiography with breath-hold targeted volumes: preliminary clinical results. Radiology 2000; 217:270–277.
22. Taylor AM, Keegan J, Jhooti P, Gatehouse PD, Firmin DN, Pennell DJ. Differences between normal subjects and patients with coronary artery disease for three different MR coronary angiography respiratory suppression techniques. J Magn Reson Imaging 1999; 9:786–793.
23. Wang Y, Vidan E, Bergmann GW. Cardiac motion of coronary arteries: variability in the rest period and implications for coronary MR angiography. Radiology 1999; 213:751–758.
24. Plein S, Jones TR, Ridgway JP, Sivananthan MU. Three-dimensional coronary MR angiography performed with subject-specific cardiac acquisition windows and motion-adapted respiratory gating. Am J Radiol 2003; 180:505–515.
25. Zhu Y, Hardy CJ, Sodickson DK, Giaquinto RO, Dumoulin CL, Kenwood G, Niendorf T, Lejay H, McKenzie CA, Ohliger MA, Rofsky NM. Highly parallel volumetric imaging with a 32-element RF coil array. Magn Reson Med 2004; 52:869–877.

4. Ausblick – differenzierte Darstellung weiterer Vorhaben

Die vorgestellten Arbeiten werden unter verschiedenen Aspekten weitergeführt. Bei den myokardialen Erkrankungen steht weiterhin die Myokarddifferenzierung im Mittelpunkt. Das T1-Mapping wird zur quantitativen Erfassung und Differenzierung akuter und chronischer Myokardschäden eingesetzt. Es ist zu erwarten, dass im Gegensatz zu den derzeitigen Techniken auch diffuse Fibrosierungen quantifiziert werden können. Die Korrelation des Fibroseausmaßes zum Grad der Obstruktion wird gegenwärtig bei der Hypertrophischen Kardiomyopathie untersucht, bisher war dies mit einer nichtinvasiven Methode am Patienten nicht möglich. Der potenzielle Nutzen der Verteilung und Ausprägung der Fibrose als Risikomarker steht im Mittelpunkt bei Patienten, die nach den Kriterien der SCD-HeFT-Studie eine Indikation zum automatischen Kardioverter-Defibrillator haben.[70]

Im März 2006 wurden auf einer Consensus-Konferenz mit den auf dem Gebiet der Myokarditis aktiven MRT-Zentren die Eckdaten einer prospektiven multizentrischen Studie definiert. Unser multisequentielles Protokoll konnte sich als Studienprotokoll gegenüber den anderen durchsetzen, die Ergebnisse sind in circa 3 Jahren zu erwarten. Untersuchungen zur myokardialen Mitbeteiligung bei systemischen Lupus erythematodes stehen kurz vor dem Abschluss.

Die Doppelbolusperfusion mit der optimierten Kontrastmitteldosis wird nicht nur zu intraindividuellen Vergleichen vor und nach neuen Therapien eingesetzt, sondern es werden auch Normwerte erstellt, die an dem Goldstandard der fraktionellen Flussreserve validiert werden.

Die weitere Entwicklung der Hard- und Software ermöglicht es uns, neue Sequenzen für die Plaquedifferenzierung einzusetzen und zu optimieren. Dabei

können wir unsere Erfahrung aus dem Bereich der T2*-Bildgebung und des T1-Mapping nutzen.[71, 72]

Eine völlig neue Perspektive entwickelt sich durch den Aufbau der Imaging-Facility am Max-Delbrück-Zentrum, damit können unsere Erfahrungen auf das Tiermodell übertragen werden und insbesondere bei Geno-Phänotypisierung neue Wege beschritten werden.

IV Zusammenfassung

In der vorliegenden Arbeit wurden neue Aspekte und Ansätze zu folgenden Themen vorgestellt:

- MRT-Methode zur Quantifizierung des linksventrikulären Ausflusstraktes bei der Hypertrophischen Kardiomyopathie
- Etablierung von Normwerten zur Differenzierung der Obstruktion bei Patienten mit Hypertrophischer Kardiomyopathie
- Darstellung der Beziehung zwischen Abnahme der Obstruktion, Verbesserung der klinischen Symptomatik und der myokardialen Infarktnarbe nach Septumarterienembolisation bei Patienten mit Hypertrophischer Kardiomyopathie
- Frühe Differenzierung von myokardialem Ödem und Nekrose/Fibrose nach Koronararterienokklusion
- Multisequentieller MRT-Ansatz zur Diagnose einer akuten Myokarditis
- Myokarddifferenzierung bei Sarkoidose
- Anwendung einer 3D-Steady-State-Free-Precession-Sequenz zur Darstellung von Koronararterien

Die meisten der genannten Ansätze konnten bei uns und in anderen Zentren in die Routine bei der kardialen Magnetresonanztomographie eingeführt werden. Die Erfahrungen bei den myokardialen Erkrankungen umfassen im eigenen Zentrum ca. 1000 Untersuchungen bei hypertrophischer Kardiomyopathie und ca. 10.000 Untersuchungen bei Verdacht auf inflammatorische Myokard-erkrankungen. Die genannten Ansätze werden gegenwärtig in weiteren mono- und multizentrischen Studien weiterverfolgt.

V Literaturverzeichnis

1. Richardson P, McKenna W, Bristow M, Maisch B, Mautner B, O'Connell J, Olsen E, Thiene G, Goodwin J, Gyarfas I, Martin I, Nordet P. Report of the 1995 World Health Organization/International Society and Federation of Cardiology Task Force on the Definition and Classification of cardiomyopathies. Circulation. Mar 1 1996;93(5):841-842.
2. Watkins H, McKenna WJ, Thierfelder L, Suk HJ, Anan R, O'Donoghue A, Spirito P, Matsumori A, Moravec CS, Seidman JG, et al. Mutations in the genes for cardiac troponin T and alpha-tropomyosin in hypertrophic cardiomyopathy. N Engl J Med. Apr 20 1995;332(16):1058-1064.
3. Niimura H, Bachinski LL, Sangwatanaroj S, Watkins H, Chudley AE, McKenna W, Kristinsson A, Roberts R, Sole M, Maron BJ, Seidman JG, Seidman CE. Mutations in the gene for cardiac myosin-binding protein C and late-onset familial hypertrophic cardiomyopathy. N Engl J Med. Apr 30 1998;338(18):1248-1257.
4. Maron BJ, Niimura H, Casey SA, Soper MK, Wright GB, Seidman JG, Seidman CE. Development of left ventricular hypertrophy in adults in hypertrophic cardiomyopathy caused by cardiac myosin-binding protein C gene mutations. J Am Coll Cardiol. Aug 2001;38(2):315-321.
5. Maron BJ, McKenna WJ, Danielson GK, Kappenberger LJ, Kuhn HJ, Seidman CE, Shah PM, Spencer WH, 3rd, Spirito P, Ten Cate FJ, Wigle ED. American College of Cardiology/European Society of Cardiology Clinical Expert Consensus Document on Hypertrophic Cardiomyopathy. A

report of the American College of Cardiology Foundation Task Force on Clinical Expert Consensus Documents and the European Society of Cardiology Committee for Practice Guidelines. Eur Heart J. Nov 2003;24(21):1965-1991.

6. Kizilbash AM, Heinle SK, Grayburn PA. Spontaneous variability of left ventricular outflow tract gradient in hypertrophic obstructive cardiomyopathy. Circulation. 1998;97(5):461-466.

7. Paz R, Jortner R, Tunick PA, Sclarovsky S, Eilat B, Perez JL, Kronzon I. The effect of the ingestion of ethanol on obstruction of the left ventricular outflow tract in hypertrophic cardiomyopathy. N Engl J Med. Sep 26 1996;335(13):938-941.

8. Maron MS, Olivotto I, Betocchi S, Casey SA, Lesser JR, Losi MA, Cecchi F, Maron BJ. Effect of left ventricular outflow tract obstruction on clinical outcome in hypertrophic cardiomyopathy. N Engl J Med. Jan 23 2003;348(4):295-303.

9. Maron BJ. Hypertrophic cardiomyopathy: a systematic review. Jama. Mar 13 2002;287(10):1308-1320.

10. Feldman AM, McNamara D. Myocarditis. N Engl J Med. Nov 9 2000;343(19):1388-1398.

11. Kawai C. From myocarditis to cardiomyopathy: mechanisms of inflammation and cell death: learning from the past for the future. Circulation. Mar 2 1999;99(8):1091-1100.

12. Magnani JW, Dec GW. Myocarditis: current trends in diagnosis and treatment. Circulation. Feb 14 2006;113(6):876-890.

13. Iwai K, Tachibana T, Takemura T, Matsui Y, Kitaichi M, Kawabata Y. Pathological studies on sarcoidosis autopsy. I. Epidemiological features of 320 cases in Japan. Acta Pathol Jpn. Jul-Aug 1993;43(7-8):372-376.

14. Sharma OP. Cardiac and neurologic dysfunction in sarcoidosis. Clin Chest Med. Dec 1997;18(4):813-825.

15. Guillevin L, Pagnoux C, Mouthon L. Churg-strauss syndrome. Semin Respir Crit Care Med. Oct 2004;25(5):535-545.

16. Falk RH. Diagnosis and management of the cardiac amyloidoses. Circulation. Sep 27 2005;112(13):2047-2060.

17. Kyle RA, Gertz MA, Greipp PR, Witzig TE, Lust JA, Lacy MQ, Therneau TM. A trial of three regimens for primary amyloidosis: colchicine alone, melphalan and prednisone, and melphalan, prednisone, and colchicine. N Engl J Med. Apr 24 1997;336(17):1202-1207.

18. Moder KG, Miller TD, Tazelaar HD. Cardiac involvement in systemic lupus erythematosus. Mayo Clin Proc. Mar 1999;74(3):275-284.

19. Doherty NE, Siegel RJ. Cardiovascular manifestations of systemic lupus erythematosus. Am Heart J. Dec 1985;110(6):1257-1265.

20. Badui E, Garcia-Rubi D, Robles E, Jimenez J, Juan L, Deleze M, Diaz A, Mintz G. Cardiovascular manifestations in systemic lupus erythematosus. Prospective study of 100 patients. Angiology. Jul 1985;36(7):431-441.

21. Guyton JR. Clinical assessment of atherosclerotic lesions: emerging from angiographic shadows. Circulation. Sep 10 2002;106(11):1308-1309.

22. Davies SW. Clinical presentation and diagnosis of coronary artery disease: stable angina. Br Med Bull. 2001;59:17-27.

23. Jennings RB, Steenbergen C, Jr., Reimer KA. Myocardial ischemia and reperfusion. Monogr Pathol. 1995;37:47-80.

24. Braunwald E. Heart Disease, A Textbook of Cardiovascular Medicine. 5th Edition, W.B. Saunders Company.

25. Kupferwasser I, Mohr-Kahaly S, Stahr P, Rupprecht HJ, Nixdorff U, Fenster M, Voigtlander T, Erbel R, Meyer J. Transthoracic three-dimensional echocardiographic volumetry of distorted left ventricles using rotational scanning. J Am Soc Echocardiogr. Oct 1997;10(8):840-852.

26. Wagner A, Schulz-Menger J, Dietz R, Friedrich MG. Long-term follow-up of patients paragraph sign with acute myocarditis by magnetic paragraph sign resonance imaging. Magma. Feb 2003;16(1):17-20.

27. Klein C, Nekolla SG, Bengel FM, Momose M, Sammer A, Haas F, Schnackenburg B, Delius W, Mudra H, Wolfram D, Schwaiger M. Assessment of myocardial viability with contrast-enhanced magnetic resonance imaging: comparison with positron emission tomography. Circulation. 2002;105(2):162-167.

28. Knuesel PR, Nanz D, Wyss C, Buechi M, Kaufmann PA, von Schulthess GK, Luscher TF, Schwitter J. Characterization of dysfunctional myocardium by positron emission tomography and magnetic resonance: relation to functional outcome after revascularization. Circulation. Sep 2 2003;108(9):1095-1100.

29. Parkka JP, Niemi P, Saraste A, Koskenvuo JW, Komu M, Oikonen V, Toikka JO, Kiviniemi TO, Knuuti J, Sakuma H, Hartiala JJ. Comparison of

MRI and positron emission tomography for measuring myocardial perfusion reserve in healthy humans. Magn Reson Med. Apr 2006;55(4):772-779.

30. Schwitter J, von Schulthess GK. MR perfusion imaging: correlation with PET and quantitative angiography. Magma. Nov 2000;11(1-2):71-72.

31. Simonetti OP, Finn JP, White RD, Laub G, Henry DA. "Black blood" T2-weighted inversion-recovery MR imaging of the heart. Radiology. Apr 1996;199(1):49-57.

32. Abdel-Aty H, Zagrosek A, Schulz-Menger J, Taylor AJ, Messroghli D, Kumar A, Gross M, Dietz R, Friedrich MG. Delayed enhancement and T2-weighted cardiovascular magnetic resonance imaging differentiate acute from chronic myocardial infarction. Circulation. May 25 2004;109(20):2411-2416.

33. Kim RJ, Wu E, Rafael A, Chen EL, Parker MA, Simonetti O, Klocke FJ, Bonow RO, Judd RM. The use of contrast-enhanced magnetic resonance imaging to identify reversible myocardial dysfunction. N Engl J Med. 2000;343(20):1445-1453.

34. Moon JC, McKenna WJ, McCrohon JA, Elliott PM, Smith GC, Pennell DJ. Toward clinical risk assessment in hypertrophic cardiomyopathy with gadolinium cardiovascular magnetic resonance. J Am Coll Cardiol. May 7 2003;41(9):1561-1567.

35. Weishaupt D, Köchli V, Marincek B. Wie funktioniert MRI?
Eine Einführung in Physik und Funktionsweise der Magnetresonanzbildgebung. Springer Verlag. 2002 (4. Auflage).

36. Alfakih K, Plein S, Thiele H, Jones T, Ridgway JP, Sivananthan MU. Normal human left and right ventricular dimensions for MRI as assessed by turbo gradient echo and steady-state free precession imaging sequences. J Magn Reson Imaging. Mar 2003;17(3):323-329.

37. Kunz RP, Oellig F, Krummenauer F, Oberholzer K, Romaneehsen B, Vomweg TW, Horstick G, Hayes C, Thelen M, Kreitner KF. Assessment of left ventricular function by breath-hold cine MR imaging: Comparison of different steady-state free precession sequences. J Magn Reson Imaging. Feb 2005;21(2):140-148.

38. Kim RJ, Shah DJ, Judd RM. How we perform delayed enhancement imaging. J Cardiovasc Magn Reson. Jul 2003;5(3):505-514.

39. Eichstaedt HW, Felix R, Dougherty FC, Langer M, Rutsch W, Schmutzler H. Magnetic resonance imaging (MRI) in different stages of myocardial infarction using the contrast agent gadolinium-DTPA. Clin Cardiol. Nov 1986;9(11):527-535.

40. Friedrich MG, Strohm O, Schulz-Menger J, Marciniak H, Luft FC, Dietz R. Contrast media-enhanced magnetic resonance imaging visualizes myocardial changes in the course of viral myocarditis. Circulation. May 12 1998;97(18):1802-1809.

41. Bock P, Abdel-Aty H, Dahme S, Greiser A, Boyé P, Kumar A, Wassmuth R, Dietz R, Friedrich M, Schulz-Menger J. Normal values of myocardial global relative enhancement. J Cardiovasc Magn Reson. 2005;7(1):abstract.

42. Bohl S, Wassmuth R, Rudolph A, Dietz R, Schulz-Menger J. Pattern of Delayed Enhancement in Non-Ischemic Cardiomyopathies. Journal Cardiovasc Mag Res. 2006;8(1):abstract.

43. Pruessmann KP, Weiger M, Scheidegger MB, Boesiger P. SENSE: sensitivity encoding for fast MRI. Magn Reson Med. Nov 1999;42(5):952-962.

44. Sodickson DK, Manning WJ. Simultaneous acquisition of spatial harmonics (SMASH): fast imaging with radiofrequency coil arrays. Magn Reson Med. Oct 1997;38(4):591-603.

45. Niendorf T, Sodickson D. [Acceleration of cardiovascular MRI using parallel imaging: basic principles, practical considerations, clinical applications and future directions]. Rofo. Jan 2006;178(1):15-30.

46. Zhu Y, Hardy CJ, Sodickson DK, Giaquinto RO, Dumoulin CL, Kenwood G, Niendorf T, Lejay H, McKenzie CA, Ohliger MA, Rofsky NM. Highly parallel volumetric imaging with a 32-element RF coil array. Magn Reson Med. Oct 2004;52(4):869-877.

47. Brasch RC, Weinmann HJ, Wesbey GE. Contrast-enhanced NMR imaging: animal studies using gadolinium-DTPA complex. AJR Am J Roentgenol. Mar 1984;142(3):625-630.

48. Niendorf HP, Haustein J, Cornelius I, Alhassan A, Clauss W. Safety of gadolinium-DTPA: extended clinical experience. Magn Reson Med. Dec 1991;22(2):222-228; discussion 229-232.

49. Mahrholdt H, Wagner A, Judd RM, Sechtem U, Kim RJ. Delayed enhancement cardiovascular magnetic resonance assessment of non-ischaemic cardiomyopathies. Eur Heart J. Aug 2005;26(15):1461-1474.

50. Schulz-Menger J, Friedrich MG. Magnetic resonance imaging in patients with cardiomyopathies: when and why. Herz. Jun 2000;25(4):384-391.

51. Schulz-Menger J, Strohm O, Waigand J, Uhlich F, Dietz R, Friedrich MG. The value of magnetic resonance imaging of the left ventricular outflow tract in patients with hypertrophic obstructive cardiomyopathy after septal artery embolization. Circulation. Apr 18 2000;101(15):1764-1766.

52. Gross CM, Schulz-Menger J, Kramer J, Siegel I, Pilz B, Waigand J, Friedrich MG, Uhlich F, Dietz R. Percutaneous transluminal septal artery ablation using polyvinyl alcohol foam particles for septal hypertrophy in patients with hypertrophic obstructive cardiomyopathy: acute and 3-year outcomes. J Endovasc Ther. Dec 2004;11(6):705-711.

53. Schulz-Menger J, Gross M, Messroghli D, Uhlich F, Dietz R, Friedrich MG. Cardiovascular magnetic resonance of acute myocardial infarction at a very early stage. J Am Coll Cardiol. Aug 6 2003;42(3):513-518.

54. Schulz-Menger J, Abdel-Aty H, Busjahn A, Wassmuth R, Pilz B, Dietz R, Friedrich M. Left Ventricular Outflow Tract Planimetry by Cardiovascular Magnetic Resonance Diffrentiates Obstructive from Non-Obstructive Hypertrophic Cardiomyopathy. J Cardiovasc Magn Reson. 2006;in press.

55. Abdel-Aty H, Boye P, Zagrosek A, Wassmuth R, Kumar A, Messroghli D, Bock P, Dietz R, Friedrich MG, Schulz-Menger J. Diagnostic performance of cardiovascular magnetic resonance in patients with suspected acute

myocarditis: comparison of different approaches. J Am Coll Cardiol. Jun 7 2005;45(11):1815-1822.

56. Abdel-Aty H, Dietz R, Schulz-Menger J. Letter regarding article by Sharkey et al, "Acute and reversible cardiomyopathy provoked by stress in women from the United States". Circulation. Jul 19 2005;112(3):e51; author reply e51.

57. Zagrosek A, Abdel-Aty H, Wassmuth R, Boyé P, Kumar A, Bock P, Dietz R, Friedrich M, Schulz-Menger J. Langzeit follow-up von Patienten mit akuter Myokarditis: Vergleich verschiedener MRT-Techniken. Z Kardiol, suppl. 2005:666, abstract.

58. Schulz-Menger J, Strohm O, Dietz R, Friedrich MG. Visualization of cardiac involvement in patients with systemic sarcoidosis applying contrast-enhanced magnetic resonance imaging. Magma. Nov 2000;11(1-2):82-83.

59. Schulz-Menger J, Wassmuth R, Abdel-Aty H, Siegel I, Franke A, Dietz R, Friedrich MG. Patterns of myocardial inflammation and scarring in sarcoidosis as assessed by cardiovascular magnetic resonance. Heart. Mar 2006;92(3):399-400.

60. Maceira AM, Joshi J, Prasad SK, Moon JC, Perugini E, Harding I, Sheppard MN, Poole-Wilson PA, Hawkins PN, Pennell DJ. Cardiovascular magnetic resonance in cardiac amyloidosis. Circulation. Jan 18 2005;111(2):186-193.

61. Wassmuth R, Bohl S, Dietz R, Schulz-Menger J. Combined Early and Delayed Myocardial Contrast Enhancement in Cardiac Amyloidosis. Journal Cardiovasc Mag Res. 2006;8(1):abstract.

62. Messroghli DR, Niendorf T, Schulz-Menger J, Dietz R, Friedrich MG. T1 mapping in patients with acute myocardial infarction. J Cardiovasc Magn Reson. 2003;5(2):353-359.

63. Messroghli D, Greiser A, Froehlich M, Dietz R, Schulz-Menger J. Myocardial T1 mapping: Implementation and Validation of an Optimized Pulse sequence Variant for Modified Look-Locker Inversion-Recovery (MOLLI) in Phantoms and in Healthy Subjects. Journal Cardiovasc Mag Res. 2006;8(1):abstract.

64. Abdel-Aty H, Friedrich MG, Schulz-Menger J. Myocardial infarction after coronary revascularization: role of cardiovascular magnetic resonance oedema imaging. Eur Heart J. Dec 2004;25(23):2172.

65. Zagrosek A, Noeske R, Abdel-Aty H, Friedrich MG, Dietz R, Schulz-Menger J. MR coronary angiography using 3D-SSFP with and without contrast application. J Cardiovasc Magn Reson. 2005;7(5):809-814.

66. Giang TH, Nanz D, Coulden R, Friedrich M, Graves M, Al-Saadi N, Luscher TF, von Schulthess GK, Schwitter J. Detection of coronary artery disease by magnetic resonance myocardial perfusion imaging with various contrast medium doses: first European multi-centre experience. Eur Heart J. Sep 2004;25(18):1657-1665.

67. Taylor AJ, Al-Saadi N, Abdel-Aty H, Schulz-Menger J, Messroghli DR, Gross M, Dietz R, Friedrich MG. Elective percutaneous coronary intervention immediately impairs resting microvascular perfusion assessed by cardiac magnetic resonance imaging. Am Heart J. Apr 2006;151(4):891 e891-897.

68. Taylor AJ, Al-Saadi N, Abdel-Aty H, Schulz-Menger J, Messroghli DR, Friedrich MG. Detection of acutely impaired microvascular reperfusion after infarct angioplasty with magnetic resonance imaging. Circulation. May 4 2004;109(17):2080-2085.

69. Utz W, Wassmuth R, Dietz R, Schulz-Menger J. Contrast-Dose Relation in TurboFLASH and Echoplanar First Pass perfusion Imaging. Journal Cardiovasc Mag Res. 2006;8(1):abstract.

70. Klein H, Auricchio A, Reek S, Geller C. New primary prevention trials of sudden cardiac death in patients with left ventricular dysfunction: SCD-HEFT and MADIT-II. Am J Cardiol. Mar 11 1999;83(5B):91D-97D.

71. Utz W, Jordan J, Niendorf T, Stoffels M, Luft FC, Dietz R, Friedrich MG. Blood Oxygen Level-Dependent MRI of Tissue Oxygenation. Relation to Endothelium-Dependent and Endothelium-Independent Blood Flow Changes. Arterioscler Thromb Vasc Biol. May 12 2005.

72. Friedrich MG, Niendorf T, Schulz-Menger J, Gross CM, Dietz R. Blood oxygen level-dependent magnetic resonance imaging in patients with stress-induced angina. Circulation. Nov 4 2003;108(18):2219-2223.

VI Danksagung

Wenn man sich viele Jahre mit einer Methode beschäftigt, gehören viele Menschen dazu, die einem helfen, die Mühen der Ebenen (B. Brecht) zu überwinden. Leider benötigt man beim Schreiben eine Reihenfolge, die aber keine Wertfolge darstellt.

Vermutlich hätte ich ohne Matthias G. Friedrich den Weg zur kardialen MRT gar nicht oder nur schwer gefunden. Ich bewundere ihn für seine Ideen und immer währende Kraft unmöglich Erscheinendes anzugehen. Es war eine wunderbare Zeit gemeinsam neugierig und mit viel Spaß ungewisse Wege zu beschreiten. Auch wenn ich mich immer noch nicht freue, dass er nicht mehr in unseren Landen seine Arbeit fortsetzt, ist es doch möglich weiter gemeinsam der kardialen MRT Tür und Tore zu öffnen.

Meinem Chef und Lehrer, Prof. Rainer Dietz, möchte ich danken, dass er der kardialen MRT in unserem Hause den Weg bereitet hat, dass er durch sein aus der gesamten Kardiologie und der Grundlagenforschung stammenden Wissens unseren Ideen den Weg gewiesen hat. Seine konstruktive Kritik hat viele Arbeiten erst zu dem werden lassen, was sie heute sind. Vor allem aber hat er es mir ermöglicht, meine wissenschaftlichen und klinischen Interessen mit meinem persönlichen familiären Weg in Übereinklang zu bringen. Er ist mir ein Vorbild in der klinischen, wissenschaftlichen Arbeit und als Mensch.

Der Weg einer Doktorarbeit kann prägend sein für die Zukunft und so möchte ich den Professoren Wolfgang Mohnike und Jürgen Schmidt danken, dass ich die insbesondere zur damaligen Zeit große Freiheit genoss, an der neuen SPECT-Kamera frisch aus der Literatur erworbenes Wissen umzusetzen und neue Ideen auszuprobieren.

Es ist mir ein großes Bedürfnis, ehemaligen und gegenwärtigen Mitgliedern der AG Kardiale MRT zu danken. Ohne die unglaublich gute, offene und freundliche Atmosphäre wäre alle Arbeit nicht möglich gewesen. Dank dieser Gruppe ist es eine tägliche Freude zur Arbeit zu gehen und die Probleme des Alltags treten in den Hintergrund. Es ist unmöglich, auf alles einzugehen, was den Einzelnen und die Gruppe ausmacht. Stellvertretend möchte ich Oliver Strohm nennen, der bereits in den Anfängen mit seiner sehr zügigen, effektiven Arbeitsweise Dinge vorantrieb. Ralf Wassmuth ist nicht nur einer der verlässlichsten Kollegen, den ich kennen lernen durfte, er stellt sein breites Wissen jedem zur Verfügung – ohne ihn wäre die AG nicht da, wo sie heute ist. Daniel R. Messroghli ist es gelungen, neue Wege zu gehen und damit unseren Alltag zu bereichern. Besonders danken möchte ich ihm für die konstruktiven Kritiken, die sowohl das geschriebene Wort, aber auch die geplante wissenschaftliche Arbeit vorantreiben. Wolfgang Utz brachte insbesondere durch sein physikalisches Vorwissen einen anderen Gang des Denkens in unsere Diskussionen, seine ruhig-ausgeglichene Art ist ein mir sehr willkommener Gegenpol. Bei Phillip Boye möchte ich mich bedanken, da man sich auf ihn stets verlassen kann und er zu jeder Zeit bereit ist, auch artfremde Probleme für die AG zu lösen und seine eigenen Interessen in den Hintergrund zu

stellen. Genau wie die Anderen, bereicherte auch Steffen Bohl durch seine offene Freundlichkeit unsere AG und auch ihm ist es eigen, seine Ideen in gut durchdachten Projekte zu Ende zu bringen. Es ist mir ein besonderes Bedürfnis Anja Zagrosek zu nennen, die hochschwanger eine Veröffentlichung zum erfolgreichen Ende gebracht hat und ich freue mich darauf, ihre verantwortungsbewusste Mitarbeit wieder genießen zu dürfen. Hassan Abdel-Aty gehört zu den uneigennützigsten Wissenschaftlern, die ich jemals kennen lernen durfte. Ich freue mich darauf, seine konstruktiven Diskussionen und seine Hilfsbereitschaft wieder in der AG begrüßen zu können. Auch ohne Petra Bock, Mirko Fröhlich und Christoph Tillmanns wäre die wissenschaftliche Arbeit deutlich schwerer, da das Tägliche nicht so verlässlich vorangetrieben werden würde und die Köpfe nicht für Fragen geöffnet würden.

Die strengsten, aber konstruktiven Kritiken und unbedingte Unterstützung habe ich durch meinem Mann, Dr. Olaf Schulz, erfahren. Als klinisch und wissenschaftlich tätiger Kardiologe hat er sich in die Aspekte meiner Arbeit eingedacht und sie durch völlig andere Blickwinkel bereichert. Ich bin aber insbesondere auch dankbar, weil es nur durch ein gemeinsames Agieren möglich ist, ein glückliches Kind zu haben und trotzdem so zu arbeiten, wie man es sich wünscht.

Meinem Sohn Alex möchte ich für die Geduld danken, mit der er die Zeit akzeptierte, die von einer gemeinsam Verbrachten verloren ging. Aber ich hoffe, dass er einen Lebensweg findet, auf dem auch er seinen neugierigen Fragen nachgehen kann und dass er gesehen hat, dass Arbeit nicht allein zum

Geldverdienen gut ist. Seine Fröhlichkeit, seine Liebe und seine Energie sind auch mein Motor.

Nicht zuletzt möchte ich die Beiden erwähnen, die die ersten Schritte in meinem Leben begleitet haben und geduldig Irrwege ertragen haben. Meine leider längst verstorbene Grossmutter Lilly Salm und meine Mutter Angelika Menger haben mich gelehrt mit Widerständen umzugehen und Ideen nicht aufzugeben.

ERKLÄRUNG

§ 4 Abs. 3 (k) der HabOMed der Charité

Hiermit erkläre ich, daß

- weder früher noch gleichzeitig ein Habilitationsverfahren durchgeführt oder angemeldet wird bzw. wurde,
- die vorgelegte Habilitationsschrift ohne fremde Hilfe verfaßt, die beschriebenen Ergebnisse selbst gewonnen sowie die verwendeten Hilfsmittel, die Zusammenarbeit mit anderen Wissenschaftlern/Wissenschaftlerinnen und mit technischen Hilfskräften sowie die verwendete Literatur vollständig in der Habilitationsschrift angegeben wurden.
- mir die geltende Habilitationsordnung bekannt ist.

Datum Unterschrift